Superconducting Quantum Computation: Devices, Gate Design and Quantum Simulation

by

Emily J. Pritchett

(Under the direction of Michael Geller and Andrew Sornborger)

Abstract

Quantum computers have the potential to solve certain problems with a significant reduction in resources from their classical counterparts. For this reason, quantum information science has grown into an extremely active field of physics with constant theoretical and experimental development. Superconducting devices provide the functionality necessary to store and process quantum information in a large-scale quantum computer. In this dissertation, a survey of existing and proposed superconducting quantum bits (qubits) is given while demonstrating the mathematical formalism that is necessary to treat superconducting circuits quantum mechanically.

High fidelity demonstration of universal gates is one of the current focuses of both theoretical and experimental work in quantum computation. Of the established universal two qubit logic gates, the most well-known and useful in algorithm design is the controlled-NOT (CNOT). Protocols for performing the CNOT gate are surveyed here and generalized to a protocol that applies to any configuration of weakly coupled two-level system. In this context, a technique for quantum gate design is described.

A certain superconducting quantum computing architecture is focused on, that of a large-area, current-biased Josephson-junction phase qubit coupled to the dilatational mode of a nanomechanical resonator. While the Josephson phase qubit has proven repeatedly to have

the functionality to store and process quantum information, certain other quantum devices, like mechanical or LC oscillators, can store information longer with less interaction from the environment. However, quantum state prepared in a superconducting qubit can be stored and later retrieved from an attached high-Q resonator. Here the memory capabilities of a such a qubit-resonator system are studied.

Quantum logic gates are the building blocks of quantum algorithms, an important class of which are quantum simulation algorithms. Here, we introduce an alternative approach to quantum simulation that does not involve logic gate decomposition. Alternatively, a direct mapping is given between the control parameters of a tunable quantum computer and the matrix element of $H_{\rm s}(t)$, an arbitrary, real, time-dependent $n \times n$ dimensional Hamiltonian that is simulated in the n-dimensional 'single excitation' subspace of the quantum computer. Simulation of a molecular collision with three Josephson phase qubits is demonstrated and the fidelity of the simulation is studied.

INDEX WORDS: Superconducting qubits, CNOT, quantum logic gate, quantum simulation

Superconducting Quantum Computation: Devices, Gate Design and Quantum Simulation

by

Emily J. Pritchett

B.S., The University of Georgia, 2003

A Dissertation Submitted to the Graduate Faculty
of The University of Georgia in Partial Fulfillment
of the
Requirements for the Degree

Doctor of Philosophy

Athens, Georgia

2010

Superconducting Quantum Computation: Devices, Gate Design and Quantum Simulation

by

Emily J. Pritchett

Approved:

Major Professors: Michael Geller
Andrew Sornborger

Committee: Chad Fertig
Phillip Stancil

Electronic Version Approved:

Maureen Grasso
Dean of the Graduate School
The University of Georgia
August 2010

Acknowledgments

This work was funded by IARPA under grant no. $W911NF-08-1-0336$ (Michael Geller and John Martinis, Principal Investigators), and the National Science Foundation under Grant No. CMS-0404031 (Michael Geller, Principal Investigator), CAREER Grant No. DMR-0093217 (Michael Geller, Principal Investigator), and grants PHYS-0939849 and PHYS-0939853 from the Physics at the Information Frontier Program (Michael Geller, Andrew Sornborger and Phillip Stancil, Principal Investigators).

I would like to thank my family for their support throughout my education.

Table of Contents

List of Figures

Chapter 1

Introduction

Quantum computers promise to solve many important problems more efficiently than currently thought possible with classical computers. These problems include searching [47], factoring [106], approximating Jones Polynomials [2], and other problems of interest in mathematics and computer science. Furthermore, quantum computers are inherently able to simulate certain other quantum systems efficiently [32]. If implemented, quantum computation could impact many branches of physics where systems of many interacting particles are studied.

While many of these algorithms have been demonstrated on small scale quantum computers [118, 72, 66, 93, 27], it is not clear if and how quantum computers will scale to 100's or more quantum bits (qubits). Qubits are the basic unit of quantum information, two level quantum systems that can be prepared in an arbitrary superposition. To accommodate a large scale quantum computation, one must be able to prepare qubits in arbitrary superpositions, perform arbitrary single qubit state transformations, entangle pairs of qubit on demand, and accurately measure the state of the qubit. Despite this high level of outside control, qubits must also remain decoupled from their environment to preserve the coherent quantum superpositions that they store.

There are many quantum systems that are currently considered as qubits that meet all of these requirements to varying degrees. The qubit architectures described in this dissertation are constructing from superconducting electrical circuits, the study of which has become an extremely active theoretical and experimental subfield of solid state physics. With the goal

of eventually implementing large scale, coherent superconducting networks, researchers currently tackle the problems of decoherence, quantum logic gate implementation, and accurate measurement for systems of fewer than ten superconducting qubits.

This dissertation is divided into three parts: devices (Chs. 2-4), gate design (Chs. 5-6), and quantum simulation (Ch. 7). These units represent areas of my research, not in any way the basic subfields of superconducting quantum computation. Many interesting topics relating to superconducting quantum computation, such as decoherence and measurement, will not be addressed here.

Chapter 2 surveys the broader categories of superconducting qubits while introducing the basic physics of superconducting devices. There is a short introduction to quantum circuits, superconductivity, and the Josephson effect, all of which are necessary background for the study of superconducting qubits. The broad categories of phase, charge, and flux qubits are described while reporting experimental progress toward implementing each.

Superconducting circuits are a uniquely *scalable* implementation of quantum bits as many can be fabricated on the same chip and coupled through electronic circuitry that is itself in the quantum regime. However, exactly what type of circuitry should be used to best couple superconducting qubits is still an answered question. A few approaches to coupling superconducting qubits are discussed in Chapter 3.

Chapter 4 focuses on a particular architecture, a superconducting phase qubit capacitively coupled to a nanomechanical resonator, and shows how the natural evolution of the system in a certain regime generates useful operations such as quantum state storage and transfer. The fidelity of the 'memory' operation is studied as a function of qubit-resonator coupling strength and the actual state that is being transferred. This chapter is a stand alone journal article, reprinted with permission of *Physical Review A*.

In Ch. 5, a short mathematical digression allows us to generalize all the superconducting devices covered so far with a surprisingly simple Hamiltonian. These generalization allows us to develop the theory of gate design and quantum simulation in the following chapters

in a platform independent way. After making some connection with the physical systems discussed in Chs. 2-4, the direction of this dissertation will become fairly independent of the details of the superconducting circuits its directed towards. This keeps theoretical results from become obsolete in an environment where superconducting architectures are constantly evolving and improving.

Using the generalized Hamiltonian derived in Ch. 5, the basic principles of gate design are discussed in Ch. 6. We have developed a very general algorithmic approach to two qubit logic gate design that applies to any of the circuits described above, based on the notation of 'local equivalence' and Lie algebra theory. In this chapter, our procedure for gate design is described using as a target gate the controlled-NOT (CNOT), a universal two qubit gate that is very useful in many quantum computation algorithms and thus has become an experimental benchmark for any system being considered as a candidate for a quantum computer.

Ch. 7 moves away from discussions of universal gate design whereby superconducting circuits are analyzed within the standard quantum computation regime and asks how the unique features of superconducting circuits can add to the standard quantum computation regime. In particular, we show that the possibility of complex connectedness and tunable couplings offered by superconducting circuits opens up a new class of quantum simulation, one in which the Hamiltonian of different quantum systems can be directly embed into the Hamiltonian of the superconducting circuit. The Hamiltonian is simulated as Schrodinger evolution propels the superconducting circuit forward in time. If the coupling between qubits is tunable, real but otherwise arbitrary $n \times n$-dimensional Hamiltonians can be simulated on n-qubit quantum circuits in this way. This final chapter contains a stand alone journal article that has been recently submitted for peer review, reprinted with permission of *Physical Review Letters*.

If there is one theme pervasive throughout this dissertation, it is the accurate modeling, prediction, and control of Schrodinger dynamics. In the first few chapters, the basic principles of classical Lagrangian and Hamiltonian mechanics are reviewed as well as the procedure

of first quantization so that superconducting circuit Hamiltonians, and consequently their quantum evolution, can be predicted accurately. In Chs. 5-6, we are less concerned with whether the accuracy of these Hamiltonians, but rather assume they are correct and ask what interesting quantum logic gates they can generate. In the final chapter, we demand some control over the Hamiltonian of a superconducting circuit, and use that control to emulate the Schrodinger dynamics of other quantum systems.

Chapter 2

Superconducting Devices as Qubits

Superconducting circuits are one of the leading candidates for quantum bits (qubits) as they exhibit robust, macroscopic quantum behavior and the external controllability necessary for quantum computation. This chapter presents a basic description and survey of superconducting qubits.

To understand the quantum limit of electrical circuits, we first study a simple example: a quantum limited LC circuit. In this discussion, the theory of modeling a circuit in the quantum regime is developed by reviewing basic principles of quantum mechanics and first quantization.

An LC circuit does not, however, have the functionality required of qubits. All currently accepted superconducting qubit architectures have a common feature that makes them spectroscopically controllable: a Josephson junction. The second section of this chapter introduces the Josephson effect and explains how Josephson junctions affect the Schrodinger dynamics of a superconducting circuit.

In a superconducting circuit containing a Josephson junction, a tunnel barrier is placed between two superconducting electrodes. The canonically conjugate quantum variables that describe circuits with Josephson junctions are related to the number of Cooper pairs charging the junction, N_{c}, and the phase differenceof the superconducting wave functions across the barrier, φ.

All superconducting qubit architectures can be organized into three broad categories based on which of these quantum variables is localized while the other experiences large variations according to the uncertainty principle of quantum mechanics. Circuits containing a

Josephson junction where the phase φ is localized are called *phase qubits*. Energy quantization in a current-biased Josephson junction, which would later become the phase qubit, was one of the first experimental demonstrations of macroscopic quantum coherence [80]. The third section of the chapter discusses the basic features of the phase qubit.

In many superconducting qubits, a Josephson junction isolates a small branch of circuit, referred to as an 'island' or a 'Cooper-pair box.' The amount of charge Q trapped on the island is localized while φ fluctuates, hence the name *charge qubit*. The energy levels between qubit states are externally controlled by changing the gate voltage across the junction. Charge qubits are discussed in the fourth section of this chapter.

Complete superconducting loops broken by one ore more Josephson junctions are called flux qubits. Typically neither φ nor N_{c} is more localized, but rather the flux is localized and qubit states are superpositions of persistent supercurrents in the clockwise and counterclockwise directions. *Flux qubits* are discussed in the fifth section of this chapter.

This chapter and the next follows the discussion in our review article Ref. [41], updating experimental results since its publication and elaborating where appropriate.

2.1 The quantum limited LC circuit

The quantum limited LC-oscillator forms the perfect introduction into superconducting devices as it bridges a well known classical electronic circuit to a well known quantum system, the quantum harmonic oscillator. This section explains what is meant by the quantum limit of an electrical circuit while developing the mathematical tools necessary to analyze more complex superconducting circuits.

The time evolution of any closed, nonrelativistic system in the quantum regime can be described by a time evolution operator $U(t)$ acting on initial state $|\psi(0)\rangle$:

$$|\psi(t)\rangle = U(t)|\psi(0)\rangle. \tag{2.1}$$

The time evolution operator $U(t)$ is determined by Schrodinger's equation,

$$i\hbar\frac{dU(t)}{dt} = H(t)U(t), \tag{2.2}$$

the solution of which is

$$U(t) = \mathcal{T}e^{-\frac{i}{\hbar}\int_{t_0}^{t} H(t')dt'} \tag{2.3}$$

where $\mathcal{T}$ is the time-ordering operator. As long as the system is closed (i.e. there are no outside systems interacting with it), $U(t)$ completely describes the dynamical behavior of the quantum system.

When describing a quantum computer, this time evolution operator *is* the quantum computation; therefore, understanding how to control $U(t)$ of a superconducting circuit is the fundamental problem faced by both theoretical and experimental researchers aspiring to build a superconducting quantum computer. When interaction with the environment is negligible, $U(t)$ depends only on $H(t)$. Therefore, accurately modeling the Hamiltonian of a superconducting circuit is the first step toward understanding its functionality as a qubit.

To derive the Hamiltonian of a given circuit, we can first establish the classical equations of motion governing that circuit. These should depend on a set of generalized coordinates, q_1, ..., q_n, and their corresponding velocities, $\dot{q}_1$, ...,$\dot{q}_2$, and/or accelerations $\ddot{q}_1$, ...,$\ddot{q}_2$. The equations of motion can be expressed as

$$F^{(i)}(q_1, ...q_n; \dot{q}_1..., \dot{q}_2; \ddot{q}_1..., \ddot{q}_2) = 0. \tag{2.4}$$

for some set of functions $F^{(1)}, ..., F^{(n)}$. There should be as many equations of motion (and thus $F^{(i)}$) as there are independent coordinates in order for the motion of the system to be determined classically. We seek a Lagrangian $L(q_1, ...q_n; \dot{q}_1..., \dot{q}_2)$ that has as its Euler-Lagrange equation of motions

$$F^{(i)} = \frac{d}{dt}\frac{\partial L}{\partial \dot{q}_i} - \frac{\partial L}{\partial q_i} = 0. \tag{2.5}$$

Once established, the Lagrangian can be Legendre transformed to a Hamiltonian

$$H(q_1, ..., q_n; p_{q_1}..., p_{q_n}) = \sum_i p_{q_i}\dot{q}_i - L \tag{2.6}$$

where $p_{\mathrm{q_i}} = \partial L/\partial \dot{q}_i$ is the momentum conjugate to the generalized coordinate q_i [65]. The system is 'quantized' by introducing an uncertainty relation between the generalized coordinates and momenta:

$$[q_i, p_{q_i}] = i\hbar \tag{2.7}$$

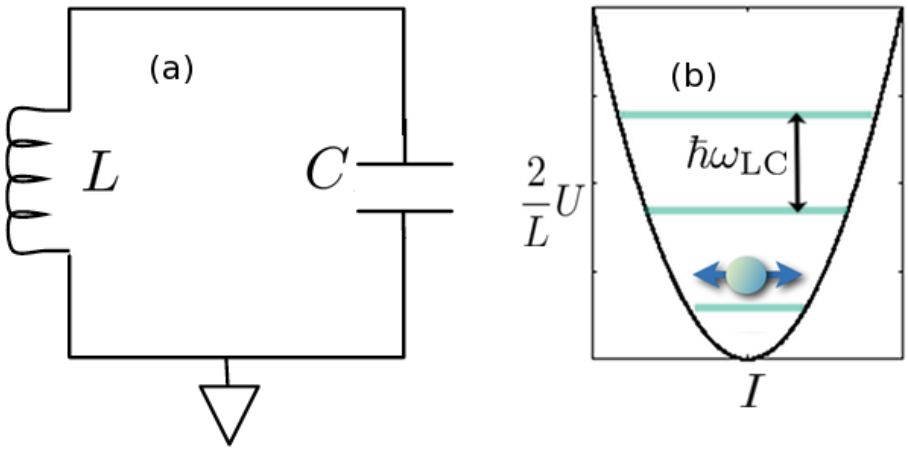

Figure 2.1: (a) A circuit with inductance L and capacitance C. (b) A quantum limited LC circuit behaves like a fictitious particle with mass M_{LC} in potential $U = \frac{1}{2}LI^2$, drawn here in arbitrary units. The energy eigenstates of the quantum limited LC circuit are equally spaced with $E_{\mathrm{n+1}} - E_n = \hbar\omega_{\mathrm{LC}}$.

This procedure of first quantization is followed for a simple closed LC circuit with inductance L and capacitance C, as shown in Fig. 2.1 (a). The characteristic equations for current and voltage drop across the inductor and capacitor separately, $V_{\mathrm{L}} = L\dot{I}_{\mathrm{L}}$ and $I_{\mathrm{C}} = C\dot{V}_{\mathrm{C}}$, together with Kirchoff's voltage and current laws applied to the loop, $V_{\mathrm{L}} = -V_{\mathrm{C}} \equiv V$ and $I_{\mathrm{C}} = I_{\mathrm{L}} \equiv I$, give the familiar harmonic oscillator equation of motion for the current:

$$\ddot{I} + \tfrac{1}{LC} I = 0. \tag{2.8}$$

Because the equation of motion depends on I and $\ddot{I}$, we take I to be the generalized coordinate describing the circuit. There is only one classical degree of freedom in this system. We can always change the generalized coordinate by a coordinate transform; for example,

the LC circuit Hamiltonian is written in terms of generalized coordinate $\Phi = IL$ below. A generalized coordinate should be chosen for convenience as long as its equation of motion can be derived from a valid Lagrangian. I is chosen here only for the familiarity of the classical equation of motion Eqn. (2.8).

The Lagrangian producing Eqn. (2.8) as its Euler-Lagrange equation of motion is

$$L_{\mathrm{LC}}(I, \dot{I}) = \frac{1}{2} C L^2 \dot{I}^2 - \tfrac{1}{2} L I^2, \tag{2.9}$$

so the conjugate momentum to generalized coordinate I is

$$p_I = \frac{\partial L_{\mathrm{LC}}}{\partial \dot{I}} = C L^2 \dot{I} = M_{\mathrm{LC}} \dot{I} \tag{2.10}$$

where $M_{\mathrm{LC}} = CL^2$ is the effective 'mass' of the circuit with current I, which actually has units of $\mathrm{kg} \cdot \mathrm{m}^2 \cdot \mathrm{s/C}$. The corresponding Hamiltonian is

$$\begin{aligned} H(I, p_I) &= \dot{I} C L^2 \dot{I} - L_{\mathrm{LC}}(I, \dot{I}) \\ &= \frac{p_i^2}{2 M_{\mathrm{LC}}} + \frac{1}{2} L I^2, \end{aligned}$$

which is completely analogous to that of a mass on a spring with current replacing position and inductance replacing spring constant.

So far our treatment of the LC circuit has been purely classical; however, this circuit can be 'quantized' by introducing a commutation relation

$$[I, p_i] = i\hbar. \tag{2.11}$$

Whether or not the circuit *should* be quantized depends on its thermal energy kT compared to the energy level spacing, $\hbar\omega_{\mathrm{LC}}$ where $\omega_{\mathrm{LC}} = (LC)^{-1/2}$. The state of an electrical circuit in the quantum limit can no longer be described by a single value for current; instead, it is better described as a wave function in the current *representation*, $\psi(I, t)$. $|\psi(I, t)|^2$ tells us the probability of finding the circuit with current I at time t upon measurement; however, before measurement, the circuit may be in a superposition of different currents, even those

going in opposite directions. The wave function $\psi(I,t)$ obeys Schrodinger's equation with the Hamiltonian derived above,

$$i\hbar\frac{d\psi(I,t)}{dt} = -\frac{\hbar^2}{2M_{\rm LC}}\frac{\partial\psi(I,t)}{\partial I^2} + \frac{1}{2}LI^2. \tag{2.12}$$

Stationary states will have energies $E_n = \hbar\omega_{\rm LC}(n+\frac{1}{2})$ for $n = 1,..,\infty$, forming a ladder of allowed energy levels $\hbar\omega_{\rm LC}$ as shown in Fig. 2.1 (b) [99].

In some cases it is more more convenient to choose the flux through the inductor $\Phi \equiv IL$ as the generalized coordinate of the circuit, in which case the charge Q on the capacitor is the generalized momentum. When quantized,

$$[\Phi, Q] = i\hbar \tag{2.13}$$

and the Hamiltonian is

$$H(\Phi,Q) \;\; = \;\; \frac{1}{2C}Q^2 + \frac{1}{2L}\Phi^2, \tag{2.14}$$

which has the same eigenstate energies as Eqn. (2.12). The wave function can be expressed in many representation, e.g. I, Φ, Q, .., depending on what is convenient.

2.1.1 The Josephson Effect

While it is certainly possible to observe an LC circuit in the quantum limit [107, 54], an LC circuit itself cannot be used a qubit. Because the energy levels are linear with n, i.e. they are equally spaced, transitions cannot be selectively driven between only two energy states of an LC circuit. This makes preparing an arbitrary superposition of exactly two energy states of an LC oscillator impossible without the assistance of a nonlinear circuit device.

Here we introduce a circuit element that, when placed in a circuit like the one described above, causes the energy levels to become unequally spaced by adding nonquadratic terms to the potential of the quantum variable of interest. This device is called a Josephson junction, based on the Josephson effect described below. In order to observe the Josephson effect we

need our circuit to be superconducting, but up until now, none of the properties described for the LC circuit in the quantum limit required superconductivity.

Here we briefly review some of the main results of superconductivity theory. Phenomenologically, a superconducting material becomes a perfect conductor exhibiting perfect diamagnetism (the Meissner effect) when cooled below its critical temperature T_{C}. In 1950, Ginzburg and Landau proposed a theory of superconductivity that successfully described these phenomenological properties by assigning to superconductors a complex-order parameter

$$\psi_{\mathrm{GL}}(\mathbf{r}) = |\psi(\mathbf{r})|e^{i\phi(\mathbf{r})}. \tag{2.15}$$

They argued based on thermodynamic considerations that this order parameter would obey a differential equation similar to Schrodinger's equation [114]. The modulus squared of the order parameter represents the local density of superconducting electrons. In 1957, the microscopic behavior of superconductors was described by the Bardeen, Cooper and Schrieffer (BCS) theory of superconductivity [7]. According to this theory, at low temperatures, electrons would become weakly attracted to each other and form 'Cooper pairs.' These pairs have Bosonic statistics and can condense into a macroscopic wave function like Eqn. (2.15), except that $|\psi_{\mathrm{BCS}}(\mathbf{r})|^2 = n_{\mathrm{C}}(\mathbf{r})$ is interpreted as the local density of Cooper pairs instead of superconducting electrons. Cooper pairs are considered the basic charge carriers in the superconductor, each having a charge of $2e$ where e is the charge of a single electron [7, 101, 114].

In 1962, Brian Josephson described the low energy dynamics of two superconductors separated by a barrier in terms of the complex phases of the two superconductor's BCS wave function. He predicted that the dynamical behavior of supercurrent through the insulating barrier would depend on the *difference* in complex phases of the two superconductors,

$$\varphi = \phi_2 - \phi_1, \tag{2.16}$$

according to what are now called the Josephson's equations:

$$I = I_0 \sin\varphi \quad \text{and} \quad V = \alpha\frac{d\varphi}{dt}.$$

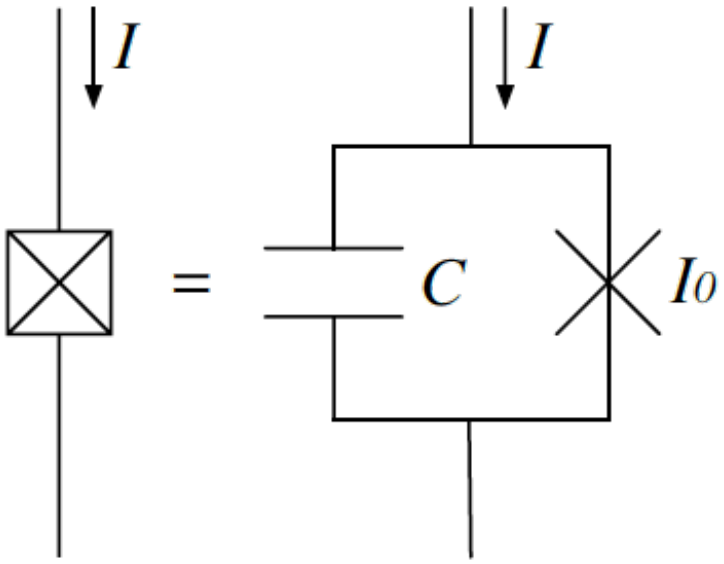

Figure 2.2: The symbol for Josephson junction with intrinsic capacitance C is box with an X inside. It is equivalent to a circuit containing in parallel a capacitor C and a circuit device marked by X that strictly obeys Josephson's equations (2.17).

I is the superconducting current through the insulating barrier, I_0 is the critical current of the system above which the tunneling effect breaks down, V is the voltage change across the barrier, and $\alpha = \hbar/2e$.

Josephson junctions are added to superconducting circuits to add nonlinearity to the circuit's energy levels. Adding a Josephson junction to a superconducting circuit not only forces the circuit to obey Josephson's equation at the junction, but also introduces an intrinsic capacitance at the junction. In circuit diagrams, a Josephson junction is often represented by an X inside a box, as shown in Fig. 2.2. This is equivalent to a circuit containing the intrinsic capacitance C of the junction in parallel to a circuit element that strictly obeys Josephson's equations, denoted by the symbol X.

Consider a 'current-biased Josephson junction' through which the current bias I is externally controlled. Some of this current, denoted $I_{\rm C}$ may pass through the effective capacitor C, and the rest of the current, denoted $I_{\rm J}$, must pass through the element obeying Josephson's equation's. These currents are controlled by the characteristic equations of the circuit elements through which they pass,

$$\begin{aligned} I_{\rm J} &= I_0 \sin\varphi \\ I_{\rm C} &= \dot{Q}_{\rm C} = C\dot{V}_{\rm C}. \end{aligned} \tag{2.17}$$

Kirchoff's laws for the circuit, $I = I_{\rm J} + I_{\rm C}$ and $V_{\rm C} = V_{\rm J}$, connect these equation giving an overall equation of motion in φ:

$$\begin{aligned} I_{\rm C} = I - I_{\rm J} = C\dot{V}_{\rm J} & \\ \Rightarrow \quad C\alpha\ddot{\varphi} + I_0 \sin\varphi - I = 0. & \end{aligned} \tag{2.18}$$

It is common to define two energy scales, one that is proportional to I_0 and describes the strength of coupling across the junction,

$$E_{\rm J} \equiv \frac{\hbar I_0}{2e}, \tag{2.19}$$

and another that gives the energy stored in the effective capacitor when charged by a Cooper pair,

$$E_{\rm c} \equiv \frac{(2e)^2}{2C} \tag{2.20}$$

(e is the charge of an electron). Written in terms of these energies and an effective 'mass' $M = \hbar^2/2E_{\rm c}$ (which actually has dimensions of mass$\times$length^2), the equations of motion for the Josephson junction are

$$M\ddot{\varphi} + E_{\rm J}\left(\sin\varphi - \frac{I}{I_0}\right) = 0. \tag{2.21}$$

The Lagrangian that gives Eq. (2.21) as its Euler-Lagrange equation of motion is

$$\begin{aligned} L_{\rm JJ} &= \frac{1}{2}M\dot{\varphi}^2 + E_{\rm J}\left(\cos(\varphi) - \frac{I}{I_0}\right) \\ &= \frac{1}{2}M\dot{\varphi}^2 - U(\varphi) \end{aligned} \tag{2.22}$$

where

$$U(\varphi) \equiv -E_{\mathrm{J}} \left(\cos\varphi + \frac{I}{I_0}\varphi \right). \tag{2.23}$$

$U(\varphi)$ is the characteristic washboard potential of a current-biased Josephson junction. The overall slope of the potential, and consequently the depth of its wells, is determined by the current bias I. The effect of applying a current I depends on the critical current of a particular Josephson junction, so we define a dimensionless bias current

$$s \equiv \frac{I}{I_0} \tag{2.24}$$

so that $U(\varphi, s)/E_{\mathrm{J}} = -(\cos(\varphi) + s\varphi)$ is independent of specific junction parameters. A plot of $U(\varphi)/E_{\mathrm{J}}$ is given in Fig. 2.3 for a particular s-value.

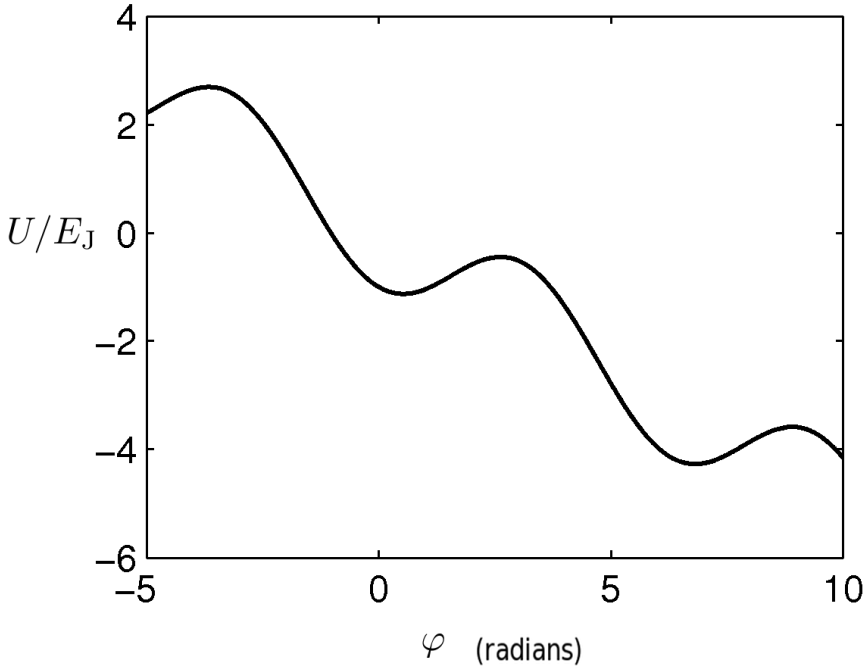

Figure 2.3: The characteristic washboard potential (over E_{J}) of a current-biased Josephson junction with $s = 0.5$.

The momentum conjugate to the generalized coordinate φ is

$$p_\varphi = \frac{\partial L_{\mathrm{JJ}}}{\partial \dot{\varphi}} = M\dot{\varphi} = \frac{\hbar Q}{2e}; \tag{2.25}$$

therefore, the Hamiltonian describing a Josephson junction is

$$\begin{aligned} H_{\mathrm{JJ}}(\varphi, p_\varphi) &= \dot{\varphi} p_\varphi - L_{\mathrm{JJ}} \\ &= \frac{p_\varphi^2}{2M} + U(\varphi). \end{aligned} \tag{2.26}$$

The Josephson junction is quantized by introducing the commutation relation,

$$[\varphi, p_\varphi] = i\hbar. \tag{2.27}$$

Note that $p_\varphi = \hbar N_{\mathrm{c}}$ where $N_{\mathrm{c}} = Q/2e$ is the number of Cooper pairs charging the junction's effective capacitor. Often the Hamiltonian is written as a function of N_{c} and φ:

$$H_{\mathrm{JJ}}(\varphi, N_{\mathrm{c}}) = E_{\mathrm{c}} N_{\mathrm{c}}^2 + U(\varphi), \tag{2.28}$$

and (2.27) becomes

$$[\varphi, N_{\mathrm{c}}] = i. \tag{2.29}$$

2.2 Superconducting Qubits

In order for a superconducting circuit to be considered a qubit, it must have two energy levels that can be prepared in an arbitrary superposition, the state of the circuit must be measurable, and the circuit must be well isolated from its environment so that it decoheres slowly.

While all of the superconducting qubits described below satisfy these basic properties, improving coherence times, state preparation and readout accuracies are all ongoing directions of research. Here the *phase*, *flux*, and *charge* qubits are defined without addressing all of these points in detail.

With knowledge of the basic Hamiltonian (2.28), the basic categories of qubits can be identified by thir relative energy scales. The phase qubit, for which φ is the localized quantum variable, is in the regime $E_{\mathrm{J}} \gg E_{\mathrm{c}}$. $E_{\mathrm{c}} \gg E_{\mathrm{J}}$ for the charge qubit, for which N_{c} is the localized quantum variable. The flux qubit, for which neither φ or N_{c} is highly localized, is in the regime $E_{\mathrm{J}} \sim E_{\mathrm{c}}$.

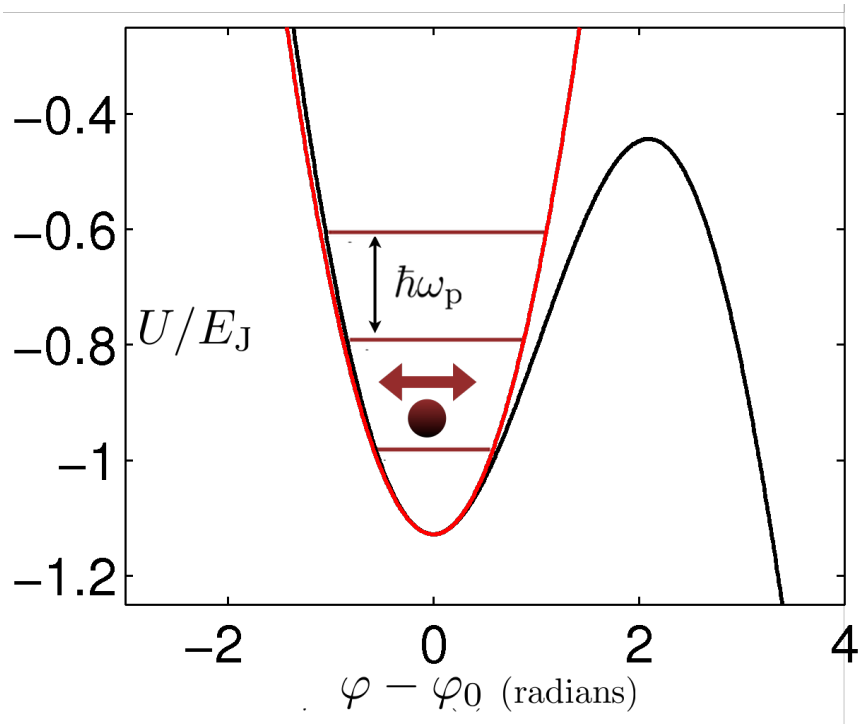

Figure 2.4: Dimensionless potential U/E_J plotted near the minima at $\varphi = \sin^{-1}(s)$ for $s = 0.5$ (black curve). In the harmonic approximation, the phase qubit potential is approximated as quadratic (red curve).

2.2.1 Josephson Phase Qubits

In the regime that $E_J \gg E_c$, quasibound states of the potential U will be stationary states of the superconducting circuit. As shown in Fig. 2.4, the wells of the washboard potential are approximately quadratic near their minimum. By solving $dU/d\varphi = 0$, one finds the minima of U are located at phase φ_0 where

$$\varphi_0 = \sin^{-1}(s). \tag{2.30}$$

The Josephson potential U shown in Fig. 2.3 is approximately quadratic in regions close to minima, as shown in Fig. 2.4, with curvature (effective spring constant)

$$\left.\frac{\partial^2 U(\varphi)}{\partial \varphi^2}\right|_{\varphi_0} = E_J \cos(\sin^{-1}(s)) = E_J(1-s^2)^{\frac{1}{2}}. \tag{2.31}$$

The energy level spacing of the phase qubit is therefore *approximately*

$$\hbar\omega_{\rm p} = \sqrt{E_{\rm J}(1-s^2)^{\frac{1}{2}} \cdot 2E_{\rm c}} = \hbar\omega_{\rm p0}(1-s^2)^{\frac{1}{4}} \tag{2.32}$$

where $\hbar\omega_{p0} = \sqrt{2E_{\rm J}E_{\rm c}}$. However, it is corrections to this harmonic approximation of order $\sim \varphi^4$ and higher that allow the individual levels of the phase qubit to be addressed spectroscopically. Quasibound states trapped in the well become more closely spaced the larger their excitation energy above the ground state. The qubit states $|0\rangle$ and $|1\rangle$ are defined to be the two quasibound states lowest in energy.

It was in a current-biased Josephson junction that quantized energy levels for a macroscopic variable were first observed in the research group of John Clarke at UC Berkeley in 1985 [80, 26]. In 2002, the group of John Martinis began to explore the suitability of a current-biased Josephson junction as a superconducting qubit by demonstrating Rabi oscillations between the $|0\rangle$ and $|1\rangle$ state of what would become the phase qubit [81]. Shortly after, it was shown that the phase qubit could be prepare in an arbitrary superposition of the $|0\rangle$ and $|1\rangle$ state [112]. Decoherence [103, 61, 91], measurement [57, 58], and state preparation [73] are all actively researched and continuously improved for phase qubits.

2.2.2 Charge Qubits

In the regime that $E_{\rm c} \gg E_{\rm J}$, the number $N_{\rm c}$ of Cooper pairs charging the Josephson junction is well determined, while the phase φ across the superconductors experiences large fluctuations. Note that $E_{\rm c}$ is inversely proportional to C and $E_{\rm J}$ is proportional to I_0, so this limit can be obtained by having a small junction so that both I_0 and C are very small. This is often achieved by separating a small 'Cooper-pair box' or 'island' from the rest of the circuit. A charge qubit is normally voltage-biased, not current-biased like the phase qubit, as shown by the circuit in Fig. 2.5. It is typically constructed from a small Cooper pair island separated by two Josephson junctions from a larger superconducting reservoir. The beige material forms electrodes that are used to produce a gate voltage $V_{\rm g}$ across the junction.

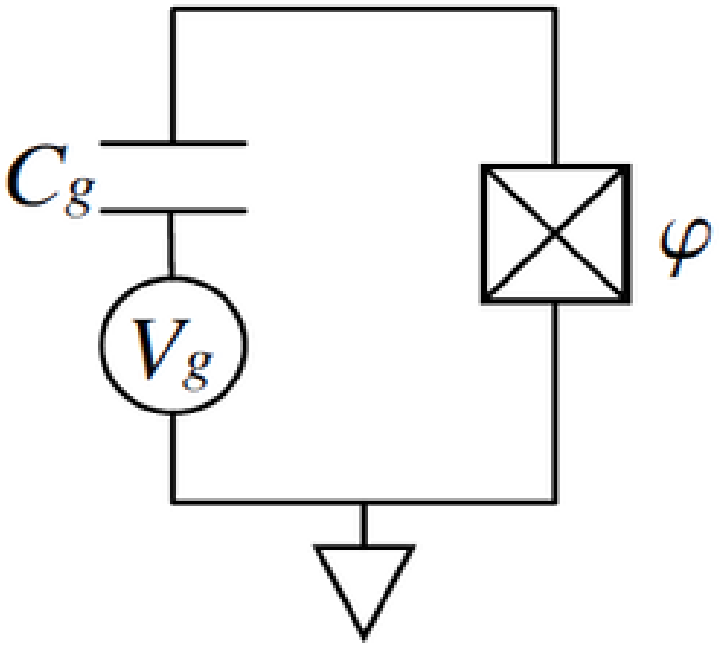

Figure 2.5: A circuit equivalent to a superconducting charge qubit.

The equation of motion for the charge qubit is the same as for the current-biased Josephson junction derived above, except that the current into the qubit I is not controlled directly. This current, which passes over the capacitor $C_{\rm g}$, is controlled indirectly by the gate voltage $V_{\rm g}$:

$$\begin{aligned} I &= \dot{Q}_{\rm g} = C_{\rm g}\frac{d}{dt}\left(V_{\rm g} - \alpha\dot{\varphi}\right) \\ &= C_{\rm g}\dot{V}_{\rm g} - \alpha C_{\rm g}\ddot{\varphi} \end{aligned} \tag{2.33}$$

Combing this with Eqn. (2.18), the equation of motion for the charge qubit is

$$\alpha^2(C + C_{\rm g})\ddot{\varphi} + I_0 \sin\varphi = C_{\rm g}\dot{V}_{\rm g}, \tag{2.34}$$

which corresponds to Lagrangian

$$L_{CQ} = \frac{1}{2}\alpha^2(C + C_{\rm g})\dot{\varphi}^2 + E_{\rm J}\cos\varphi - \alpha C_{\rm g}V_{\rm g}\dot{\varphi}. \tag{2.35}$$

The conjugate momentum to the generalized coordinate φ is

$$\begin{aligned}\frac{\partial L_{\mathrm{CQ}}}{\partial \dot{\varphi}} = p_{\varphi} &= \alpha^2 (C + C_{\mathrm{g}})\dot{\varphi} - \alpha C_{\mathrm{g}} V_{\mathrm{g}} \\ &= \alpha \left[CV - C_{\mathrm{g}}(V_{\mathrm{g}} - V) \right] \\ &= \frac{\hbar}{2e} \left[Q - Q_{\mathrm{g}} \right] \\ &\equiv \hbar N_{\mathrm{I}} \end{aligned} \tag{2.36}$$

where N_{I} is defined as the total number of Cooper pairs on the island, the portion of the circuit between the Josephson junction and C_{g}. The Hamiltonian describing a charge qubit is typically written as

$$H(\varphi, N) = E_{\mathrm{c}} \left(N_{\mathrm{I}} - N_{\mathrm{g}} \right)^2 - E_{\mathrm{J}} \cos \varphi \tag{2.37}$$

where $E_{\mathrm{c}} = (2e)^2/2(C + C_{\mathrm{g}})$ and $N_{\mathrm{g}} = C_{\mathrm{g}} V_{\mathrm{g}}/(2e)$. The charge qubit is quantized by introducing

$$[\varphi, N_{\mathrm{I}}] = i. \tag{2.38}$$

Macroscopic quantum states were first shown spectroscopically in a charge qubit in 1997 by Nakamura *et al.* [86]. The charge qubit was the first superconducting circuits considered as a *qubit* in 1999 when Rabi oscillations were driven between the state where no excess Cooper pair are on the island, labeled $|0\rangle$, and the state where one excess pair is on the island, labeled $|1\rangle$ [87]. Decoherence [6, 88, 31], measurement [37], and state preparation [20] are all actively researched and continuously improved for charge qubits. Researchers at Yale University have implemented a charge qubit that is remarkably immune to decoherence which they refer to as the *transmon* qubit [63, 100, 51, 52].

2.2.3 Flux Qubits

If a superconducting circuit containing one or more Josephson junctions is closed, the magnetic flux through the superconducting loop becomes quantized to maintain the single-valuedness of the superconducting wave function. *Flux qubits* are formed from superpositions of persistent currents in the clockwise and counterclockwise directions. Typicallly, flux

qubits are in the regime that the charging energy E_{C} and Josephson Energy E_{J} are of similar magnitude,

$$E_{\mathrm{J}}/E_{\mathrm{c}} \sim 1 - 10^3. \tag{2.39}$$

A diagram of a simple flux qubit containing only one Josephson junction is shown in Fig. 2.6 (a), which can be compared to the SEM of a flux qubit with four junctions in Fig. 2.2 (a) coupled to a RF-SQUID, which is also superconducting loop with two larger Josephson junctions.

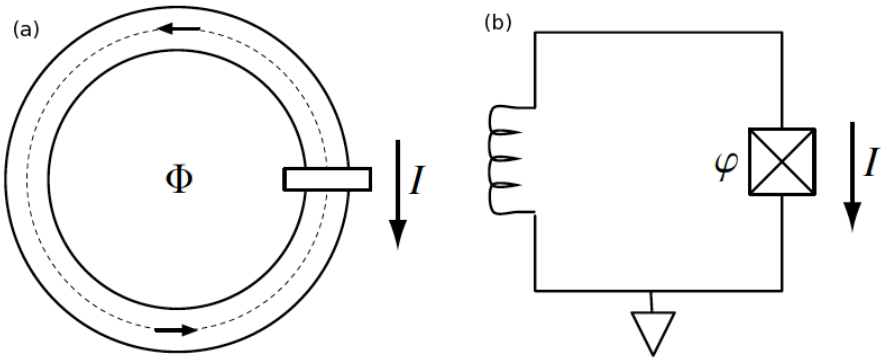

Figure 2.6: (a) A cartoon of a superconducting loop broken by one Josephson junction. (b) An equivalent circuit.

A superconducting loop without a direct current source or potential change can be controlled by applying flux through the loop. A loop with steady current I has a self-induced flux $\Phi_{\mathrm{ind}} = cIL$ opposed to that of the applied flux Φ_{ext} so that the total flux through the superconducting loop is

$$\Phi(t) = \Phi_{\mathrm{ext}} - \Phi_{\mathrm{ind}} \tag{2.40}$$

The current through the inductor I_{L} will obey the characteristic equation $V_{\mathrm{L}} = L\frac{dI}{dt}$, but with only one Josephson junction in the loop, $V_{\mathrm{L}} = V = \alpha\dot{\varphi}$, so

$$\begin{aligned} I_{\mathrm{L}} &= \frac{1}{L}\int_{-\infty}^{t} V(t)dt \\ &= \frac{\alpha}{L}\int_{-\infty}^{t} d\varphi \\ &= \frac{\alpha}{L}\varphi(t) \end{aligned} \tag{2.41}$$

where $\varphi(-\infty)$ is assumed to be zero. When passing through the Josephson junction, current from the inductor will branch into a current passing over the capacitor I_{C} and a current governed by Josephson's equation I. This gives the equation of motion

$$\begin{aligned} I_{\mathrm{L}} &= I_{\mathrm{C}} + I \\ &\Rightarrow \quad C\alpha\ddot{\varphi} + I_0 \sin\varphi - c\frac{\alpha}{L}\varphi = 0 \end{aligned} \tag{2.42}$$

There is a relationship between the phase variable φ and the total flux through the loop,

$$\frac{\Phi}{\Phi_0} = \frac{\varphi}{2\pi} \mod 1, \tag{2.43}$$

that is a consequence of the order parameter of the superconducting loop being single-valued.

$$\Phi_0 \equiv \frac{h}{2e} \tag{2.44}$$

is the fundamental quanta of magnetic flux. Using Eqn. (2.43) to express φ in terms of the externally applied flux $\Phi_{\mathrm{ext}} = \Phi - \Phi_{\mathrm{ind}}$, the Lagrangian producing equation of motion in Eq. (2.42) is

$$L_{\mathrm{FQ}} = \frac{1}{2}\alpha^2 C\dot{\varphi}^2 + E_{\mathrm{J}}\cos\varphi - \frac{\hbar^2\omega_{\mathrm{LC}}^2}{4E_{\mathrm{C}}}\left(\varphi - \frac{2\pi\Phi_{\mathrm{ext}}}{\Phi_0}\right)^2. \tag{2.45}$$

The generalized coordinate φ has conjugate momentum $p_\varphi = Q$, the charge on C, like the flux of an LC circuit. However, the Hamiltonian of a flux qubit has a more complicated potential than the LC circuit:

$$H = E_{\mathrm{c}}N^2 - E_{\mathrm{J}}\cos\varphi + \frac{\hbar\omega_{\mathrm{LC}}^2}{4E_{\mathrm{c}}}\left(\varphi - \frac{2\pi\Phi_{\mathrm{ext}}}{\Phi_0}\right)^2 \tag{2.46}$$

Macroscopic persistent-current states were first demonstrated experimentally in 2000 by van der Wal *et al.* [116] and Friedman *et al.* [34]. Decoherence [10] and measurement [43] are actively researched for flux qubits. It should be noted that modern phase qubits are actually a hybrid of the flux qubit and the original current-biased phase qubit described above. While still in the regime that φ is localized and $E_{\mathrm{J}} \sim 10^4 E_{\mathrm{c}}$, phase qubits are now fabricated in loops with large inductances where the persistent current is controlled inductively. This makes

Hamiltonian (2.46) the appropriate description of the modern phase qubit, the distinguishing factor between the phase and flux qubit being their relative energy scales [112, 103, 61, 91, 57, 58, 73].

Chapter 3

Coupling Superconducting Qubits

All of the superconducting circuits surveyed in the last chapter exhibit robust macroscopic quantum behavior and externally controllability that make them good candidates for quantum bits. However, the most attractive feature of superconducting qubits will be discussed in this chapter: namely, the ease with which superconducting qubits are coupled together in a larger circuit to form a *scalable* quantum computer.

In the first two sections of this chapter, we describe how superconducting qubits can be coupled together using a fixed capacitor. This successful method of coupling superconducting qubits was the first to be realized experimentally. We derive the Hamiltonian for capacitively coupled phase qubits, followed by the Hamiltonian for capacitively coupled charge qubits.

While straightforward to describe mathematically and implement experimentally, fixed capacitive coupling has the disadvantage that it can never be turned off. This produces errors during portions of a quantum computation when entanglement is undesirable, such as state preparation and read out. One approach to this problem is to separate the qubits by adding an intermediate circuit element. The additional circuit element may be an LC oscillator, a mechanical resonator, or a another superconducting circuit containing a Josephson junction. In the third section we discuss how qubits can couple to an LC oscillator.

Not only does an intermediate resonator turn off the interaction between qubits more effectively, but resonators may be used in tandem with the qubits as memory devices. Resonators are typically more stable and less affected by environmental interaction than qubits. Furthermore, there is a whole direction of experimental research whereby people explore the quantum properties of resonators using coupled Josephson junction to aid in state storage

and preparation. In the following chapter, which is a stand alone journal article, nanomechanical resonators coupled to superconducting qubits are studied as memory (state storage) devices.

Throughout this chapter we build on the mathematical framework developed in the last chapter to accurately model the Hamiltonians of systems with multiple qubits coupled together. For each coupled superconducting circuit that is considered, the equation of motion and Hamiltonians are derived.

3.1 Capacitive Coupling

The most experimentally tested method of coupling two superconducting qubits involves placing a fixed capacitor in a circuit branch connecting the two qubits. In the next section we discuss the circuit design for such a two qubit system in detail, and compare it to similar models in following sections.

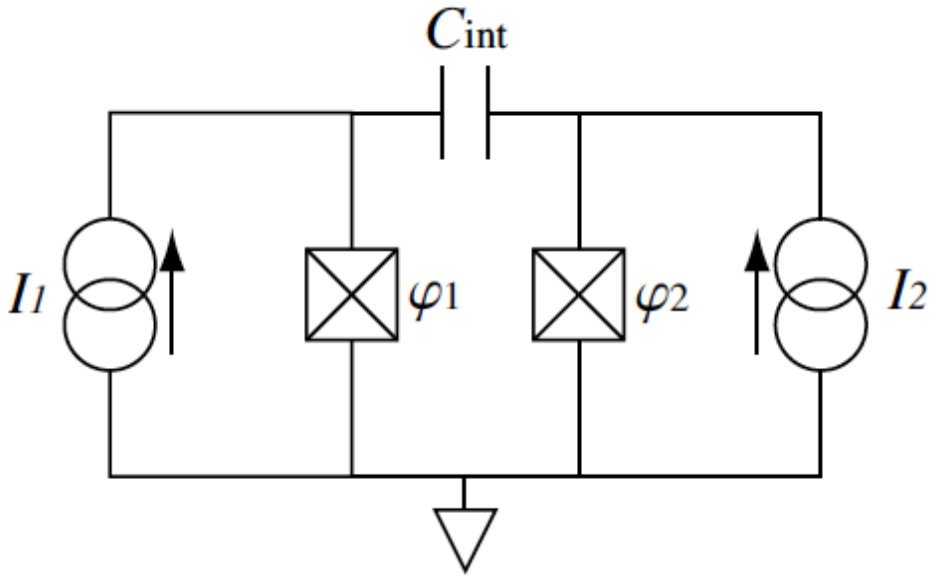

Figure 3.1: A circuit model describing the capacitively coupled phase qubits.

3.1.1 Capacitively Coupled Phase Qubits

Two phase qubits coupled capacitively as in Fig. 3.1 are controlled independently by external current sources I_1 and I_2. The equations of motions for each of the qubits are the same as in Eqn. (2.21) except that the current passing through the ith junction is no longer just the external bias current I_i, but also has a contribution from the connecting branch with coupling capacitor $C_{\rm int}$. Assuming that the current $I_{\rm int}$ flows from right to left across $C_{\rm int}$, the equations of motion for the qubit on the left are:

$$\begin{aligned} I_1 + I_{\rm int} &= I_{\rm C} + I_J \\ \Rightarrow I_1 + \dot{Q}_{\rm int} &= \dot{Q}_{\rm C_1} + I_0^{(1)} \sin\varphi \\ \Rightarrow I_1 + C_{\rm int}\dot{V}_{\rm int} &= C_1\dot{V}_1 + I_0^{(1)} \sin\varphi \\ \Rightarrow 0 &= \alpha^2(C_1 + C_{\rm int})\ddot{\varphi}_1 + E_{\rm J}^{(1)}(\sin\varphi_1 - s_1) - \alpha^2 C_{\rm int}\ddot{\varphi}_2 \end{aligned} \tag{3.1}$$

where $V_{\rm int} = V_2 - V_1$. Similarly,

$$\alpha^2(C_2 + C_{\rm int})\ddot{\varphi}_2 + E_{\rm J}^{(1)}(\sin\varphi_2 - s_2) - \alpha^2 C_{\rm int}\ddot{\varphi}_1 = 0. \tag{3.2}$$

The corresponding two qubit Lagrangian is

$$L_{CCPQ}(\varphi_1, \dot{\varphi}_1, \varphi_2, \dot{\varphi}_2) = \sum_i \left[\frac{\alpha^2}{2}(C_i + C_{\rm int})\dot{\varphi}_i^2 + E_{\rm J}^{(i)}\left(\cos\varphi_i + s_i\varphi_i\right)\right] - \alpha^2 C_{\rm int}\dot{\varphi}_1\dot{\varphi}_2. \tag{3.3}$$

The conjugate momentum to the generalized coordinate φ_1 is

$$\begin{aligned} p_{\varphi_1} &= \alpha^2 C_1\dot{\varphi}_1 + \alpha^2 C_{\rm int}(\dot{\varphi}_1 - \dot{\varphi}_2) \\ &= \alpha(Q - Q_{\rm int}) \\ &\equiv \hbar N_{I1} \end{aligned} \tag{3.4}$$

where N_{I1} is the number of excess Cooper pairs charging the 'island' between the junction on the left and the coupling capacitor. Similarly,

$$p_{\varphi_2} = \hbar(Q_2 + Q_{\rm int}) \equiv \hbar N_{I2} \tag{3.5}$$

where N_{I2} is the number of excess Cooper pairs charging the 'island' between the second junction and the coupling capacitor. Because the momenta p_{φ_1} and p_{φ_2} mix the generalized coordinates φ_1 and φ_2, it is not obvious how to write the Hamiltonian

$$\begin{aligned} H(\varphi_1, p_{\varphi_1}, \varphi_2, p_{\varphi_2}) &= \dot{\varphi}_1 p_{\varphi_1} + \dot{\varphi}_2 p_{\varphi_2} - L(\varphi_1, \dot{\varphi}_1, \varphi_2, \dot{\varphi}_2) \\ &= \frac{1}{2}\alpha^2 C_1 \dot{\varphi_1}^2 + \frac{1}{2}\alpha^2 C_2 \dot{\varphi}_2^2 + \alpha^2 C_{\rm int}(\dot{\varphi}_1^2 - 2\dot{\varphi}_1\dot{\varphi}_2 + \dot{\varphi}_2^2) \\ &\quad -E_{\rm J}^{(1)}(\cos\varphi_1 + s_1\varphi_1) - E_{\rm J}^{(2)}(\cos\varphi_2 + s_2\varphi_2) \end{aligned} \tag{3.6}$$

explicitly in terms of p_{φ_1} and p_{φ_2}. Note that $\vec{p}/\alpha^2 = \hat{C}\cdot\vec{\dot{\varphi}}$ where

$$\vec{p} \equiv \begin{pmatrix} p_{\varphi_1} \\ p_{\varphi_2} \end{pmatrix},\ \hat{C} \equiv \begin{pmatrix} C_1 + C_{\rm int} & -C_{\rm int} \\ -C_{\rm int} & C_2 + C_{\rm int} \end{pmatrix},\ \text{and } \vec{\dot{\varphi}} \equiv \begin{pmatrix} \dot{\varphi}_1 \\ \dot{\varphi}_2 \end{pmatrix}. \tag{3.7}$$

By inverting $\hat{C}$ we can express the velocites $\dot{\varphi}_i$ in terms of the generalized momenta p_{φ_i}:

$$\begin{pmatrix} \dot{\varphi}_1 \\ \dot{\varphi}_2 \end{pmatrix} = \hat{C}^{-1}\cdot\vec{p} = \begin{pmatrix} (C_2 + C_{\rm int})p_{\varphi_1} + C_{\rm int}p_{\varphi_2} \\ (C_1 + C_{\rm int})p_{\varphi_2} + C_{\rm int}p_{\varphi_1} \end{pmatrix} /\alpha^2.(C_1C_2 + C_{\rm int}(C_1 + C_2)). \tag{3.8}$$

After some algebra we find,

$$\begin{aligned} H(\varphi_1, p_{\varphi_1}, \varphi_2, p_{\varphi_2}) = \frac{p_{\varphi_1}^2}{2\alpha^2\tilde{C}_1} &- E_{\rm J}^{(1)}(\cos\varphi_1 + s_1\varphi_1) \\ &+ \frac{p_{\varphi_2}^2}{2\alpha^2\tilde{C}_2} - E_{\rm J}^{(2)}(\cos\varphi_2 + s_2\varphi_2) + \frac{p_{\varphi_1}p_{\varphi_2}}{\alpha^2\tilde{C}_{\rm int}}. \end{aligned} \tag{3.9}$$

where

$$\begin{aligned} \tilde{C}_1 &\equiv C_1 + (C_{\rm int}^{-1} + C_2^{-1})^{-1} \\ \tilde{C}_2 &\equiv C_2 + (C_{\rm int}^{-1} + C_1^{-1})^{-1} \\ \tilde{C}_{\rm int} &\equiv C_1C_2(C_1^{-1} + C_2^{-1} + C_{\rm int}^{-1})^{-1}. \end{aligned} \tag{3.10}$$

The two-qubit Hamiltonian is quantized by introducing the commutation relations

$$\begin{aligned} [\varphi_1, N_{I1}] &= i \\ [\varphi_2, N_{I2}] &= i. \end{aligned} \tag{3.11}$$

Capacitively coupled phase qubits were one of the first two-qubit superconducting circuits considered, both theoretically [13, 55, 113] and experimentally [9, 82, 111, 124]. Moreover, the two-qubit Hamiltonian (3.9) is easily scalable to an n-qubit Hamiltonian. Each qubit contributes to the Hamiltonian a kinetic and potential energy term uncoupled to the other qubits,

$$H_0^{(i)} = \frac{p_{\varphi_i}^2}{2\alpha^2 \tilde{C}_i} - E_{\mathrm{J}}^{(i)}(\cos\varphi_i + s_i\varphi_i), \tag{3.12}$$

and every pair of qubits that is interacting via a fixed capacitive coupling contributes an interaction term to the Hamiltonian of the form

$$H_{\mathrm{int}}^{(ij)} = \frac{p_{\varphi_i} p_{\varphi_j}}{\alpha^2 \tilde{C}_{\mathrm{int}}^{ij}}. \tag{3.13}$$

For example, in a recent experiment [89], maximally entangled GHZ states were created between three of the four superconducting phase qubits on a chip. Each qubit couples capacitively to each other qubit. The total Hamiltonian is modeled as $H_{4\mathrm{Q}} = H_0 + H_{\mathrm{int}}$ where

$$\begin{aligned} H_0 &= \sum_{i=1}^{4} H_0^{(i)} \\ H_{\mathrm{int}} &= \frac{1}{2}\sum_{i=1}^{4}\sum_{j=1}^{4} H_{\mathrm{int}}^{(ij)} \end{aligned} \tag{3.14}$$

and the factor of $1/2$ in the interaction Hamiltonian prevents double counting.

3.1.2 Capacitively Coupled Charge Qubits

In this section the Hamiltonian is derived for two capacitively coupled charge qubits. The circuit description of this system is given in Fig. 3.2.

Each of the charge qubits are controlled independently by gate voltages V_{g1} and V_{g2}, and there are two independent generalized coordinates φ_1 and φ_2. The equations of motion are like that of a single charge qubit, the current modified by a small addition from the coupling capacitor:

$$\begin{aligned} \alpha^2(C_1 + C_{\mathrm{g1}} + C_{\mathrm{int}})\ddot{\varphi}_1 + E_{\mathrm{J}}^{(1)}\sin\varphi_1 - \alpha^2 C_{\mathrm{int}}\ddot{\varphi}_2 - \alpha C_{\mathrm{g1}}\dot{V}_{\mathrm{g1}} = 0 \\ \alpha^2(C_2 + C_{\mathrm{g2}} + C_{\mathrm{int}})\ddot{\varphi}_2 + E_{\mathrm{J}}^{(2)}\sin\varphi_2 - \alpha^2 C_{\mathrm{int}}\ddot{\varphi}_1 - \alpha C_{\mathrm{g2}}\dot{V}_{\mathrm{g2}} = 0. \end{aligned} \tag{3.15}$$

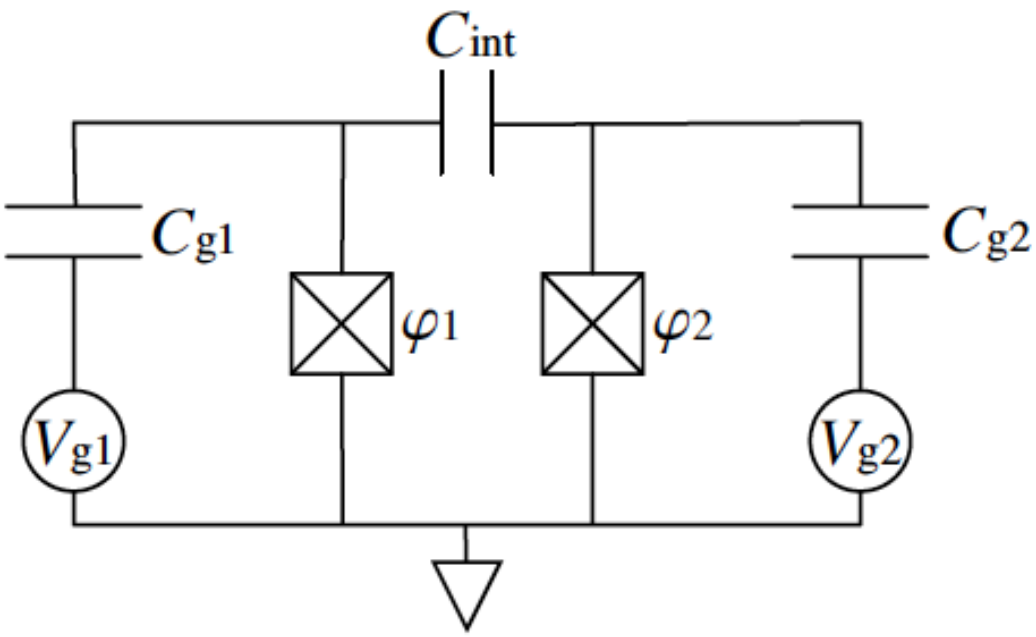

Figure 3.2: A circuit description of capacitively coupled phase qubits.

.

The corresponding Lagrangian is

$$\begin{aligned} L(\varphi_1, \dot{\varphi}_1, \varphi_2, \dot{\varphi}_2) &= \frac{\alpha^2}{2}\left(C_1 + C_{\rm g1} + C_{\rm int}\right)\dot{\varphi}_1^2 + \frac{\alpha^2}{2}\left(C_2 + C_{\rm g2} + C_{\rm int}\right)\dot{\varphi}_2^2 + E_{\rm J}^{(1)}\cos\varphi_1 + E_{\rm J}^{(2)}\cos\varphi_2 \\ &- \alpha C_{\rm g1} V_{\rm g1}\dot{\varphi}_1 - \alpha C_{\rm g2} V_{\rm g2}\dot{\varphi}_2 - \alpha^2 C_{\rm int}\dot{\varphi}_1\dot{\varphi}_2, \end{aligned} \tag{3.16}$$

and the phase variables φ_1 and φ_2 have conjugate momenta

$$\Pi_1 = p_{\varphi_1} + \alpha C_{\rm g1} V_{\rm g1}$$

$$\Pi_2 = p_{\varphi_2} + \alpha C_{\rm g2} V_{\rm g2}$$

where p_{φ_1} and p_{φ_2} are the conjugate momenta of capacitively coupled phase qubits in Eqn. (3.4). Following the same analysis that was applied to phase qubits, the Hamiltonian of two capacitively coupled charge qubits can be written as

$$H = \frac{\Pi_1^2}{2\alpha^2\tilde{C}_1} + \frac{\Pi_2^2}{2\alpha^2\tilde{C}_2} - E_{\rm J}^{(1)}\cos\varphi_1 - E_{\rm J}^{(2)}\cos\varphi_2 + \frac{\Pi_1\Pi_2}{\alpha^2\tilde{C}_{\rm int}} \tag{3.17}$$

where

$$\begin{aligned}
\tilde{C}_1 &\equiv C_1 + C_{\rm g1} + \left[C_{\rm int}^{(-1)} + (C_2 + C_{\rm g2})^{(-1)}\right]^{(-1)} \\
\tilde{C}_2 &\equiv C_2 + C_{\rm g2} + \left[C_{\rm int}^{(-1)} + (C_1 + C_{\rm g1})^{(-1)}\right]^{(-1)} \\
\tilde{C}_{\rm int} &\equiv C_1 + C_{\rm g1} + C_2 + C_{\rm g2} + (C_1 + C_{\rm g1})(C_2 + C_{\rm g2})C_{\rm int}^{-1}.
\end{aligned} \tag{3.18}$$

The first superconducting qubit coupling scheme to be successfully implemented experimentally was that of two charge qubits coupled capacitively [92, 125].

3.2 Coupling Qubits to Resonators

Coupling qubits to resonators has become a popular way to build a scalable superconducting quantum computer [74, 107, 54, 3, 50, 49, 120, 102, 119, 77, 105, 76, 84, 126, 127, 13, 96, 131, 18, 12, 96, 119, 23, 39, 133, 78, 132, 94]. In this section, the Hamiltonian is derived for a phase qubit coupled to an intermediate superconducting LC circuit, as shown in Fig. 3.3, using the techniques developed in this and the previous chapter. In the following section, several other qubit-resonator models are surveyed, with emphasis on the phase qubit coupled to a NEMS resonator model of Refs.[39, 23] that will be used in the following chapter.

3.2.1 A Phase Qubit Coupled to an LC circuit

Here we derive the Hamiltonian of the circuit in Fig. 3.3. The generalized coordinate of the Josephson junction is φ while we take the generalized coordinate for the LC circuit to be $\Phi = I_{\rm res}L_{\rm res}$. The equation of motion for φ will be a slight modification of Eqn. (3.1):

$$\alpha^2(C + C_{\rm int})\ddot{\varphi}_1 + E_{\rm J}^{(1)}(\sin\varphi - s) - \alpha^2 C_{\rm int}\ddot{\Phi} = 0. \tag{3.19}$$

The equation of motion for the LC oscillator is

$$\alpha(C_{\rm res} + C_{\rm int})\ddot{\Phi} + \frac{\alpha}{L_{\rm res}}\Phi - \alpha C_{\rm int}\ddot{\varphi} = 0. \tag{3.20}$$

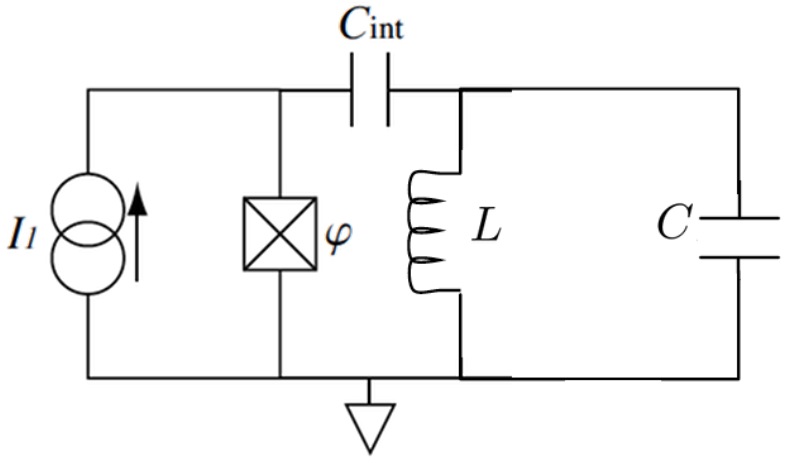

Figure 3.3: A circuit description of a phase qubit coupled capacitively to an LC-circuit
.

The Lagrangian giving these equations of motion is

$$\begin{aligned} L(\varphi,\dot{\varphi},\Phi,\dot{\Phi}) &= \frac{\alpha^2}{2}(C+C_{\text{int}})\dot{\varphi}^2 + E_{\text{J}}(\cos\varphi + s\varphi) \\ &+ \frac{\alpha^2}{2}(C_{\text{res}}+C_{\text{int}})\dot{\Phi}^2 - \frac{\alpha^2}{2L_{\text{res}}}\Phi^2 - \alpha^2 C_{\text{int}}\dot{\Phi}\dot{\varphi}, \end{aligned} \tag{3.21}$$

therefore the canonical momenta are

$$\begin{aligned} p_\varphi &= \alpha^2(C+C_{\text{int}})\dot{\varphi} - \alpha^2 C_{\text{int}}\dot{\Phi} \\ p_\Phi &= \alpha^2(C_{\text{res}}+C_{\text{int}})\dot{\Phi} - \alpha^2 C_{\text{int}}\dot{\varphi} \end{aligned} \tag{3.22}$$

$$\tag{3.23}$$

Following the procedure for capacitively coupled phase qubits,

$$\begin{aligned} H(\varphi,p_\varphi,\Phi,p_\Phi) &= \frac{p_\varphi^2}{2\alpha^2\tilde{C}} - E_{\text{J}}(\cos\varphi + s\varphi) \\ &+ \frac{p_\Phi^2}{2\alpha^2\tilde{C}_{\text{res}}} + \frac{\alpha^2\dot{\Phi}^2}{2L_{\text{res}}} + \frac{p_\varphi p_\Phi}{\alpha^2\tilde{C}_{\text{int}}}, \end{aligned} \tag{3.24}$$

where

$$\begin{aligned} \tilde{C} &\equiv C + (C_{\rm int}^{-1} + C_{\rm res}^{-1})^{-1} \\ \tilde{C}_{\rm res} &\equiv C_{\rm res} + (C_{\rm int}^{-1} + C^{-1})^{-1} \\ \tilde{C}_{\rm int} &\equiv C C_{\rm res} (C^{-1} + C_{\rm res}^{-1} + C_{\rm int}^{-1})^{-1}. \end{aligned} \tag{3.25}$$

An experiment at NIST in Boulder in the group of Raymond Simmonds has shown that energy quanta can be transferred between two phase qubits coupled via an intermediate LC oscillator [107]. A similar experiment has also been performed in a quantum circuit containing a flux qubit and an LC oscillator [54].

3.2.2 Other Qubit-Resonator Models

Recall that the Hamiltonian of a resonator in the quantum limit with energies $E_n = \hbar\omega_{\rm res}(n + \frac{1}{2})$ can be written as

$$H_{\rm res} = \hbar\omega_{\rm res} a^\dagger a \tag{3.26}$$

where a and $a^\dagger$ are creation and annihilation operators of the resonator's energy quanta (phonons for a mechanical resonator, photons for a transmission line). This second quantization notation is more natural to describe resonators other than the LC oscillator. To transform between the notations, recall that the quantum variable and coordinate of the oscillator can be written as

$$\begin{aligned} q &= \sqrt{\frac{\hbar}{2 m_{\rm res}\omega_{\rm res}}}(a^\dagger + a) \\ p_q &= i\sqrt{\frac{\hbar m_{\rm res}\omega_{\rm res}}{2}}(a^\dagger - a) \end{aligned} \tag{3.27}$$

where $m_{\rm res}$ is its effective mass.

In all three of the examples given in this chapter so far, the final coupling between qubits, or qubit and resonator, has been very similar. In particular, it is of the form 'momentum-momentum', where the exact form of the momentum depends on the system that is being considered.

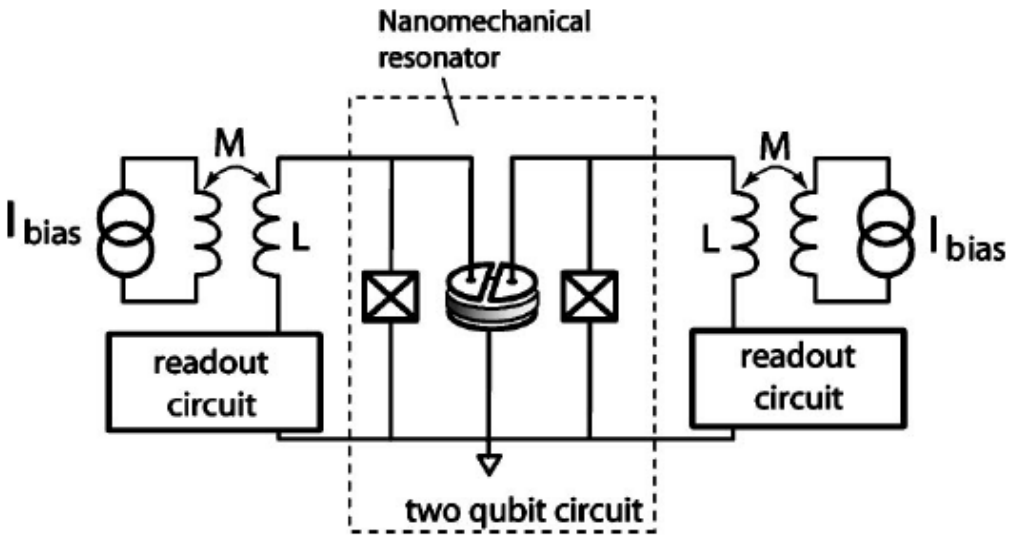

Figure 3.4: A circuit description of two charge qubits coupled capacitively, from Ref. [39]
.

In the following chapter, we consider a qubit-resonator model whereby a superconducting phase qubit is coupled capacitively to a high-Q nanoelectromechanical (NEMS) resonator. This architecture, first proposed by Michael Geller and Andrew Cleland in Refs. [39, 23], is shown in the circuit diagram of Fig. 3.4. The resonator should be made of a piezoelectric material, such as AlN, so that its mechanical oscillations produce an oscillating electric field that can couple to the current of capacitively coupled Josephson junctions. The Hamiltonian derived from Refs. [39, 23] to describe a single resonator coupled to n phase qubits is

$$H = \sum_{i=1}^{n} H_0^{(i)} + \hbar\omega_{\rm res} a^\dagger a - ig(a - a^\dagger) \sum_{i=1}^{n} \varphi_i \tag{3.28}$$

where $H_0^{(i)}$ is the uncoupled phase qubit Hamiltonian given above and g is a coupling constant of dimensions of energy that depends on the fabrication of the resonator and the coupling circuit. This interaction Hamiltonian is seemingly different from those derived earlier, in particular, it is of the form 'momentum-position,' and it is not symmetric with respect to

circuit devices. It is for these types of variations in superconducting circuits that we derive a more general model of interaction in Ch. 5 and implement quantum logic in Ch. 6.

Several experimental demonstrations of the usefulness of coupling phase qubits to resonators have come from the combined efforts of John Martinis and Andrew Cleland at UCSB. Bell's inequality was violated for entangled superconducting phase qubits separated by a stripline resonator [3], which can be modeled as a quantum harmonic oscillator with photonic excitations. Phase qubits have been used to prepare pure photon Fock states [50], arbitrary superpositions of Fock states [49], and study the decoherence of photons [120]. Using the qubit-resonator model, oscillations between phase qubits and microscopic spurious resonances in their Josephson junction tunnel junction materials have been measured [24].

At Yale University, the experimental groups of Rob Schoelkopf and Michele Deverot, consider charge qubits coupled to microwave transmission lines. They have demonstrated coherent coupling between the qubit and resonator [74], strong coupling of single photons to charge qubits [119], and also prepared photon fock states in the resonator [102].

Chapter 4

QUANTUM MEMORY FOR SUPERCONDUCTING QUBITS

[0] Pritchett, E. J. and M. R. Geller, *Physical Review A* **72**, 010301(R), 2010.] Copyrighted material reprinted here with permission of publisher.

4.1 Introduction

The macroscopic quantum properties of superconductors make Josephson junctions strong candidates for large-scale quantum information processing [77]. Several proposed architectures involve coupling Josephson-junction (JJ) flux, phase, or charge qubits together with LC resonators [77, 105, 76, 84, 126, 127, 13, 96, 131], superconducting cavities [18, 12, 96, 119], mechanical resonators [23, 39, 133], or other types of oscillators [78, 132, 94]. Such resonator-based coupling schemes have the advantage of additional functionality resulting from the ability to tune the qubits relative to the resonator frequency, as well as to each other. Although the lowest pair of levels in a harmonic oscillator cannot be frequency selected by an external driving field, resonators are quite desirable as coupling elements because of their potential for having extremely high quality factors.

In JJ-resonator architectures, the resonators store qubits states, transfer states from one JJ to another, entangle two or more JJs, and mediate two-qubit quantum logic. In this paper we discuss the speed and accuracy with which a qubit state can be stored in a resonator and later retrieved, which depends on both the JJ-resonator coupling strength and the location of the state on the Bloch sphere. The specific architecture we consider is a large-area, current-biased JJ phase qubit coupled to a nanoelectromechanical resonator [23, 39]. The Hamiltonian is similar to that of a tunable few-level atom in a single-mode electromagnetic cavity, and many of our results will apply to other qubit-oscillator models. However, the precise tradeoff between memory speed and fidelity depends on the detailed form of the JJ-resonator interaction Hamiltonian, which varies from architecture to architecture.

Transfer of simple qubit states from a JJ to a weakly coupled resonator has been considered previously in Refs. [23, 39]. Here we study a complete memory operation, where the qubit is stored in the resonator and then transferred back to the JJ, for a large range of JJ-resonator coupling strengths and for a variety of qubit states. Furthermore, we show that a dramatic improvement in memory performance can be obtained by a numerical optimization procedure where the resonant interaction times and off-resonant detunings are varied to max-

imize the overall gate fidelity. This allows larger JJ-resonator couplings to be used, leading to faster gates and therefore more operations carried out within the available coherence time. Our results suggest that it should be possible to demonstrate a fast quantum memory using existing superconducting circuits, which would be a significant accomplishment in solid-state quantum computation.

In addition to its relevance for quantum information processing, our paper builds on recent interesting proposals to entangle a nanomechanical resonator with a Cooper-pair box [4, 53]. There is considerable interest in pushing a variety of nanoelectromechanical systems (NEMS) to the quantum limit [4, 53, 62, 64, 14], and the memory operation described here would provide a particularly clean demonstration of quantum effects.

4.2 Phase Qubit Coupled to NEMS Resonator

The low-energy dynamics of a JJ is determined by the phase difference φ between the phases of the spatially uniform order parameters in the superconductors forming the junction. The Hamiltonian for the system we consider is $H = H_{\rm J} + H_{\rm res} + \delta H$, where $H_{\rm J} \equiv -E_{\rm c}(d^2/d\varphi^2) + U(\varphi)$ is the Hamiltonian for the JJ with current bias $I_{\rm b}$, with $U \equiv -E_{\rm J}(\cos\varphi + s\varphi)$ and $s \equiv I_{\rm b}/I_0$. $E_{\rm c} \equiv (2e)^2/2C$ is the charging energy, and $E_{\rm J} \equiv \hbar I_0/2e$ is the Josephson energy, with C the junction capacitance and I_0 the critical current. In the large-area JJ of interest here, $E_{\rm J} \gg E_{\rm c}$. $\omega_{\rm p0} \equiv \sqrt{2E_{\rm c}E_{\rm J}}/\hbar$ is the zero-bias plasma frequency. The lowest two eigenstates, $|0\rangle$ and $|1\rangle$, are used to make a qubit. $H_{\rm res} \equiv \hbar\omega_0 a^\dagger a$ is the Hamiltonian for the resonator, with $a^\dagger$ and a the creation and annihilation operators for dilatational-mode phonons of frequency $\omega_0 < \omega_{\rm p0}$. The resonator is a piezoelectric disk sandwiched between two capacitor plates. Finally, the interaction term is $\delta H = -ig(a - a^\dagger)\varphi$, where g is a coupling constant with dimensions of energy that depends on the geometric and material properties of the resonator [23, 39]. A similar interaction Hamiltonian applies to a current-biased JJ capacitively coupled to an LC circuit.

The junction Hamiltonian $H_{\rm J}$ depends on the dimensionless bias current s, which is time dependent. We expand the state of the coupled system in a basis of instantaneous eigenstates $|mn\rangle_s$ of $H_0 \equiv H_{\rm J} + H_{\rm res}$, defined by $H_0(s)|mn\rangle_s = E_{mn}(s)|mn\rangle_s$, where $|mn\rangle_s \equiv |m\rangle_{\rm J} \otimes |n\rangle_{\rm res}$. Here $|m\rangle_{\rm J}$ and $|n\rangle_{\rm res}$ are the eigenstates of the uncoupled JJ and resonator, respectively. The wave function is expanded as $|\psi(t)\rangle = \sum_{mn} c_{mn}(t) e^{-(i/\hbar)\int_{t_0}^{t} dt' E_{\rm mn}(s)} |mn\rangle_s$. The probability amplitudes in the instantaneous interaction representation then satisfy

$$i\hbar \dot{c}_{mn} = \sum_{m'n'} \langle mn|\delta H - i\hbar\partial_t|m'n'\rangle_s e^{-(i/\hbar)\int_{t_0}^{t} dt'[E_{mn}(s) - E_{m'n'}(s)]} c_{m'n'}. \tag{4.1}$$

All effects of dissipation and decoherence are assumed to be negligible over the time scales studied here. We will also assume that the JJ states are well approximated by harmonic oscillator eigenfunctions, which is an excellent approximation unless s is very close to unity. Transitions between instantaneous eigenstates caused by a nonadiabatic variation of s are described by the term $\langle mn|\partial/\partial t|m'n'\rangle_s = \langle mn|\partial/\partial s|m'n'\rangle_s \dot{s}$, which can be evaluated analytically in the harmonic limit [39].

4.3 NEMS Resonator as a Quantum Memory Element

An arbitrary qubit state,

$$|\psi\rangle_{\rm J} = \alpha|0\rangle_{\rm J} + \beta|1\rangle_{\rm J}, \tag{4.2}$$

prepared in the JJ can be stored in the ground and one-phonon states of the resonator's dilatational mode as follows: Assuming the resonator is initially in the ground state $|0\rangle_{\rm res}$ and the JJ is detuned from the resonator, the coupled system is prepared in the initial state $(\alpha|0\rangle_{\rm J} + \beta|1\rangle_{\rm J}) \otimes |0\rangle_{\rm res} = \alpha|00\rangle + \beta|10\rangle$, with $|\alpha|^2 + |\beta|^2 = 1$. The bias current s is then adiabatically varied to tune the JJ level spacing $\Delta\epsilon = \hbar\omega_{\rm p0}(1-s^2)^{1/4}$ to $\hbar\omega_0$, reaching the resonant value $s^* \equiv \sqrt{1-(\omega_0/\omega_{p0})^4}$ at time $t = 0$. Neglecting any nonadiabatic corrections, the probability amplitudes in the instantaneous interaction representation at this time are $c_{mn}(0) = (\alpha\delta_{m0} + \beta\delta_{m1})\delta_{n0}$.

If the interaction strength g is small compared with $\hbar\omega_0$, the subsequent dynamics is well described by the rotating-wave approximation (RWA) of quantum optics [104]. In this approximation, and on resonance, we can write (4.1) as

$$\dot{c}_{0n} = \frac{g}{\hbar}\sqrt{n}x_{01}c_{1,n-1} \tag{4.3}$$

$$\dot{c}_{1n} = -\frac{g}{\hbar}\sqrt{n+1}x_{01}c_{0,n+1}, \tag{4.4}$$

where $x_{01} \equiv \langle 0|\varphi|1\rangle_{\rm J} = l^*/\sqrt{2}$ is an effective dipole moment. Here $l^* \equiv (2E_{\rm c}/E_{\rm J})^{1/4}[1-(s^*)^2]^{-1/8}$ is the characteristic width in φ of the JJ eigenfunctions, when tuned to the resonator. Then we obtain, for $t \geq 0$,

$$\begin{aligned} c_{00}(t) &= \alpha \\ c_{01}(t) &= \beta\sin\left(\frac{\Omega t}{2}\right) \\ c_{10}(t) &= \beta\cos\left(\frac{\Omega t}{2}\right) \\ c_{11}(t) &= 0, \end{aligned} \tag{4.5}$$

and all $c_{mn}(t)$ with $n > 1$ equal to zero. $\Omega \equiv 2gx_{01}/\hbar$ is the resonant vacuum Rabi frequency.

After a time $\Delta t = \pi/\Omega$, a π pulse, the nonvanishing probability amplitudes are $c_{00}(t) = \alpha$ and $c_{01}(t) = \beta$, corresponding to the interaction-representation state $|0\rangle_{\rm J}\otimes(\alpha|0\rangle_{\rm res}+|\beta|1\rangle_{\rm res})$. The qubit state (4.2) has been stored in the resonator's vacuum and one-phonon states. The JJ is now adiabatically detuned from the resonator. To retrieve the stored state, we again bring the systems into resonance at time t_1. Using the stored amplitudes as initial conditions, the RWA equations now lead to (for $t \geq t_1$)

$$\begin{aligned} c_{00}(t) &= \alpha \\ c_{01}(t) &= \beta\cos\left[\frac{\Omega}{2}(t-t_1)\right] \\ c_{10}(t) &= -\beta\sin\left[\frac{\Omega}{2}(t-t_1)\right] \end{aligned} \tag{4.6}$$

the others vanishing. This time the systems are held in resonance for an interval $\Delta t = 3\pi/\Omega$, a 3π pulse, after which the original state $(\alpha|0\rangle_{\rm J} + \beta|1\rangle_{\rm J})\otimes|0\rangle_{\rm res}$ is recovered.

The above analysis, which is based on the adiabatic approximation and the RWA, suggests that perfect memory performance can be obtained with arbitrarily fast gate times (arbitrarily large $g/\hbar\omega_0$). This is incorrect, of course, because the actual quantum memory performance is controlled by the *corrections* to these approximations, which become significant if $g/\hbar\omega_0$ is not small.

4.4 Quantum Memory Fidelity

The accuracy of a storage and retrieval operations can be characterized by the absolute value of the overlap between the intended and achieved final states, or the fidelity F of the memory operation. Accounting for the fact that the intended and actual final state have the same phase factors resulting from the time evolution of the instantaneous eigenstates, F is given by the absolute value of the inner product of the intended and achieved interaction-representation probability amplitudes. We actually report the fidelity squared,

$$F^2 = |\alpha^* c_{00}(t_\mathrm{f}) + \beta^* c_{10}(t_\mathrm{f})|^2, \tag{4.7}$$

which is the probability that the memory device operates correctly. The fidelity is measured at a time t_f, 1 ns after the qubit has been transferred back to the JJ. The c_{mn} in (4.6) are obtained by numerically integrating the exact equation of motion (4.1).

Dissipation and decoherence are not included in our model and do not affect the F we calculate. Thus, any loss of fidelity we find is a consequence of the breakdown of the rotating-wave and adiabatic approximations. An alternative approach would be to introduce phenomenological dissipation and decoherence rates for the qubit and resonator, and calculate the fidelity from the density matrix equation of motion. However, the resulting fidelity versus gate speed curve would then depend sensitively on the assumed dissipation and decoherence rates, which vary considerably from system to system. By including only the pure "gate error" contributation to R, one can immediately apply our results to a given experimental system by focusing on gate times short compared with the relevant energy and phase relaxation times.

When the JJ is weakly coupled to the resonator, with $g/\hbar\omega_0$ below a few percent, the RWA memory protocol of Sec. 4.3 works well, and qubits are stored and retrieved with high fidelity. However, such gates are *slow*. As $g/\hbar\omega_0$ is increased, making the gate faster, the fidelity becomes very poor, and it becomes necessary to deviate from the RWA protocol by numerically searching for optimum values of the resonant interaction times and off-resonant detunings. By performing this optimization for a variety of coupling strengths, we find that the π and 3π pulse times should be *shortened* to $\Delta t = [1 - 0.8(g/\hbar\omega_0)]\Delta t_{\rm RWA}$, where $\Delta t_{\rm RWA}$ is the RWA values.

In Fig. 4.1 we show the result of simulating the storage and retrieval of the qubit state $2^{-1/2}(|0\rangle + |1\rangle)$, which is on the equator of the Bloch sphere. The JJ is that of Ref. [81], with parameters $E_{\rm J} = 43.05$ meV and $E_{\rm c} = 53.33$ neV, and the resonator has a dilatational-mode frequency $\omega_0/2\pi$ of 15 GHz. The JJ and resonator are somewhat strongly coupled, with $g = 0.20\ \hbar\omega_0$. The dimensionless bias current on resonance is $s^* = 0.545$, and the off-resonant values were determined by optimization. Trapezoidal bias profiles with 1 ns ramps and optimized interaction times were used. The gate takes about 10 ns to complete, disregarding times during which the system is detuned, and a squared fidelity of about 91% is achieved. As stated above, the loss of fidelity comes entirely from corrections to the rotating-wave and adiabatic approximations.

4.4.1 Memory fidelity versus coupling strength

In the upper panel of Fig. 4.2 we plot the memory fidelity for the same qubit state $2^{-1/2}(|0\rangle + |1\rangle)$ as a function of $g/\hbar\omega_0$. As expected, the fidelity gradually decreases with increasing g. The small deviations from a strictly monotonic dependence on g are caused by oscillations in the probability amplitudes occurring when the JJ is detuned from the resonator, as in the final nanoseconds of Fig. 4.1. (These could be eliminated by choosing an optimal $t_{\rm f}$ for each g.) The lower panel of Fig. 4.2 gives the gate time as a function of $g/\hbar\omega_0$, again disregarding nonresonant evolution. These results suggest that memory fidelities better than 90% can be

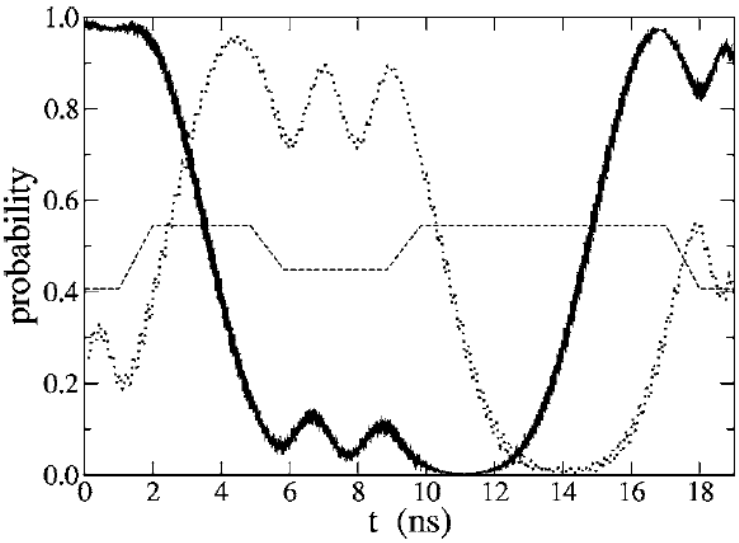

Figure 4.1: Storage and retrieval of the state $2^{-1/2}(|0\rangle + |1\rangle)$. The solid curve is the overlap squared with the initial state. After about 19 ns the qubit is successfully retrieved with a squared fidelity of 91%. The dotted curve gives the occupation of the state $2^{-1/2}(|00\rangle + |01\rangle)$, in which the qubit is stored in the resonator. $g/\hbar\omega_0$ is 20%. The dashed curve is s.

achieved using phase qubits and resonators with coherence times longer than a few tens of nanoseconds.

4.4.2 State dependence of memory fidelity

The memory fidelity depends not only on the strength of the JJ-resonator interaction, but also on the qubit state itself. This is because the fidelity is determined by the corrections to the adiabatic and rotating-wave approximations, and these corrections are state dependent. Using a Bloch sphere representation $\cos(\theta/2)|0\rangle + \sin(\theta/2)e^{i\phi}|1\rangle$ for the stored qubit, we show in Fig. 4.3. the memory fidelity along two great circles, from $|0\rangle$ to $|1\rangle$ along $\phi = 0$ (left) and around the equator (right) starting and finishing at $2^{-1/2}(|0\rangle + |1\rangle)$.

The dependence of F on θ can be understood as follows: When $\theta = 0$, the initial state of the coupled system is $|00\rangle$, because the resonator always starts in the ground state. For a

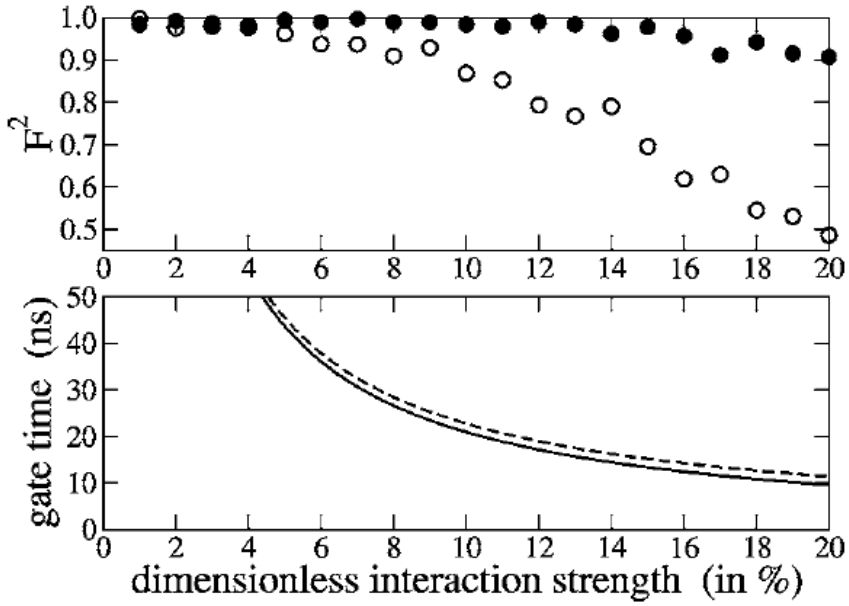

Figure 4.2: (Upper panel) Memory fidelity for the equator state $2^{-1/2}(|0\rangle + |1\rangle)$ as a function of $g/\hbar\omega_0$, using both the RWA (unfilled circles) and optimized (solid circles) pulse times. (Lower panel) The time needed to store and retrieve the state, using both the RWA (dashed curve) and optimized (solid curve) pulse times.

weakly coupled system, $|00\rangle$ is close to the exact ground state for any s, because there are no other $|mn\rangle$ states degenerate with $|00\rangle$ In the adiabatic $ds/dt \to 0$ limit, the large component of $|00\rangle$ in the exact instantaneous ground state will remain there with unit probability, a consequence of the adiabatic theorem, leading to a high memory fidelity for the qubit state $|0\rangle$. The $|1\rangle$ state, by contrast, derives no protection from the adiabatic theorem and is subject to errors caused by the corrections to the RWA. The weaker ϕ dependence is a consequence of the form of δH, which favors equator states pointing in the $2^{-1/2}(|0\rangle + |1\rangle)$ or "positive x" direction.

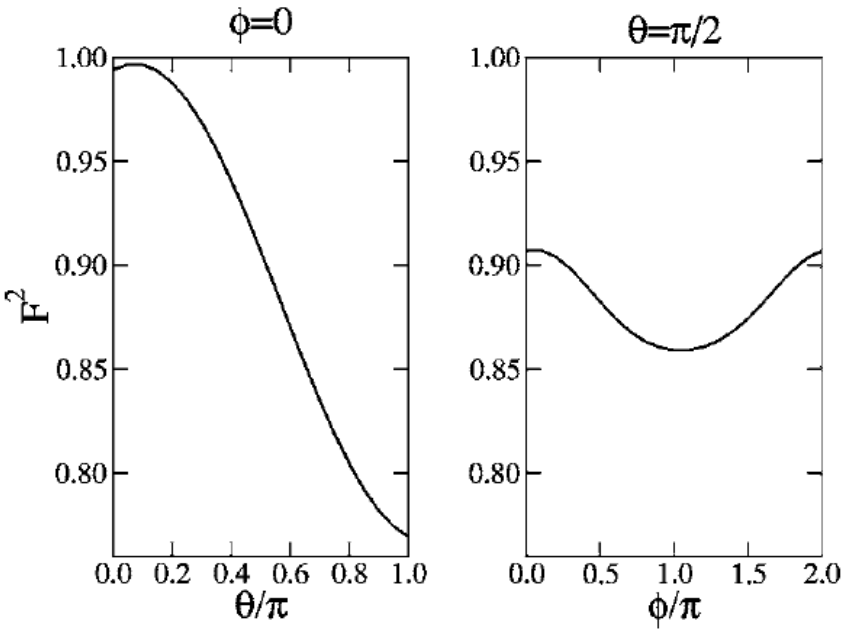

Figure 4.3: State dependence of memory fidelity, for the same JJ-resonator system studied in Fig. 1, with $g/\hbar\omega_0 = 20\%$. (Left) Fidelity as a function of θ, along the arc $\phi = 0$ on the Bloch sphere. (Right) Fidelity around the equator.

4.5 Discussion

We have explored the speed and accuracy with which a NEMS resonator can be used to store qubit states prepared in a current-biased JJ. We find that a simple optimization of resonant interaction times and off-resonant detuning leads to a tremendous improvement in gate performance compared with that resulting from the primitive RWA protocol. Finding the right balance between gate fidelity and operation time will be essential in the design of large-scale superconducting quantum computers. Overall, our simulation suggests that generic states on the Bloch sphere can be stored and retrieved in a few tens of nanoseconds with accuracies better than 90%. We expect that many of the results presented here will apply to other qubit-oscillator systems as well.

Chapter 5

Generalizing Superconducting Qubit Hamiltonians

In the previous chapters, many superconducting circuits were considered as possible building blocks of a quantum computer. In the following chapters we discuss how to implement quantum logic and simulate other systems with these superconducting circuits. This chapter serves as a bridge between the physically motivated discussions in the previous chapters to the more mathematical discussions in the following chapters.

A very general model of weakly coupled qubits is described, one that has a wide range of applicability including all of the superconducting qubit circuits described previously, and some architectures not described, such as NMR and ion traps. Assumptions are placed on this model only when the benefits of simplicity outweigh the cost of generality.

This purpose of defining such a general and abstract model is efficiency and longevity. With a model that encompasses any system of weakly coupled qubits, we can perform a calculation abstractly that applies to many different physical systems simultaneously. Also, as superconducting qubit architectures rapidly evolve, results tailored to a specific architecture become quickly obsolete.

Theory development using a general model of weakly coupled qubits also has experimental benefit. We show that certain types of interactions between qubits have no benefit to gate design or quantum simulation and are therefore expendable, while others prove crucial for effective qubit-qubit coupling. These considerations can affect circuit design and fabrication.

In the first section of this chapter, a general model Hamiltonian for weakly coupled qubits is established. This model is time dependent, and contains large energy discrepancies

between the diagonal and off-diagonal terms. This makes calculating the time evolution of the physical systems described by the Hamiltonian difficult analytically.

In the second section, we transform the general Hamiltonian into a rotating frame. In the final section we approximate the rotating frame Hamiltonian as a time-independent Hamiltonian that is used as a substitution for the more general Hamiltonian for the purposes of gate design.

Inaccuracies based on these approximations are small when qubits are coupled weakly. Gate design and simulation techniques that use these approximate Hamiltonian solutions should be considered as guidelines about which more process architecture-dependent optimizations can be performed.

5.1 Projecting Superconducting Qubit Hamiltonians into the Computational Basis

In chapters 2-4 the Hamiltonians describing superconducting circuits were written in terms of continuous quantum variables, e.g. φ_i, Q, p_φ, etc., in infinite dimensional Hilbert spaces. While this is necessary to identify the energy eigenstates of the quantum circuit, only two of the infinite number of energy levels in the quantum circuit will be used for quantum computation. The two eigenstates lowest in energy are usually defined as the qubit states of the circuit, and they are labelled $|0\rangle$ and $|1\rangle$. The 'computational subspace' of an n-qubit quantum computer is the 2^n-dimensional Hilbert space spanned by only the qubit states of each superconducting qubit.

Circuit Hamiltonians are projected into the computational basis state to simplify the process of gate design. For example, in the case of capacitively coupled phase qubits, the Hamiltonian can be written as $H = H_0 + H_{\rm int}$ where

$$H_0 \;=\; \sum_{i=1}^{n}\left[\frac{p_{\varphi_i}^2}{2\alpha\tilde{C}_i} - E_{\rm J}^{(i)}(\cos\varphi_i + s_i\varphi_i)\right] \quad \text{and} \quad H_{\rm int} = \frac{1}{2}\sum_{i\neq j}\frac{p_{\varphi_i}p_{\varphi_j}}{\alpha^2\tilde{C}_{\rm int}^{ij}}. \tag{5.1}$$

Projecting into the computational basis involves first finding energy eigenstates (or localized quasibound states) of H_0 for each qubit. For the ith qubit, suppose the energies are ϵ_i^0, ϵ_i^1, ϵ_i^2, etc. The states lowest in energy are defined to be the qubit states represented by $|0\rangle$ and $|1\rangle$, so if all other states are ignored,

$$H_0 = \sum_i -\frac{\epsilon_i}{2}\sigma_i^z \tag{5.2}$$

where $\epsilon_i = \epsilon_i^1 - \epsilon_i^0$ and an additive constant has been dropped. The following notation is used for the Pauli matrices:

$$\sigma^x = \begin{pmatrix} 0 & 1 \\ 1 & 0 \end{pmatrix}, \quad \sigma^y = \begin{pmatrix} 0 & -i \\ i & 0 \end{pmatrix}, \quad \text{and} \quad \sigma^z = \begin{pmatrix} 1 & 0 \\ 0 & -1 \end{pmatrix} \tag{5.3}$$

The sign of H_0 in Eqn. (5.2) comes from the convention of using the computational basis states in the order $|0\rangle$, $|1\rangle$. The projected interaction Hamiltonian is of the form

$$H_{\text{int}} = \frac{g}{2}\sum_{i\neq j} \sigma_i^y \otimes \sigma_j^y \tag{5.4}$$

where g is a coupling constant of dimensions of energy that depends on the properties of the junctions and their interaction capacitance. All of the 'momentum-momentum' couplings derived in Ch. 3 will be of this forms with differing g values. A 'position-position' coupling is of the form

$$H_{\text{int}} = \frac{g}{2}\sum_{i\neq j} \sigma_i^x \otimes \sigma_j^x, \tag{5.5}$$

and so forth.

Leakage out of the computational subspace is an important concern to gate design. However, the details of how the computational basis states couple to higher lying energy levels are architecture specific. We do not include any states outside of the computational subspace here, but note that techniques to reduce leakage out of the computational basis do exist and can be used in combination with theory developed in the computational subspace [85]. It is also interesting to consider the possibilty of generalizing the theory presented here in the computational subspace to allow three (or more) states per qubit.

5.2 A General Model Hamiltonian of n Weakly Coupled Qubits

The Hamiltonian of a quantum computer of n weakly coupled qubits can be written as the sum of three terms,

$$H = H_0 + H_{\rm C} + H_{\rm int}, \tag{5.6}$$

where H_0 in Eqn. (5.2) describes n noninteracting qubits, $H_{\rm C}$ describes external control on the qubits, and $H_{\rm int}$ describes qubit-qubit interaction. The Pauli matrices together with the 2×2 identity σ^0 form a basis for any operator acting on a single two level system, and will be used to describe H_0 and $H_{\rm C}$. Control Hamiltonians can vary in detail between architectures, but we assume

$$H_{\rm C} = \sum_{i=1}^{n} \Omega_i \cos(\omega_i^{\rm rf} t + \phi_i)\sigma_i^x, \tag{5.7}$$

which has a wide range of applicability in superconducting qubit architectures. Oscillations between qubit energy levels are driven by external sources of flux and/or current described with magnitude Ω, driving frequency $\omega_{\rm rf}$, and phase ϕ. Note that $\Omega = \Omega(t)$ and $\phi = \phi(t)$ are in general time dependent.

Interactions occur between pairs of qubits, and can therefore be written in a basis of tensor products of two Pauli matrices: $\sigma_i^x\sigma_j^x$, $\sigma_i^z\sigma_j^z$, etc. Interactions can cause one qubit to rotate while the other remains unchanged, so terms of the form $\sigma_i^x \otimes \sigma_j^0$, etc. appear in the most general description of interaction:

$$H_{\rm int}(t) = \frac{1}{2}\sum_{i\neq j} g_{ij}(t) J_{\mu\nu}\sigma_i^\mu \otimes \sigma_j^\nu, \tag{5.8}$$

where $\mu,\nu \in \{0,x,y,z\}$ are summed over. $g_{ij}(t) = g_{ji}(t)$ are pairwise qubit interaction strengths which have dimensions of energy and may in general be time-dependent. $J_{\mu\nu}$ is a 4×4 dimensionless tensor that describes the time-independent structure of the qubit interaction and is determined by the computer's architecture. The coefficient of a particular

tensor product $\sigma_i^\mu \otimes \sigma_j^\nu$ is determined by the element $J_{\mu\nu}$:

$$\begin{aligned} J_{\mu\nu}\sigma_i^\mu \otimes \sigma_j^\nu &= J_{00}\mathbb{I} + J_{01}\sigma_j^1 + J_{02}\sigma_j^2 + J_{03}\sigma_j^3 \\ &\quad + J_{10}\sigma_i^1 + J_{11}\sigma_i^1 \otimes \sigma_j^1 + J_{12}\sigma_i^1 \otimes \sigma_j^2 + J_{13}\sigma_i^1 \otimes \sigma_j^3 \\ &\quad + J_{20}\sigma_i^2 + J_{21}\sigma_i^2 \otimes \sigma_j^1 + J_{22}\sigma_i^2 \otimes \sigma_j^2 + J_{23}\sigma_i^2 \otimes \sigma_j^3 \\ &\quad + J_{30}\sigma_i^3 + J_{31}\sigma_i^3 \otimes \sigma_j^1 + J_{32}\sigma_i^3 \otimes \sigma_j^2 + J_{33}\sigma_i^3 \otimes \sigma_j^3. \end{aligned} \tag{5.9}$$

$J_{\mu\nu}$ can be generalized to describe systems of nonidentical two level systems where each pair of two level systems may have a different interaction, requiring $J_{\mu\nu}^{ij}$ to have four indices. The interaction between each pair of qubits is more often identical; therefore, these additional indices will be suppressed. Furthermore, when describing identical qubits, $J_{\mu\nu}$ is symmetric:

$$J_{\mu\nu} = J_{\nu\mu} \tag{5.10}$$

5.3 Rotating Frame

The time evolution generated by the quantum computer's Hamiltonian $H = H(t)$ is

$$U = e^{-i/\hbar \int_{t_0}^{t} H(t')dt'} \tag{5.11}$$

according to Schrodinger's Equation. The state of the quantum computer measured after evolving by time evolution operator U will be identical to the state measured after operation $\tilde{U} \cdot U$, so long as the operation $\tilde{U}$ commutes with measurement. One such operation is a rotation of each of the qubits about the σ_i^z 'direction',

$$\tilde{U} = e^{-i\sum_{i=1}^{n} \frac{\omega_i}{2}\sigma_i^z t}, \tag{5.12}$$

since σ_i^z is diagonal in the basis of energy eigenstates (which is the basis of measurement). We calculate the Hamiltonian that generates the product of operators $\tilde{U} \cdot U$, which we denote as $\tilde{H}$. This Hamiltonian, commonly referred to as the Hamiltonian in the 'rotating frame' , will generate a time evolution that is indistinguishable from the actual time evolution of the

computer as generated by H, not because the lab is rotating, but because $\tilde{U}$ commutes with measurement.

Since $i\hbar\partial_t U(t) = H(t)U(t)$,

$$\begin{aligned} i\hbar\partial_t[\tilde{U}(t)\cdot U(t)] &= i\hbar[\partial_t\tilde{U}]\cdot U + i\hbar\tilde{U}\cdot[\partial_t U] \\ &= \left[\sum_i \frac{\hbar\omega_i}{2}\sigma_i^z + \tilde{U}H(t)\tilde{U}^{-1}\right]\tilde{U}\cdot U, \end{aligned} \tag{5.13}$$

and the rotating frame Hamiltonian $\tilde{H}$ that generates $\tilde{U}\cdot U$ is

$$\begin{aligned} \tilde{H} &= \sum_i \frac{\hbar\omega_i}{2}\sigma_i^z + \tilde{U}H(t)\tilde{U}^{-1} \\ &= \frac{1}{2}\sum_{i=1}^{n}[\hbar\omega_i - \epsilon_i(t)]\sigma_i^z + \tilde{U}H_{\rm C}\tilde{U}^{-1} + \tilde{U}H_{\rm int}\tilde{U}^{-1} \end{aligned} \tag{5.14}$$

since H_0 and $\tilde{U}$ commute. For convenience, define $\tilde{H}_{\rm C} \equiv \tilde{U}H_{\rm C}\tilde{U}^{-1}$ and $\tilde{H}_{\rm int} = \tilde{U}H_{\rm int}\tilde{U}^{-1}$. Note that

$$\begin{aligned} \tilde{U}\sigma_i^x\tilde{U}^{-1} &= \cos(\omega_i t)\,\sigma_i^x + \sin(\omega_i t)\,\sigma_i^y \\ \tilde{U}\sigma_i^y\tilde{U}^{-1} &= \cos(\omega_i t)\,\sigma_i^y - \sin(\omega_i t)\,\sigma_i^x \end{aligned} \tag{5.15}$$

and $\tilde{U}\sigma_i^z\tilde{U}^{-1} = \sigma_i^z$, so

$$\begin{aligned} \tilde{H}_{\rm C} &= \frac{\hbar}{2}\sum_{i=1}^{N}\Omega_i\left[\cos(\omega_i^{\rm rf}t + \phi_i + \omega_i t) + \cos(\omega_i^{\rm rf}t + \phi_i - \omega_i t)\right]\sigma_i^x \\ &+ \frac{\hbar}{2}\sum_{i=1}^{N}\Omega_i\left[\sin(\omega_i^{\rm rf}t + \phi_i + \omega_i t) - \sin(\omega_i^{\rm rf}t + \phi_i - \omega_i t)\right]\sigma_i^y \end{aligned} \tag{5.16}$$

$$\begin{aligned} \tilde{H}_{\rm int} &= \frac{1}{2}\sum_{i\neq j} g_{ij}(t)\Big\{ J_{00}\mathbb{I} + J_{0z}\sigma_j^z + J_{z0}\sigma_i^z + J_{zz}\sigma_i^z\otimes\sigma_j^z \\ &+ [\cos(\omega_j t) + \sin(\omega_j t)]\cdot\left[J_{0x}\sigma_j^x + J_{zx}\sigma_i^z\otimes\sigma_j^x\right] + [\cos(\omega_i t) + \sin(\omega_i t)]\cdot\left[J_{x0}\sigma_i^x + J_{xz}\sigma_i^x\otimes\sigma_j^z\right] \\ &+ [\cos(\omega_j t) - \sin(\omega_j t)]\cdot\left[J_{0y}\sigma_j^y + J_{zy}\sigma_i^z\otimes\sigma_j^y\right] + [\cos(\omega_i t) - \sin(\omega_i t)]\cdot\left[J_{y0}\sigma_i^x + J_{yz}\sigma_i^y\otimes\sigma_j^z\right] \\ &+ \frac{1}{2}[\cos(\omega_i t + \omega_j t) + \cos(\omega_i t - \omega_j t)]\cdot\left[J_{xx}\sigma_i^x\otimes\sigma_i^x + J_{yy}\sigma_i^y\otimes\sigma_j^y + J_{xy}\sigma_i^x\otimes\sigma_j^y + J_{yx}\sigma_i^y\otimes\sigma_j^x\right] \\ &+ \frac{1}{2}[\cos(\omega_i t - \omega_j t) - \cos(\omega_i t + \omega_j t)]\cdot\left[J_{xx}\sigma_i^y\otimes\sigma_i^y + J_{yy}\sigma_i^x\otimes\sigma_j^x - J_{xy}\sigma_i^y\otimes\sigma_j^x - J_{yx}\sigma_i^x\otimes\sigma_j^y\right] \\ &+ \frac{1}{2}[\sin(\omega_i t + \omega_j t) - \sin(\omega_i t - \omega_j t)]\cdot\left[J_{xx}\sigma_i^x\otimes\sigma_i^y - J_{yy}\sigma_i^y\otimes\sigma_j^x - J_{xy}\sigma_i^x\otimes\sigma_j^x + J_{yx}\sigma_i^y\otimes\sigma_j^y\right] \\ &+ \frac{1}{2}[\sin(\omega_i t + \omega_j t) + \sin(\omega_i t - \omega_j t)]\cdot\left[J_{xx}\sigma_i^y\otimes\sigma_i^x - J_{yy}\sigma_i^x\otimes\sigma_j^y + J_{xy}\sigma_i^y\otimes\sigma_j^y - J_{yx}\sigma_i^x\otimes\sigma_j^x\right]\Big\}. \end{aligned}$$

5.4 The Rotating Wave Approximation

At first glance, going into a rotating frame does not seem to help simplify $H(t)$ as $\tilde{H}_{\rm C}$ and $\tilde{H}_{\rm int}$ are much more complicated than $H_{\rm C}$ and $H_{\rm int}$ respectively. However, by choosing the frequencies ω_i cleverly, certain terms in $\tilde{H}_{\rm C}$ and $\tilde{H}_{\rm int}$ are made time independent while others oscillate very quickly with time. For example, by taking $\omega_i = \omega = \omega_i^{\rm rf}$,

$$\begin{aligned}
\tilde{H}_{\rm C} &= \frac{\hbar}{2}\sum_{i=1}^{n}\Omega_i\left[\cos(\phi_i+2\omega t)+\cos(\phi_i)\right]\sigma_i^x \\
&+ \frac{\hbar}{2}\sum_{i=1}^{N}\Omega_i\left[\sin(\phi_i+2\omega t)-\sin(\phi_i)\right]\sigma_i^y \\
\tilde{H}_{\rm int} &= \frac{1}{2}\sum_{i\neq j} g_{ij}(t)\Big\{ J_{00}\mathbb{I} + J_{0z}\sigma_j^z + J_{z0}\sigma_i^z + J_{zz}\sigma_i^z\otimes\sigma_j^z \\
&+ \left[\cos(\omega t)+\sin(\omega t)\right]\cdot\left[J_{0x}\sigma_j^x + J_{zx}\sigma_i^z\otimes\sigma_j^x + J_{x0}\sigma_i^x + J_{xz}\sigma_i^x\otimes\sigma_j^z\right] \\
&+ \left[\cos(\omega t)-\sin(\omega t)\right]\cdot\left[J_{0y}\sigma_j^y + J_{zy}\sigma_i^z\otimes\sigma_j^y + J_{y0}\sigma_i^x + J_{yz}\sigma_i^y\otimes\sigma_j^z\right] \\
&+ \frac{1}{2}\left[(J_{xx}+J_{yy})\left(\sigma_i^x\otimes\sigma_i^x+\sigma_i^y\otimes\sigma_j^y\right)+(J_{xy}-J_{yx})\left(\sigma_i^x\otimes\sigma_j^y-\sigma_i^y\otimes\sigma_j^x\right)\right] \\
&+ \frac{1}{2}\cos(2\omega t)\left[(J_{xx}-J_{yy})\left(\sigma_i^x\otimes\sigma_i^x-\sigma_i^y\otimes\sigma_j^y\right)+(J_{xy}+J_{yx})\left(\sigma_i^x\otimes\sigma_j^y+\sigma_i^y\otimes\sigma_j^x\right)\right] \\
&+ \frac{1}{2}\sin(2\omega t)\left[(J_{xx}-J_{yy})\left(\sigma_i^x\otimes\sigma_i^y+\sigma_i^y\otimes\sigma_j^x\right)+(J_{xy}+J_{yx})\left(\sigma_i^x\otimes\sigma_j^x-\sigma_i^y\otimes\sigma_j^y\right)\right]\Big\}
\end{aligned} \tag{5.17}$$

Using a standard and very accurate approximation from quantum optics called the Rotating Wave Approximation (RWA) [104], terms that change quickly with time are averaged. leaving

$$\begin{aligned}
\tilde{H}_{\rm C} &\simeq \frac{\hbar}{2}\sum_{i=1}^{n}\Omega_i(\cos\phi_i\sigma_i^x+\sin\phi_i\sigma_i^y) \\
\tilde{H}_{\rm int} &\simeq \frac{1}{2}\sum_{i\neq j} g_{ij}(t)\Big\{ J_{00}\mathbb{I} + J_{0z}\sigma_j^z + J_{z0}\sigma_i^z + J_{zz}\sigma_i^z\otimes\sigma_j^z \\
&+ J\left(\sigma_i^x\otimes\sigma_j^x+\sigma_i^y\otimes\sigma_j^y\right)+J'\left(\sigma_i^x\otimes\sigma_j^y-\sigma_i^y\otimes\sigma_j^x\right)\Big\}
\end{aligned} \tag{5.18}$$

where $J \equiv (J_{xx}+J_{yy})/2$ and $J' \equiv (J_{xy}-J_{yx})/2$. The RWA is improved for $\tilde{H}_{\rm C}$ and $\tilde{H}_{\rm int}$ as $\Omega/\omega \to 0$ and $g||J_{\mu\nu}||/\omega \to 0$ respectively.

Evolution by $H(t)$ is indistinguishable from evolution from $\tilde{H}(t)$, which to a good approximation is equivalent to evolution generated by $\mathcal{H}_{\rm RWA} = \mathcal{H}_{\rm C} + \mathcal{H}$, where

$$\begin{aligned}
\mathcal{H}_{\rm C} &= \frac{1}{2}\sum_{i=1}^{n}\left\{\hbar\Omega_i(\cos\phi_i\sigma_i^x + \sin\phi_i\sigma_i^y) + \left[\hbar\omega - \epsilon_i(t)) + \frac{J_{z0}}{2}\sum_{j\neq i} g_{ij}(t)\right]\sigma_i^z\right\} \\
\mathcal{H} &= \frac{1}{2}\sum_{i\neq j} g_{ij}(t)\left[J\left(\sigma_i^x\otimes\sigma_j^x + \sigma_i^y\otimes\sigma_j^y\right) + J'\left(\sigma_i^x\otimes\sigma_j^y - \sigma_i^y\otimes\sigma_j^x\right) + J_{\rm zz}\sigma_i^z\otimes\sigma_j^z\right]
\end{aligned}$$

Note that the parameters $\Omega(t)$, $\phi(t)$, and $\epsilon(t)$ give complete control over $\mathcal{H}_{\rm C}(t)$. In particular, $\mathcal{H}_{\rm C}$ can be set to zero, even with J_{z0} and J_{0z} are nonzero. $\mathcal{H}$ is much simpler than the original $H_{\rm int}$, as can be seen by its matrix form:

$$\mathcal{H} = \begin{pmatrix} J_{zz} & 0 & 0 & 0 \\ 0 & -J_{zz} & \gamma & 0 \\ 0 & \gamma^* & -J_{zz} & 0 \\ 0 & 0 & 0 & J_{zz} \end{pmatrix} \tag{5.19}$$

where $\gamma(t) = 2g_{ij}(t)(J + iJ') = |\gamma(t)|e^{i\varphi}$. Note that since $J_{\mu\nu}$ is assumed time independent, only the magnitude of γ changes with time. In this approximation, which is extremely accurate in the weak coupling limit, all qubit-qubit interactions can be characterized by three parameters: J, J', and $J_{\rm zz}$, or alternatively, $|\gamma|$, θ, and $J_{\rm zz}$. These parameters depend only on 5 of the original 16 elements of the original coupling tensor $J_{\mu\nu}$: J_{xx}, J_{yy}, J_{xy}, J_{yx}, and J_{zz}. Terms involving one σ_i^z, namely $\sigma_i^x\otimes\sigma_j^z$, $\sigma_i^y\otimes\sigma_j^z$, $\sigma_i^z\otimes\sigma_i^x$, and $\sigma_i^z\otimes\sigma_j^y$, have no effect on qubit-qubit interaction in the RWA. This result will be used in the next chapter on gate design.

Chapter 6

Quantum Gate Design For Weakly Coupled Qubits

One of the first and most important discoveries in quantum information science was that any $2^n \times 2^n$ dimensional time evolution operator U can be decomposed into a universal set of one- and two-qubit logic gates on an n-qubit register [8, 90]. One of most important long term challenges to the physical implementation of a quantum computer is the fast and accurate implementation of such a universal set of gates on a physically realizable quantum system. This chapter explores gate design for weakly coupled qubits, using figures from our paper [40] unless otherwise noted.

6.1 The problem of Gate Design

Recall that any computation performed by a quantum computer *is* that computer's time evolution $U(t)$ generated by its Hamiltonian $H(t)$ according to Schrodinger's equation:

$$U(t) = \mathcal{T} e^{-\frac{i}{\hbar}\int_{t_0}^{t} H(t')dt'}. \tag{6.1}$$

In order for a physical system to be considered as a possible quantum computer, it must offer time dependent control over its Hamiltonian so that a universal set of gates can be performed on demand. Therefore, the Hamiltonian of a quantum computer must be a function of several control parameters ξ_1, ξ_2, .., ξ_k:

$$H(t) = H(\xi_1(t), \xi_2(t), ..\xi_k(t)). \tag{6.2}$$

The problem of gate design can be stated as finding the time-dependent profiles of these parameters that will cause the computer to evolve the desired target gate U_{T}. Given $H(t)$, calculating $U(t)$ according to Eqn. (6.1) is straightforward numerically and sometimes straightforward analytically when $H(t)$ has certain properties. However, inverting this equation, e.g. finding $H(t)$ given the target gate U_{T}, is much more difficult. This is precisely what makes the process of gate design challenging. In this chapter, we focus on two qubit gate design, taking the CNOT gate

$$U_{\mathrm{T}} = U_{\mathrm{CNOT}} \equiv \begin{pmatrix} 1 & 0 & 0 & 0 \\ 0 & 1 & 0 & 0 \\ 0 & 0 & 0 & 1 \\ 0 & 0 & 1 & 0 \end{pmatrix}, \tag{6.3}$$

as an example target gate when required.

In general, two-qubit gate design is a control problem in the continuous Lie group U(N) of unitary transformations on an N dimensional quantum system where $N \geq 4$. In this chapter, $N = 4$ is considered. This restriction seems reasonable since the two-qubit computational subspace is four dimensional; however, there is an important class of two-qubit gate protocols excluded by this approach that is mentioned briefly here.

Specifically, when a two-qubit system evolves a CNOT, its time evolution operator $U(t)$ may leave the computational subspace and return during the course of a gate's implementation. This technique has proven very powerful for CNOT gate design. For example, if the $|11\rangle$ state performs a 2π rotation with an auxiliary state, like the $|02\rangle$ or $|20\rangle$ states of a superconducting circuit, while the other computational basis states only evolve an overall phase, the computational subspace will evolve the Controlled-Z(CZ) gate (up to an overall phase), where

$$U_{\mathrm{CZ}} \equiv \begin{pmatrix} 1 & 0 & 0 & 0 \\ 0 & 1 & 0 & 0 \\ 0 & 0 & 1 & 0 \\ 0 & 0 & 0 & -1 \end{pmatrix}. \tag{6.4}$$

The CZ gate is itself universal for quantum computation; however, the canonical CNOT in Eqn. (6.3) is useful for algorithm implementation and may be obtained from the CZ by only single qubit (non-entangling) transformations [90]:

$$U_{\text{CNOT}} = H_2 \cdot U_{CZ} \cdot H_2 \tag{6.5}$$

where H_2 is the Hadamard gate on the second qubit, which can be constructed from single qubit rotations:

$$H_i \equiv 2^{-\frac{1}{2}} \cdot \begin{pmatrix} 1 & 1 \\ 0 & -1 \end{pmatrix}_i = i\mathcal{R}_x(\pi)_i \cdot \mathcal{R}_y\left(\frac{\pi}{2}\right)_i. \tag{6.6}$$

The notation for single qubit rotations is defined as follows:

$$\mathcal{R}_{\hat{n}}(\theta)_i \equiv e^{-i\frac{\theta}{2}\hat{n}\cdot\vec{\sigma}_i} \tag{6.7}$$

where $\hat{n}$ is any three dimensional unit vector and $\vec{\sigma}_i \equiv \sigma_i^x\hat{x} + \sigma_i^y\hat{y} + \sigma_i^z\hat{z}$.

This CNOT protocol was first proposed in 1995 by Cirac, *et al.* [21] for an ion trap quantum computer, then in 2003 by Strauch *et al.* for two capacitively coupled phase qubits [113]. It has been implemented experimentally for phase qubits [124, 89], transmon qubits [27, 28], and trapped ions [83]. While this chapter only considers evolution in the two-qubit computational subspace, it is possible that the approaches described here may be generalizable to $U(N)$ for $N \geq 5$ so that the results just mentioned may be included.

6.2 The Entangling Gates Generated by Weakly Coupled Qubits

Along with the many approaches to physically realizing a quantum computer come a variety of approaches to implementing universal logic. Often these approaches use details about the physical system being considered, or require the Hamiltonian to obey certain symmetries. For example, an exact CNOT gate construction is known when the qubits interact via an Ising interaction ($H \sim \sigma_1^z \otimes \sigma_2^z$) [90], as well as when qubits interact via a Heisenberg interaction ($H \sim \sigma_1 \cdot \sigma_2$) [71, 19].

The goal of this chapter is to develop an algorithmic approach to gate design that applies to *any* two-qubit gate and *any* interaction Hamiltonian. The model Hamiltonian derived in the last chapter is used, which only assumes a system of weakly coupled qubits. We also assume that $H_{\mathrm{C}} = 0$, which implies that the qubits are *tuned* in energy, $\epsilon_1 = \epsilon_2$, unless $J_{\mathrm{z0}} = J_{\mathrm{0z}}$ is nonzero.

The interaction part of the two-qubit RWA Hamiltonian is rewritten here for convenience:

$$\begin{aligned} \mathcal{H} &= g(t)\left[J(\sigma_1^x \otimes \sigma_2^x + \sigma_1^y \otimes \sigma_2^y) + J'(\sigma_1^x \otimes \sigma_2^y - \sigma_1^y \otimes \sigma_2^x) + J_{\mathrm{zz}}\sigma_1^z \otimes \sigma_2^z\right] \\ &= g(t)\begin{pmatrix} J_{zz} & 0 & 0 & 0 \\ 0 & -J_{zz} & \gamma & 0 \\ 0 & \gamma^* & -J_{zz} & 0 \\ 0 & 0 & 0 & J_{zz} \end{pmatrix} \end{aligned} \tag{6.8}$$

where $\gamma(t) = 2g_{ij}(t)(J + iJ') = |\gamma(t)|e^{i\varphi}$. It is straightforward to show that the time evolution generated by $\mathcal{H}(t)$ is

$$\begin{aligned} U(t) &= \mathcal{T}e^{\int_{t_0}^{t} -i\mathcal{H}(t')dt'} \\ &= e^{-i\phi(t)}\begin{pmatrix} 1 & 0 & 0 & 0 \\ 0 & e^{i2\phi(t)}\cos\Gamma(t) & e^{i(2\phi(t)+\varphi-\frac{\pi}{2})}\sin\Gamma(t) & 0 \\ 0 & e^{i(2\phi(t)-\varphi-\frac{\pi}{2})}\sin\Gamma(t) & e^{i2\phi(t)}\cos\Gamma(t) & 0 \\ 0 & 0 & 0 & 1 \end{pmatrix}. \end{aligned} \tag{6.9}$$

where $\Gamma(t) = \int_{t_0}^{t} |\gamma(t')|dt'$, $\phi(t) = J_{\mathrm{zz}}\int_{t_0}^{t} g(t')dt'$, and $\hbar = 1$. Clearly, $\mathcal{H}$ will not naturally evolve the target CNOT gate in Eqn. (6.3) after any time t.

6.3 Local Equivalence

$\mathcal{H}(t)$ cannot generate a CNOT directly; however, the single qubit control term in the RWA Hamiltonian adds three controls per qubit, $\epsilon(t)$, $\Omega(t)$ and $\phi(t)$, that have not yet been considered. There are (at least) two ways one can add single qubit control to this problem. One is by simply adding $\mathcal{H}_{\mathrm{C}}$ to $\mathcal{H}$ and using the single qubit rotation terms to 'steer' the

time evolution to the desired gate. This approach, as formulated by Zhang *et al.* in 2003 [129, 130], has been studied in detail by another member of our group Andrei Galiautdinov [35, 36].

Here a different approach is taken, namely, single qubit control is not added to $\mathcal{H}$, but arbitrary single qubit transformations are allowed before and after the time evolution $U(t)$ generated by $\mathcal{H}$. The target gate is decomposed as

$$U_{\mathrm{T}} = e^{i\varphi}\mathcal{R}^2 \cdot U_{\mathrm{ent}} \cdot \mathcal{R}^1 \tag{6.10}$$

where U_{ent} is the entangling part of the gate, φ is an overall phase, and $\mathcal{R}^{1,2}$ are pre- and post-single qubit rotations of the form in Eqn. (6.7). For most experimental implementations of a quantum computer, it is known how to perform an arbitrary single qubit rotation quickly and accurately.

Because the problem of implementing arbitrary single qubit rotations is so much easier than that of implementing arbitrary two-qubit gates, we will be satisfied if our interaction Hamiltonian $\mathcal{H}$ has evolved a gate equivalent to the target gate up to single qubit rotations and an overall phase. When the relationship between U_{ent} and U_{T} holds for some $\mathcal{R}^{1,2}$ and φ, we say that U_{ent} and U_{T} are 'locally equivalent,' denoted as

$$U_{\mathrm{T}} \sim U_{\mathrm{ent}}. \tag{6.11}$$

Both U_{T} and U_{ent} are in $U(4)$, a 16 dimensional Lie group (generated by, for example, the basis vectors of the $J_{\mu\nu}$ tensor). Single qubit rotations $\mathcal{R}^1$ and $\mathcal{R}^2$ are in the 6 dimensional Lie group $SU(2) \otimes SU(2)$, which can be generated by two copies of the three Pauli matrices: σ_1^x, σ_1^y, σ_1^z, σ_2^x, σ_2^y, σ_2^z. The overall phase $e^{i\varphi}$ is in the 1-dimensional group $U(1)$. This suggests that

$$\text{dim. of } U(4) - 2 \times (\text{dim. of } SU(2) \otimes SU(2)) - \text{dim. of } U(1) = 3 \tag{6.12}$$

degrees of freedom are required to specify an operator's 'local equivalence class.' In the next two subsections, two existing approaches to establishing an operators equivalence class are reviewed.

6.3.1 Makhlin Invariants

Yuriy Mahklin derived the condition for local equivalence in 2003 by proving that two quantities, $G_1(U)$ and $G_2(U)$, will be unchanged if local rotations are performed on U [75]. G_1 is in general complex while G_2 is always real, so this amounts to three real variables that determine a gate's local equivalence. $G_1(U)$ and $G_2(U)$ are calculated as follows:
Define $U_{\rm B} \equiv Q^\dagger U Q$ to be the transformation of U into the Bell basis, defined as

$$Q \equiv \frac{1}{\sqrt{2}} \begin{pmatrix} 1 & 0 & 0 & i \\ 0 & i & 1 & 0 \\ 0 & i & -1 & 0 \\ 1 & 0 & 0 & -i \end{pmatrix}. \tag{6.13}$$

Let $u = U_{\rm B}^{\rm T} U_{\rm B}$. Then

$$\begin{aligned} G_1(U) &= {\rm tr}^2 u \; {\rm det} U^\dagger / 16 \\ G_2(U) &= [{\rm tr}^2 u - {\rm tr}(u^2)] {\rm det} U^\dagger / 4. \end{aligned} \tag{6.14}$$

G_1 and G_2 are referred to as 'Makhlin Invariants.' This result makes it convenient to numerical check whether the time evolution of any particular Hamiltonian will ever be locally equivalent to the desired target gate. For example, in the case of $U_{\rm T} = U_{\rm CNOT}$,

$$\begin{aligned} G_1(U_{\rm T}) &= 0 \\ G_1(U_{\rm T}) &= 1. \end{aligned} \tag{6.15}$$

It is straightforward to show that for U(t) in Eqn. (6.9),

$$\begin{aligned} G_1(U(t)) &= \frac{1}{4} e^{-4i\phi(t)} \left[1 + e^{4i\phi(t)} \cos\left(2\Gamma(t)\right)\right]^2 \\ G_2(U(t)) &= \cos\left(4\phi(t)t\right) + 2\cos\left(2\Gamma(t)\right) \end{aligned} \tag{6.16}$$

This means that $U(t)$ is locally equivalent to a CNOT when

$$\begin{aligned} \frac{1}{4} e^{-4i\phi(t)} \left(1 + e^{4i\phi(t)} \cos\left(2\Gamma(t)t\right)\right)^2 &= 0 \\ \cos\left(4\phi(t)t\right) + 2\cos\left(2\Gamma(t)\right) &= 1 \end{aligned} \tag{6.17}$$

Both equations in (6.17) are satisfied only when both

$$\begin{aligned} \Gamma(t) &= 0 \mod \pi \\ \phi(t) &= \pi/4 \mod \pi/2. \end{aligned} \tag{6.18}$$

This requires that

$$\frac{J_{zz}}{|\gamma|} = \frac{1+2m}{4n} \tag{6.19}$$

for integers m and n, or that $\gamma = 0$, in which case $\mathcal{H} = J_{zz}\sigma_1^z\sigma_2^z$ and a gate locally equivalent to U_{CNOT} evolves when $\phi(t) = \pi/4$, a well-known result [90]. For superconducting qubits, the relative sizes of the coupling constants in $J_{\mu\nu}$ depend on the physical architecture of the quantum circuit as well as details of circuit fabrication. Obtaining the exact ratio in Eqn. (6.19) is very restrictive and not satisfying as a general approach to gate design. It does, however, give us some useful information: A general interaction Hamiltonian $\mathcal{H}$ only generates a $U(t)$ locally equivalent to a CNOT in special cases.

An alternate approach to evolving the target gate will be required. So far we have only explored the possibility of performing a 'single shot' CNOT, by which only one entangling pulse is applied. Instead, we can look for 'two shot solutions', by which

$$U_{\text{T}} \sim U_{\text{ent}} \cdot \mathcal{R} \cdot U_{\text{ent}} \tag{6.20}$$

where U_{ent} is the time evolution generated by $U(t)$ after some time t. Makhlin's result does not help us with this problem besides giving a numerical way to search over all possible times t and single qubit rotations $\mathcal{R}$ for solutions to Eqn. (6.20). In the next section, we explore a more intuitive, geometric approach.

6.3.2 Cartan Deomposition

To gain geometric insight into the theory of two qubit gates, we turn to Lie algebra theory to better describe the group SU(4), a subgroup of U(4) in which all elements have determinant 1. Any element of U(4) can be transformed to an element in SU(4) by multiplication of an

overall phase, so we do not lose any of the physically observable behavior of U(4) by making this simplification. A convenient representation of the Lie algebra $\mathfrak{su}(4)$ that generates the Lie group SU(4) is the set of 15 tensor products of Pauli matrices that form a basis for $J_{\mu\nu}$ (the identity is excluded).

As introduced to the field of quantum computation by Khaneja and Glaser in 2001 [60, 59], the Lie algebra $\mathfrak{su}(4)$ can be written as the direct some of two subalgebras,

$$\mathfrak{su}(4) = \mathfrak{l} \oplus \mathfrak{p} \tag{6.21}$$

where

$$\begin{aligned} \mathfrak{l} = \mathfrak{su}(2) \otimes \mathfrak{su}(2) &= \text{span}\{\sigma_1^x, \sigma_1^y, \sigma_1^z, \sigma_2^x, \sigma_2^y, \sigma_2^z\} && (6.22) \\ \mathfrak{p} = \mathfrak{su}(4)/\mathfrak{su}(2) \otimes \mathfrak{su}(2) &= \text{span}\{\sigma_1^x \otimes \sigma_2^x, \sigma_1^x \otimes \sigma_2^y, \sigma_1^x \otimes \sigma_2^z, \\ &\qquad \sigma_1^y \otimes \sigma_2^x, \sigma_1^y \otimes \sigma_2^y, \sigma_1^y \otimes \sigma_2^z, \\ &\qquad \sigma_1^z \otimes \sigma_2^x, \sigma_1^z \otimes \sigma_2^y, \sigma_1^z \otimes \sigma_2^z, \}. && (6.23) \end{aligned}$$

The subalgebra $\mathfrak{l}$ generates single qubit rotations, while the subalgebra $\mathfrak{p}$ generates entanglement between the qubits. Because the subalgebras $\mathfrak{l}$ and $\mathfrak{p}$ obey certain commutation relations,

$$[\mathfrak{l}, \mathfrak{l}] \subset \mathfrak{l}, \;\; [\mathfrak{p}, \mathfrak{l}] \subset \mathfrak{p}, \;\; [\mathfrak{p}, \mathfrak{p}] \subset \mathfrak{l}, \tag{6.24}$$

any maximal abelian (commuting) subalgebra of $\mathfrak{p}$ is a *Cartan subalgebra* of $\mathfrak{su}(4)$. Suppose $\mathfrak{a} \subset \mathfrak{p}$ is a Cartan subalgebra. For our purposes, a particularly useful property of Cartan subalgebras is that any $U \in \text{SU}(4)$ can be written as

$$U = \mathcal{R}^1 \cdot A \cdot \mathcal{R}^2 \tag{6.25}$$

where $\mathcal{R}^{1,2}$ are generated by $\mathfrak{l}$ and A is generated by $\mathfrak{a}$ [48].

There are several 3-element Cartan subalgebras in $\mathfrak{p}$. We choose one that contains generators most often found in physical Hamiltonians,

$$\mathfrak{a} \equiv \text{span}\{\sigma_1^x \otimes \sigma_2^y, \sigma_1^y \otimes \sigma_2^y, \sigma_1^z \otimes \sigma_2^z\}. \tag{6.26}$$

In this case, the Cartan decomposition of Eqn. (6.25) translates to every $U \in \mathrm{SU}(4)$ being locally equivalent to an A of the form

$$A(x, y, z) \equiv e^{-i(x\sigma_i^x \otimes \sigma_j^x + y\sigma_i^y \otimes \sigma_j^y + z\sigma_i^z \otimes \sigma_j^z)}. \tag{6.27}$$

This is a very powerful statement, as it says that only three entangling generators are needed to describe an arbitrary U, even though there are a total of 9 entangling generators in $\mathfrak{su}(4)$. Furthermore, every U can be mapped to a point in a 3-dimensional space by assigning to it the point (x, y, z) of its corresponding $A(x, y, z)$. This mapping from U to the 3d 'space of entanglers' is not unique, however. Not only do the variables x, y, and z have the 2π periodicity in x, y and z that we may expect, but there are several other ways that one can change A non-trivially by single qubit rotations. For example,

$$R_x(-\pi)A(x, y, z)R_x(\pi) = A(x, -y, -z); \tag{6.28}$$

therefore,

$$A(x, y, z) \sim A(x, -y, -z), \tag{6.29}$$

and any gate locally equivalent to $A(x, y, z)$ will also be locally equivalent to $A(x, -y, -z)$. This means that a given U is locally equivalent to many $A(x, y, z)$. For a full discussion of the geometry of the group generated by $\mathfrak{a}$, see Refs. [129, 130]. There is a continuous subspace of the full space of entanglers, called the Weyl chamber, that does have a one-to-one correspondence with the local equivalence classes of SU(4). While this is a beautiful result, allowing $U(t)$ to evolve outside of this subspace is more useful for gate design.

6.4 The Space of Entanglers

The theories of Makhlin invariance combined with Cartan decomposition give us powerful intuition toward gate design. Given a target gate U_{T}, it is not often easy to identify which $A(x, y, z)$ to which it corresponds. In [129], a very useful relationship is given between the Makhlin invariants, which can be calculated directly from U_{T}, and the arguments x, y, and

z of an equivalent A:

$$\begin{aligned} G_1 &= \cos^2(2x)\cos^2(2y)\cos^2(2z) - \sin^2(2x)\sin^2(2y)\sin^2(2z) \\ &\quad + \frac{i}{4}\sin(4x)\sin(4y)\sin(4z) \\ G_2 &= 4\cos^2(2x)\cos^2(2y)\cos^2(2z) - 4\sin^2(2x)\sin^2(2x)\sin^2(2z) \\ &\quad - \cos(4x)\cos(4y)\cos(4z) \end{aligned} \tag{6.30}$$

For example, if U_{T} is the CNOT gate, then it is straightforward to calculate the Makhlin invariants $G_1 = 0$ and $G_2 = 1$. By inspection of Eqn. (6.30), it can be seen that

$$U_{\mathrm{CNOT}} \sim A\left(\pm\frac{\pi}{4}, 0, 0\right) \sim A\left(0, \pm\frac{\pi}{4}, 0\right) \sim A\left(0, 0, \pm\frac{\pi}{4}\right). \tag{6.31}$$

These A values correspond to the green dots in the space of entanglers shown in Fig. 6.1. In the following sections, gate design is outlined for differing conditions on J, J' and J_{zz}.

Case 1: $J' = 0 \neq J$:

In this case,

$$\mathcal{H} = g_{ij}(t)\left[J(\sigma_1^x \otimes \sigma_2^x + \sigma_1^y \otimes \sigma_2^y) + J_{\mathrm{zz}}\sigma_1^z \otimes \sigma_2^z\right], \tag{6.32}$$

which is in the Cartan subalgebra $\mathfrak{a}$. Because each of the terms in $\mathcal{H}$ commute,

$$U(t) = \mathcal{T} e^{-\frac{i}{\hbar}\int_{t_0}^{t} g_{ij}(t)\left[J(\sigma_1^x\otimes\sigma_2^x + \sigma_1^y\otimes\sigma_2^y), + J_{\mathrm{zz}}\sigma_1^z\otimes\sigma_2^z)\right]dt} \tag{6.33}$$

corresponds to the trajectory $\mathbf{r}(t) = (x(t), y(t), z(t))$ where

$$\begin{aligned} x(t) = y(t) &= \int_{t_0}^{t} g_{ij}(\tau) J d\tau = J \cdot G(t) \\ z(t) &= \int_{t_0}^{t} g_{ij}(\tau) J_{\mathrm{zz}} d\tau = J_{\mathrm{zz}} \cdot G(t). \end{aligned} \tag{6.34}$$

$G(t) \equiv \int_{t_0}^{t} g_{ij}(t')dt'$ is the area swept out by the coupling strength. In the common situation where g is time independent, $G(t) = gt$. $\mathbf{r}(t)$ traces the black line in Fig. 6.1, which starts from the origin (the identity) and naturally follows the line $x = y = z\tan\theta$ where $\theta = \tan^{-1}(J/J_{\mathrm{zz}})$

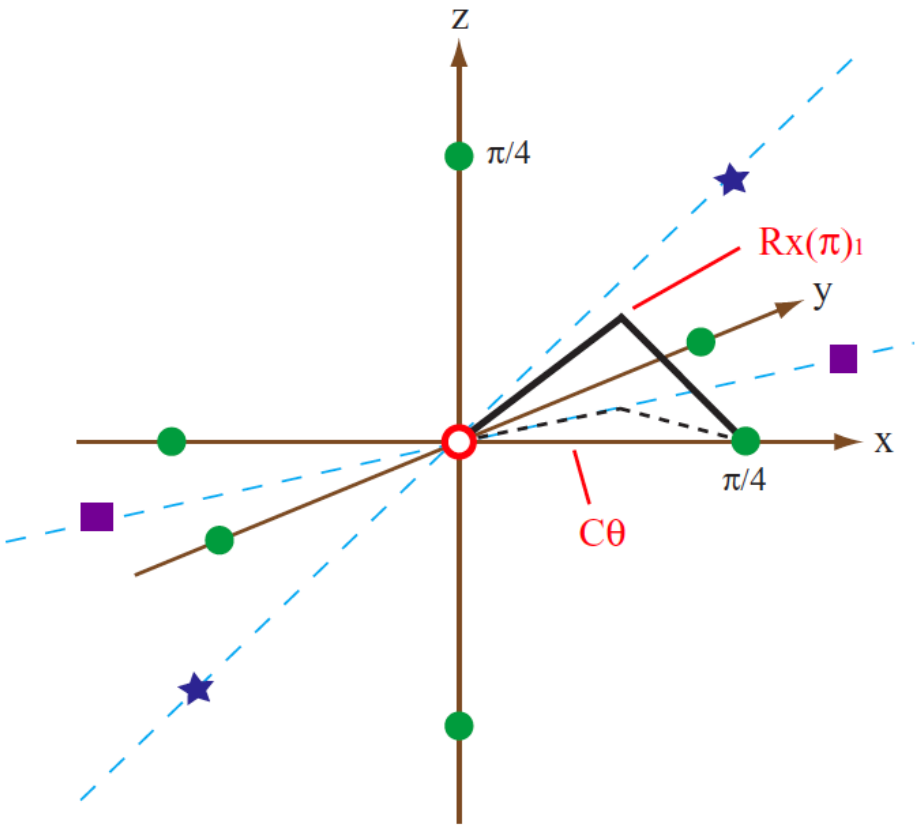

Figure 6.1: The 'space of entanglers.' Green points correspond to entanglers that are locally equivalent to a CNOT. The blue stars are locally equivalent to the swap gate, and the purple squares are locally equivalent to SWAP×CNOT. The black curve represents a possible trajectory corresponding to Schrodinger evolution with $J' = 0$. A π-puse is applied at $A\left(\frac{\pi}{8}, \frac{\pi}{8}, z\right)$ to 'refocus' the trajectory back the x-axis.

.

is the angle taken from the z-axis. In order for $\mathbf{r}(t)$ to intersect a green dot (indicating $U(t)$ is locally equivalent to a CNOT), the special condition given in Eqn. (6.19) is required.

Alternatively, the path of $U(t)$ can be turned by inserting a single qubit rotation. Recall that a 'π-pulse' applied one of the qubits before and after the entangler $A(x, y, z)$ produces the entangler $A(x, -y, -z)$, as shown in Eqn. (6.28). Suppose a time evolution operator $U(t)$

sweeps out a line $\mathbf{r}(t)$ in the space of entanglers, indicated by the correspondence

$$U(t) \leftrightarrow \mathbf{r}(t) = (x(t), y(t), z(t)). \tag{6.35}$$

If a π-pulse is applied on one of the qubits before and after evolution by $U(t)$, the resulting path in the space of entanglers is the reflection of $\mathbf{r}(t)$ over the x-axis:

$$\mathcal{R}_{\mathrm{x}}(-\pi)_i U(t) \mathcal{R}_x(\pi)_i \leftrightarrow \mathbf{r}'(t) = (x(t), -y(t), -z(t)). \tag{6.36}$$

The combined effect of evolution by $U(t)$ followed by $\mathcal{R}_{\mathrm{x}}(\pi)_i U(t) \mathcal{R}_x(\pi)_i$ is to reach a point exactly on the x-axis:

$$\mathcal{R}_{\mathrm{x}}(-\pi)_i U(t) \mathcal{R}_x(\pi)_i U(t) \leftrightarrow \mathbf{r}'(t) + \mathbf{r}(t) = (2x(t), 0, 0). \tag{6.37}$$

By this sequence with $G(t) = \pi/8J$, the trajectory in the space of entanglers ends exactly at the point $\left(\frac{\pi}{4}, 0, 0\right)$, which corresponds to a net time evolution that is locally equivalent to the CNOT.

Note that if the angle θ had been less that $\pi/4$, in other words $J_{\mathrm{zz}} > J$, then $G(t_z) = \pi/8J_{\mathrm{zz}}$ for a $t_z < t$. In other words, a gate locally equivalent to a CNOT could be implemented faster by applying the π-pulses about the z-axis and turning the trajectory toward the point $\left(0, 0, \frac{\pi}{4}\right)$, which is also locally equivalent to a CNOT.

Case 2: $J = J' = 0$:

When $J = J' = 0$, $\mathcal{H} = g_{ij}(t) J_{\mathrm{zz}} \sigma_1^z \otimes \sigma_2^z$, so

$$U(t) = e^{-\frac{i}{\hbar} J_{\mathrm{zz}} \int_{t_0}^{t} g_{ij}(t') dt'} \leftrightarrow \left(0, 0, \frac{\pi}{4}\right) \tag{6.38}$$

after $G(t) = \pi/4J_{\mathrm{zz}}$. This is the well known Ising case, mentioned before.

Case 3: $J = 0 \neq J'$:

Note that $\sigma_1^x \otimes \sigma_2^y, \sigma_1^y \otimes \sigma_2^z, \sigma_1^z \otimes \sigma_2^z$ also form a Cartan subalgebra where (6.31) holds. The result from Case 1 is therefore applicable, with the modification that $G(t) = \pi/8J'$ when $J' > J_{\mathrm{zz}}$.

Case 4: $J \neq 0$ and $J' \neq 0$

In this case, the phase of γ, $\varphi \equiv \arg(J + iJ')$, is nonzero. The identity

$$R_z(-\varphi)_2 U(t) R_z(\varphi)_2 = A(\Gamma(t), \Gamma(t), \phi(t)) \tag{6.39}$$

tells us that the following gate sequence

$$R_z(-\varphi)_2 R_x(-\pi)_1 U(t) R_x(\pi)_1 U(t) R_z(\varphi)_2 \leftrightarrow \left(\frac{\pi}{4}, 0, 0\right) \tag{6.40}$$

produces a gate locally equivalent to a CNOT when $\Gamma(t) = |\gamma| \cdot G(t) = \pi/8\cdot$.

6.5 A General CNOT

The procedure for gate design applied to U_{CNOT} described in the last section can be summarized as follows: Define t so that $G(t) = \pi/8|\gamma|$. Execute the gate sequence

$$\begin{aligned} U_{\mathrm{ent}} &\equiv R_z(-\varphi)_2 R_x(-\pi)_1 U(t) R_x(\pi)_1 U(t) R_z(\varphi)_2 \\ &\sim A\left(\frac{\pi}{4}, 0, 0\right) \end{aligned} \tag{6.41}$$

which produces a gate that is locally equivalent to a CNOT. The canonical CNOT can be obtained exactly with the following pre- and post- single qubit rotations and overall phase:

$$U_{\mathrm{CNOT}} = e^{i\frac{3\pi}{4}} \left[\mathcal{R}_y\left(-\frac{\pi}{2}\right)_1 \otimes \mathcal{R}_x\left(-\frac{\pi}{2}\right)_2\right] \cdot U_{\mathrm{ent}} \cdot \mathcal{R}_y\left(\frac{\pi}{2}\right)_1. \tag{6.42}$$

This generalization includes all but the second case above, the Ising limit. In this case, after a time t defined so that $G(t) = \pi/4J_{\mathrm{zz}}$, the system evolves $A\left(0, 0, \frac{\pi}{4}\right)$ exactly, which is related to the CNOT gate according to

$$U_{\mathrm{CNOT}} = e^{-i\frac{\pi}{4}} H_2 \left[\mathcal{R}_z\left(-\frac{\pi}{2}\right)_1 \otimes \mathcal{R}_z\left(-\frac{\pi}{2}\right)_2\right] \cdot A\left(0, 0, \frac{\pi}{4}\right) \cdot H_2. \tag{6.43}$$

Another member of our group, Joydip Ghosh, has investigated the numerical accuracy of this general approach with differing J, J', and J_{zz} values in Ref. [42]

6.6 An Alternative to CNOT

Local equivalence simplifies the analysis of two qubit gates by removing the effect of single qubit rotations which are straightforward to perform experimentally. There is a two qubit operation that is simple to perform at the level of compiling a gate sequence, namely, the action of swapping two qubits. This is implemented simply by swapping the labels of the qubits. The action of swapping qubits is equivalent to the unitary transformation

$$U_{\text{swap}} \equiv \begin{pmatrix} 1 & 0 & 0 & 0 \\ 0 & 0 & 1 & 0 \\ 0 & 1 & 0 & 0 \\ 0 & 0 & 0 & 1 \end{pmatrix}. \tag{6.44}$$

When searching for an implementation of a particular U_{T}, one may also search for that target gate before and after swapping. For the case of CNOT, the points corresponding to

$$\begin{aligned} &\text{CNOT} \times \text{SWAP} \\ &\text{SWAP} \times \text{CNOT} \end{aligned} \tag{6.45}$$

(which are locally equivalent to each other) are indicated by purple squares in Fig. 6.1. In the case that $J' = J_{\text{zz}} = 0$,

$$U(t) = A\left(\frac{\pi}{4}, \frac{\pi}{4}, 0\right) \sim \text{SWAP} \times \text{CNOT} \sim \text{CNOT} \times \text{SWAP} \tag{6.46}$$

after $G(t) = \pi/4 \cdot J$. The canonical SWAP$\times$CNOT can be obtained by the following sequence of pre- and post- single qubit rotations:

$$\begin{aligned} \text{SWAP} \times \text{CNOT} &= i\left[\mathcal{R}_x\left(\frac{\pi}{2}\right)_1 \otimes \mathcal{R}_x\left(\frac{\pi}{2}\right)_2\right] \cdot \left[\mathcal{R}_y\left(\frac{\pi}{2}\right)_1 \otimes \mathcal{R}_y\left(\frac{\pi}{2}\right)_2\right] \mathcal{R}_x\left(\frac{\pi}{2}\right)_2 \\ &\times A\left(\frac{\pi}{4}, \frac{\pi}{4}, 0\right) \cdot \mathcal{R}_y\left(-\frac{\pi}{2}\right)_2. \end{aligned} \tag{6.47}$$

The canonical CNOT can be obtained by from the SWAP $\times$ CNOT by simply relabeling the qubits.

Chapter 7

QUANTUM SIMULATION OF MOLECULAR COLLISIONS WITH SUPERCONDUCTING QUBITS

[0]Pritchett, E. J., C. Benjamin, A. Galiautdinov, M. R. Geller, A. T. Sornborger, P. C. Stancil and J. M. Martinis. Submitted to *Physical Review Letters*, 07/08/2010.

Quantum simulation algorithms can significantly reduce the resources necessary to simulate quantum mechanical systems [32]. Typically, these algorithms construct the simulated system's time evolution operator, energies and/or eigenstates from a universal set of gates [70, 29, 121, 128, 16, 1, 123, 17, 109, 56, 5, 67, 30]. Alternatively, ultracold atoms, trapped ions, and liquid-state NMR have directly emulated the time evolution of certain other quantum systems [44, 115, 68, 33, 108]. Recent experimental progress suggests that quantum simulation will be one of the first practical applications of quantum computation [67, 30, 44, 115, 68, 33, 108, 15].

In principle, an n-qubit quantum computer can store the state of any $N = 2^n$ dimensional quantum system, an exponential reduction in the resources necessary to store quantum information on a classical computer. However, simulation may require $\sim N^2 = 2^{2n}$ elementary gates per time step unless the simulated Hamiltonian has special properties, e.g. locality [8, 70, 29]. Even for these special Hamiltonians, fully digital quantum simulation often requires an excessive number of gates for current quantum computing technology [17, 56, 5].

In this Letter, we show that a subspace of a tunable n-qubit quantum computer can emulate an arbitrary n-dimensional quantum system, trading an exponential reduction in resources for simulations of a wider variety of Hamiltonians. This subspace simulates other quantum systems very different from the computer itself in an amount of time that is independent of n. By comparison, classical simulation of an n-dimensional quantum system requires $\sim n^3$ elementary operations per time step. While the most efficient quantum simulation algorithms offer an exponential reduction in both qubits and elementary operations, they typically apply to specific, fundamental time-independent Hamiltonians, or those already similar to that of the computer itself. We show that with a more modest polynomial reduction in resources, a subspace of a tunable quantum computer can simulate any real, time-dependent Hamiltonian.

We begin by outlining the theory behind our approach to simulation. To this effect, we identify an n-dimensional invariant subspace suitable for quantum simulation. Then we define

a time dependent energy/time rescaling that maximizes the speed of the simulation within the constraints of the quantum computer. Finally, we explicitly give the control parameters of the quantum computer as a function of the matrix elements of $H_{\rm s}(t)$.

This theory is tested by performing a simulation of a molecular collision with a circuit of tunably coupled Josephson phase qubits. Molecular collisions and electronic structure calculations are widely studied as important applications of quantum simulation techniques [56, 5, 30]. We show in detail how a superconducting circuit of three tunably coupled Josephson phase qubits simulates a three channel Na-He collision. Finally, we discuss the relationship between simulation fidelity and total simulation time for this particular example.

An n-Dimensional Subspace of the full quantum computer's Hilbert space, $\mathcal{H}$, can emulate another quantum system at all times only if it is invariant to the time evolution generated by the computer's Hamiltonian $H_{\rm qc}$ (so that the subspace is well-isolated from the rest of $\mathcal{H}$ and evolves unitarily). We model $H_{\rm qc}$ as

$$H_{\rm qc}(t) = \sum_{i=1}^{n} -\frac{\epsilon_i(t)}{2}\sigma_i^z + \frac{1}{2}\sum_{i\neq j} g_{ij}(t) J_{\mu\nu}\sigma_i^\mu \otimes \sigma_j^\nu, \tag{7.1}$$

where $\mu, \nu \in \{0, 1, 2, 3\}$ are summed over. $\epsilon_i(t)$ are the uncoupled qubit energies and $g_{ij}(t) = g_{ji}(t)$ are the pairwise qubit interaction strengths, both of which may in general be time-dependent. $J_{\mu\nu}$ is a 4×4 tensor that describes the time-independent structure of the qubit interaction which is determined by the computer's architecture, as explained in detail in Chapter 5.

In the weak coupling limit, $|g_{ij}||J_{\mu\nu}||/\epsilon_i \ll 1$, subspaces of $\mathcal{H}$ are invariant to time evolution generated by $H_{\rm qc}$ if spanned by computational basis states having the same number of excited (tunable) qubits. The 'single excitation subspace', denoted as $\mathcal{H}_n$, is an n-dimensional invariant subspace spanned by $|i\rangle_n \equiv |00..01_i..0_n\rangle$ for all $i = 1, 2..., n$.

The control parameters $\epsilon_i(t)$ and $g_{ij}(t)$ directly control the Hamiltonian that $\mathcal{H}_n$ simulates. We define H_n as $H_{\rm qc}$ projected into the single excitation subspace,

$$H_n(t) \equiv P H_{\rm qc}(t) P^\dagger \tag{7.2}$$

where P is an $n \times 2^n$ dimensional operator that projects $\mathcal{H}$ onto $\mathcal{H}_n$. Up to an additive energy shift, H_n has matrix elements

$$H_n^{ij}(t) \equiv \begin{cases} \epsilon_i(t) - \alpha \sum_{k \neq i} g_{ik}(t), \ i = j \\ g_{ij}(t), \ i \neq j \end{cases} \tag{7.3}$$

with $\alpha \equiv 2(J_{zo} + J_{zz})$. We assume $J_{xx} + J_{yy} \neq 0$ and normalize $J_{\mu\nu}$ so that $J_{xx} + J_{yy} = 1$. In the weak coupling limit, $\mathcal{H}_n$ is approximately invariant and generated by H_n:

$$\begin{aligned} U_n(t) &\equiv P U_{\rm qc}(t) P^\dagger \\ &\simeq \mathcal{T} e^{-\frac{i}{\hbar}\int_0^t H_n(t')dt'} \end{aligned} \tag{7.4}$$

where $\mathcal{T}$ is the time-ordering operator. H_n generates U_n exactly when no matrix elements of $H_{\rm qc}$ mix $\mathcal{H}_n$ with the rest of $\mathcal{H}$ (i.e. $J_{0x} = J_{0y} = J_{zx} = J_{zy} = 0$). The $(n^2+n)/2$ parameters $\epsilon_i(t)$ and $g_{ij}(t)$ independently control each of the $(n^2+n)/2$ matrix elements of the real H_n and can therefore be used to simulate any arbitrary, real Hamiltonian in $\mathcal{H}_n$.

While we can simulate H_s in $\mathcal{H}_n$ by choosing $\epsilon_i(t)$ and $g_{ij}(t)$ so that $H_n(t) = H_{\rm s}(t)$ for all t, a direct mapping between Hamiltonians limits the computer to simulating other quantum systems with similar energy scales over lengths of time within the computer's coherence time. Fortunately, simulation of $H_{\rm s}$ only requires equality up to an overall phase between U_n and the time evolution operator generated by $H_{\rm s}$:

$$\begin{aligned} U(t) &\equiv \mathcal{T} e^{-\frac{i}{\hbar}\int_{t_{\rm i}}^t H_{\rm s}(t')dt'} \\ &= e^{i\phi(t)} U_n(t_{\rm qc}(t)). \end{aligned} \tag{7.5}$$

The time elapsed on the quantum computer, $t_{\rm qc}(t)$, is a strictly increasing function of simulated time t, admitting a much less restrictive relationship between Hamiltonians:

$$H_{\rm s}(t) + c(t) = \lambda(t) H_n(t_{\rm qc}(t)). \tag{7.6}$$

$c(t)$ is a time-dependent, additive energy shift giving the overall phase difference $\phi(t) = \frac{1}{\hbar}\int_{t_{\rm i}}^t c(t')dt'$, and we have introduced a positive, time-dependent energy/time scaling

$$\lambda(t) \equiv dt_{\rm qc}/dt. \tag{7.7}$$

The energy/time scaling $\lambda(t)$ determines the speed of the simulation. By carefully minimizing $\lambda(t)$, we reduce the total simulation time and, consequently, the error due to decoherence. $\lambda(t)$ is bounded from below by experimental constraints on the allowed values of control parameters $\epsilon_i(t)$ and $g_{ij}(t)$ as well as their maximum rates of change. Suppose qubit interaction strengths can vary in a range $g_{ij}(t) \in [-g_{\max}, g_{\max}]$, and the uncoupled qubit energies can vary in a range $\epsilon_i(t) \in [\epsilon_{\min}, \epsilon_{\max}]$. For convenience, we define a simulated energy $E_i(t)$ analogous to $\epsilon_i(t)$ when diagonal contributions from qubit interactions are anticipated:

$$E_i(t) \equiv H_{\rm s}^{ii}(t) + \alpha \sum_{j \neq i} H_{\rm s}^{ij}(t). \tag{7.8}$$

Using this definition together with equations (3) and (6), we relate the control parameters of the quantum computer to the simulated energies in $H_{\rm s}(t)$:

$$\begin{aligned} g_{ij}(t) &= H_{\rm s}^{ij}(t)/\lambda(t) \\ \epsilon_i(t) &= [E_i(t) - c(t)]/\lambda(t). \end{aligned} \tag{7.9}$$

By choosing $c(t) = E_{\max}(t) - \lambda(t)\epsilon_{\max}$ where $E_{\max}(t)$ is the largest value obtained by the $E_j(t)$ at a particular t, we force each ϵ_i to be as large as possible and therefore minimize leakage out of $\mathcal{H}_n$.

Each of the computer's control parameters remains within its allowed range when $\lambda(t)$ is larger than $(n^2+n)/2$ energy ratios at all times:

$$\lambda(t) \geq \begin{cases} |H_{\rm s}^{ij}(t)|/g_{\max}, \ i \neq j \\ \Delta E_i(t)/\Delta\epsilon_{\max} \end{cases} \tag{7.10}$$

where $\Delta E_i(t) \equiv E_{\max}(t) - E_i(t)$ and $\Delta\epsilon \equiv \epsilon_{\max} - \epsilon_{\min}$. $\lambda(t)$ is also bounded by constraints on the speeds with which control parameters can change. Suppose $v_i^{\epsilon}(t_{\rm qc}) \equiv d\epsilon_i(t_{\rm qc})/dt_{\rm qc}$ and $v_{ij}^{g}(t_{\rm qc}) \equiv dg_{ij}(t_{\rm qc})/dt_{\rm qc}$ can never be larger in magnitude than $v_{\max}^{\epsilon}$ and $v_{\max}^{g}$ respectively. Then for all t,

$$v_{\max}^{g} \geq \frac{1}{\lambda^2}\left|\frac{dH_{\rm s}^{ij}(t)}{dt} - \frac{H_{\rm s}^{ij}(t)}{\lambda}\frac{d\lambda}{dt}\right| \tag{7.11}$$

(and similarly for $v^{\epsilon}_{\max}$).

To simulate $H_s(t)$ in $\mathcal{H}_n$, we first choose $\lambda(t)$ as small as both inequalities (10) and (11) allow, guaranteeing a fast simulation within the experimental constraints of the quantum computer. We integrate over $\lambda(t)$ to calculate $t_{\rm qc}$ as a function of t:

$$t_{\rm qc}(t) = \int_{t_{\rm i}}^{t} \lambda(t')dt' + t_{\rm qc}(t_{\rm i}). \tag{7.12}$$

With both $\lambda(t)$ and $t_{\rm qc}(t)$ known, we can explicitly map the matrix elements of $H_{\rm s}$ to the control parameters of the quantum computer:

$$\begin{aligned} \epsilon_i(t_{\rm qc}(t)) &= \epsilon_{\max} + \Delta E_i(t)/\lambda(t) \\ g_{ij}(t_{\rm qc}(t)) &= H_{\rm s}^{ij}(t)/\lambda(t). \end{aligned} \tag{7.13}$$

To demonstrate our theory in detail, we describe three Josephson phase qubits simulating a three-channel collision between a sodium and a helium atom. For three phase qubits with tunable inductive coupling,

$$H_{\rm qc}(t) = \sum_{i=1}^{3} -\frac{\epsilon_i(t)}{2}\sigma_i^z + \frac{1}{2}\sum_{i\neq j} g_{ij}(t)\hat{\Phi}_i \otimes \hat{\Phi}_j \tag{7.14}$$

where $\hat{\Phi}_i$ is defined in terms of the matrix elements $\varphi_{jk} = \langle j|\hat{\varphi}_i|k\rangle$ of the local Josephson phase operator in the computational basis of the ith qubit:

$$\hat{\Phi}_i \equiv \sigma_i^x + \frac{\varphi_{00}-\varphi_{11}}{2\varphi_{01}}\sigma_i^z + \frac{\varphi_{11}+\varphi_{00}}{2\varphi_{01}}\sigma_i^0. \tag{7.15}$$

Both the ϵ_i and the φ_{jk} depend on Φ_x, the externally applied flux through the superconducting circuit. External flux bias is quantified by a dimensionless parameter $s_i(t) = \Phi_x/\Phi_x^*$ where Φ_x^* is the qubit's critical flux bias, or alternatively, by the dimensionless well depth $\Delta U/\hbar\omega_p$ [22, 79]. We consider external bias values for which $s \in [.89, .90]$ and $\Delta U/\hbar\omega_p \in [13.7, 15.5]$. In this range, $\Delta\epsilon/h = 190$MHz while $\hat{\Phi}_i \simeq \sigma_i^1 + 11\sigma_i^0$ varies little. A tunable mutual inductance independently controls the couplings $g_{ij}(t)$ between each pair of qubits. We have assumed Josephson junction parameters $I_0 = 2.93\ \mu$A, $C = 1.52$ pF, and $L = 808$ pH.

An n-dimensional subspace can simulate a molecular collision only after we project the full, many-body Hamiltonian of the interacting electrons and nuclei into an n-dimensional basis. We construct the collision Hamiltonian from Born-Oppenheimer energies and nonadiabatic couplings calculated previously for three molecular channels: Na($3s$) + He($1s^2$) [$1\ ^2\Sigma^+$] and Na($3p$) + He($1s^2$)[$1\ ^2\Pi$; $2\ ^2\Sigma^+$] [69], labeled as $|1\rangle_{\rm s}$, $|2\rangle_{\rm s}$ and $|3\rangle_{\rm s}$ respectively. The energies are stored for fixed values of the internuclear distance R, which we assume takes straight-line trajectories in a standard semiclassical approximation: $R(t) = \sqrt{b^2 + v^2t^2}$ where v is the incoming particle's velocity and b is the impact parameter of the collision.

Figure 7.1 outlines our simulation protocol for $H_{\rm s}(t)$ describing a three-channel Na-He collision. The matrix elements of $H_{\rm s}(t)$ are displayed in Fig. 7.1(a) for a given semiclassical trajectory $R(t)$. Directly below, we plot the energy/time scaling parameter $\lambda(t)$ as a black curve enveloping the six energy ratios given in Eq. (10). A small $\lambda(t)$ speeds the quantum computer through times when the internuclear distance R is large, but as R decreases ($t \to 0$), a relatively small $g_{\rm max}$ value constrains the growing couplings. $\lambda(t)$ increases over two orders of magnitude, creating a highly nonlinear relationship between $t_{\rm qc}$ and t, as shown in Fig. 7.1(c). This effectively stretches the portion of the collision when internuclear distance is small over the entire simulation, as can be seen in the plot of the quantum computer's control parameters as a function of $t_{\rm qc}$ in Fig. 7.1(d).

To study the fidelity of the simulation, we compare the exact and simulated time evolution operators, $U(t)$ and $U_n(t_{\rm qc}(t))$ respectively, by plotting (in Fig. 7.2) transition probabilities out of $|1\rangle$:

$$P_{1i}(t) \equiv |\langle i|U(t)|1\rangle|^2. \tag{7.16}$$

Because the exact transition probabilities evolve differently with t than the simulated evolve with $t_{\rm qc}$, we define a time-dependent transition fidelity which accounts for time scaling,

$$F(t) \equiv |{}_{\rm s}\langle 1|U^\dagger(t)U_n(t_{\rm qc}(t))|1\rangle_n|^2, \tag{7.17}$$

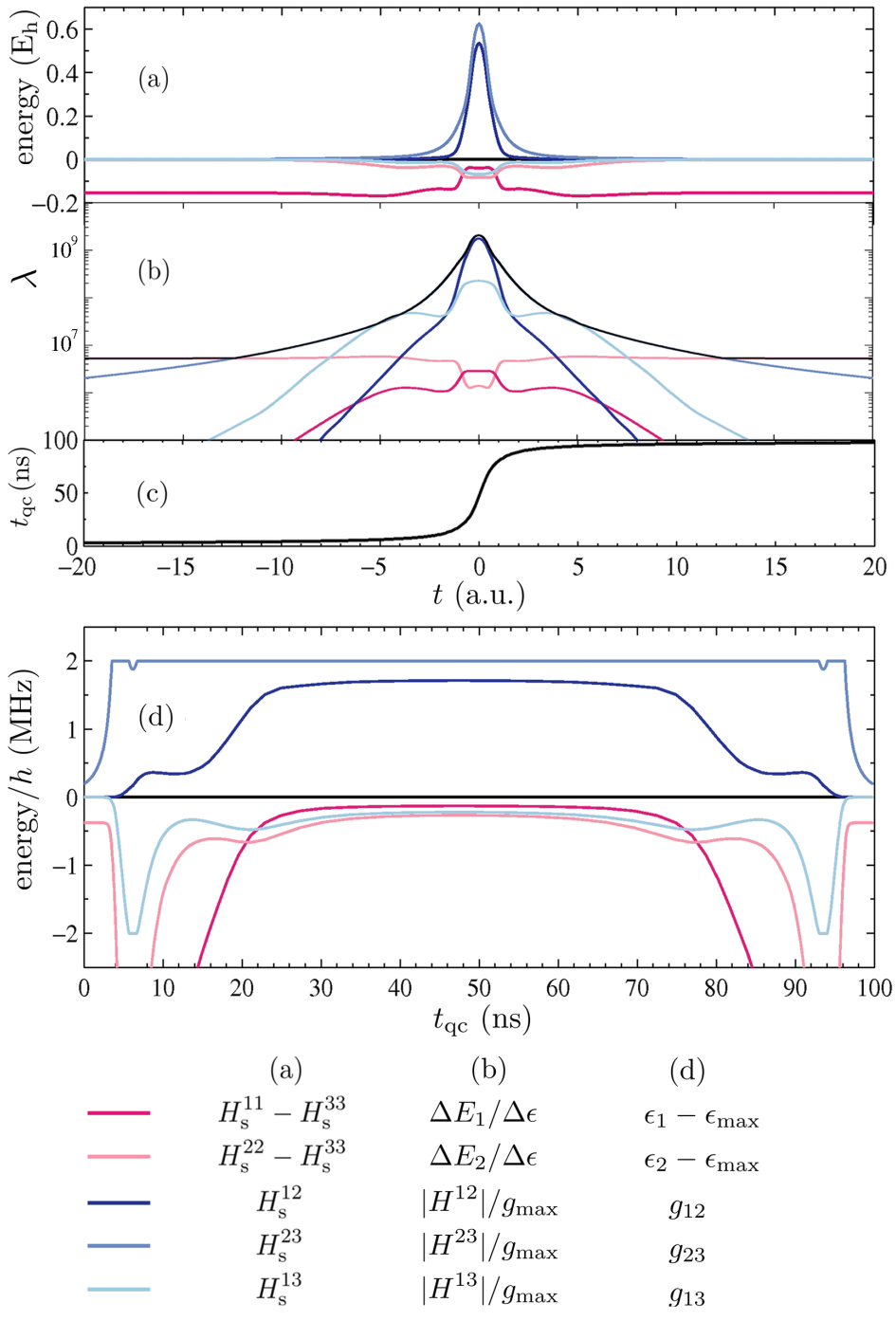

Figure 7.1: (color online) $H_{\rm s}(t)$ describes a three channel Na-He collision with $b = 0.5$ and $v = 1.0$. (a) Diagonal energy differences $H_{\rm s}^{ii} - H_{\rm s}^{33}$ and couplings $H_{\rm s}^{ij}$ $(i \neq j)$ are plotted as a function of time in atomic units. (b) The dimensionless time scaling parameter $\lambda(t)$ envelopes the six energy ratios $\Delta E_i/\Delta\epsilon$ and $|H_{\rm s}^{ij}|/g_{\rm max}$ ($\Delta E_3 = 0$ for all t). We assume $g_{\rm max}/h = 2.0$ MHz and $\Delta\epsilon_{\rm max}/h = 190$ MHz. (c) $t_{\rm qc}(t)$ plotted when $t_{\rm qc}(t_{\rm i}) = 0$, $t_{\rm i} = -40$ a.u.. (d) Control parameters g_{ij}/h and $(\epsilon_i - \epsilon_{\rm max})/h$ that simulate $H_{\rm s}(t)$ are plotted as a function of $t_{\rm qc}$ ($\epsilon_3 = \epsilon_{\rm max}$ for all $t_{\rm qc}$).

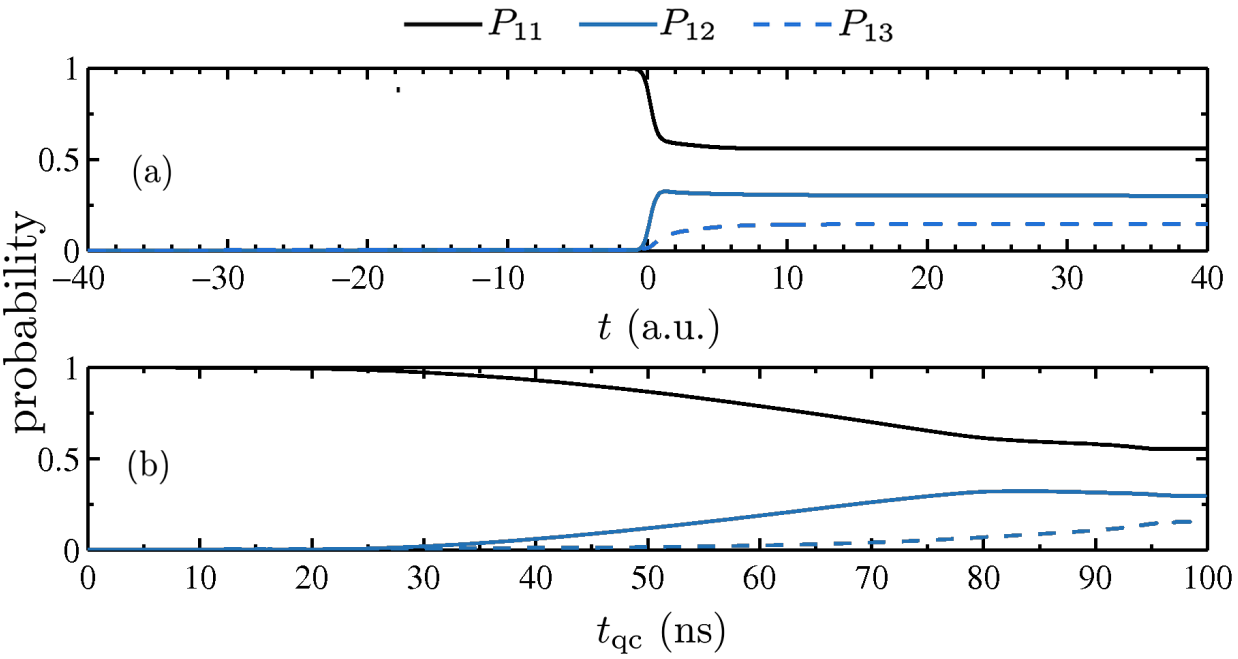

Figure 7.2: (upper) Exact transition probabilities generated by $H_{\rm s}(t)$ plotted in Fig. 7.1(a). (lower) Transition probabilities simulated with parameter profiles given in Fig. 7.1(d). Final simulation fidelity is .998.

and a time-dependent leakage out of $\mathcal{H}_n$,

$$L(t) \equiv \sum_{\perp} |{}_{\perp}\langle i|U_{\rm qc}(t_{\rm qc}(t))|1\rangle_n|^2 \tag{7.18}$$

where $\sum_{\perp}$ is the sum over all computational basis states $|i\rangle_{\perp}$ orthogonal to $\mathcal{H}_{\rm n}$. In the upper part of Fig. 7.3, fidelity and leakage are plotted together for four different $g_{\rm max}$ values.

Minimizing $g_{\rm max}||J_{\mu\nu}||/\epsilon_{\rm min}$, either by decreasing $g_{\rm max}$ or by increasing $\epsilon_{\rm min}$, reduces leakage and thus improves simulation fidelity. In this example, we find simulation fidelity more sensitive to the cutoff in $g_{\rm max}$ because leakage is most prominent when the interatomic distances are small ($t \to 0$) and the diabatic couplings between channels are the dominant terms. By reducing $g_{\rm max}$ we also increase $\lambda(t)$ and thus the total simulation time, as studied in the lower plot of Fig. 7.3. To increase fidelity from .9990 to .9999 we need to increase the simulation time by a factor of ~ 3, a relationship that is independent of n. While

not introducing specific models of decoherence, we note that high fidelity simulations are possible on superconducting qubits with coherence times around 100 ns.

When applied to molecular collisions, our approach to quantum simulation requires classical overhead to project the fundamental, time-independent, many-body Hamiltonian into an R-dependent, n-channel H_{s}. The quantities of physical interest, cross sections, are obtained by integrating the final transition probabilities over many semiclassical trajectories with different impact parameters, which requires no further classical overhead. A classical simulation of transition probabilities requires $\sim n^3$ elementary operations per time step for a single impact parameter, thus cross section calculations are computationally intensive for large n. Alternatively, simulation time is independent of n using our protocol, so once the R-dependent H_{s} has been calculated, cross sections can be obtained quickly.

In summary, we present a straightforward protocol for quantum simulation that can be implemented with currently available superconducting quantum computing technology. While a promising application of quantum computation, current quantum simulation protocols require a threshold number of gates and qubits that prohibits fully digital quantum simulations from being demonstrated on available quantum computers. However, we have shown how quantum computers of only a few qubits can simulate arbitrary quantum systems accurately and quickly even before they reach the regime of fault tolerant quantum computation.

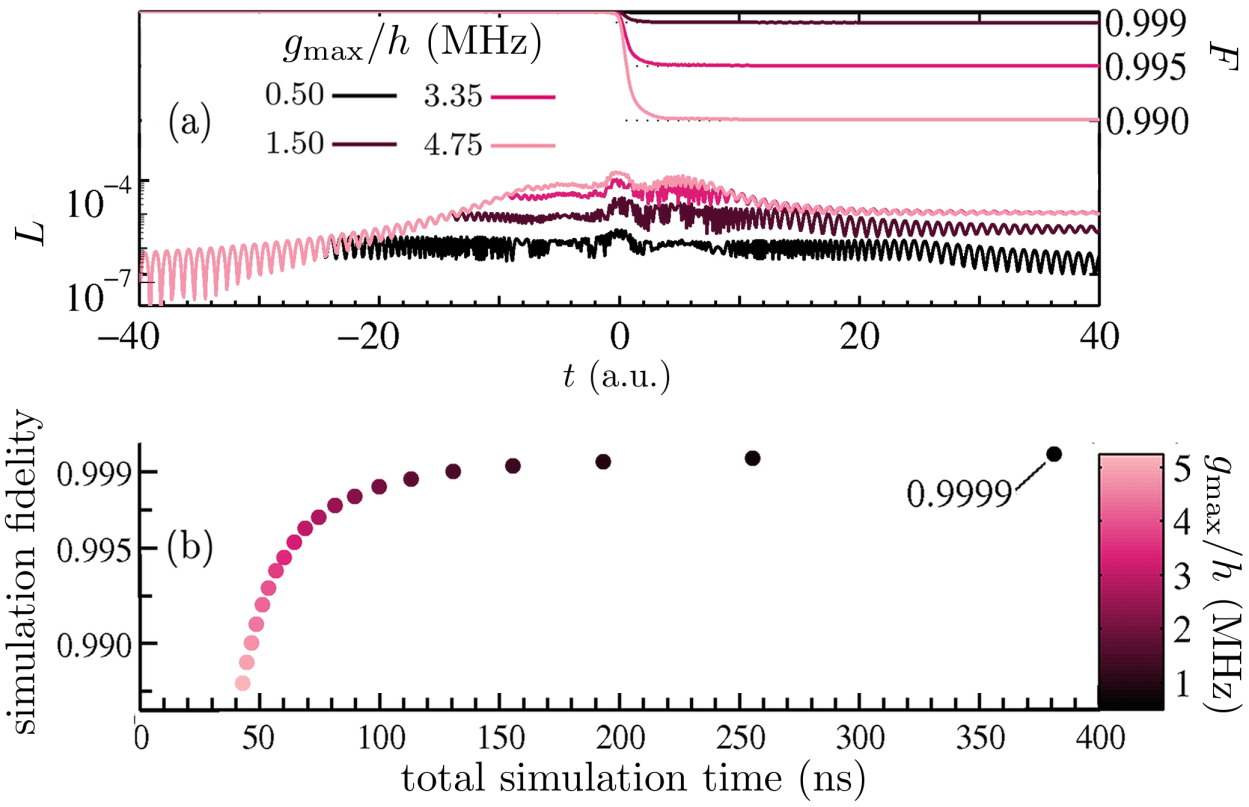

Figure 7.3: (upper) Fidelity and leakage as a function of simulation time for four different $g_{\max}$ values, all other parameters the same as in figure 1. (lower) Final simulation fidelity compared with total simulation time for varying $g_{\max}$. The $g_{\max}$ value referenced by the shade of the data point.

Bibliography

[1] D.S. Abrams and S. Lloyd: *Physical Review Letters* **79**, 'Simulation of Many-Body Fermi Systems on a Universal Quantum Computer,' 1997, p 2586.

[2] D. Aharonov, V. Jones, Z. Landau: 'A Polynomial Quantum Algorithm for Approximating the Jones Polynomial,' arXiv:quant-ph/0511096.

[3] M. Ansmann, H. Wang, R. C. Bialczak, M. Hofheinz, E. Lucero, M. Neeley, A. D. O'Connell, D. Sank, M. Weides, J. Wenner, A. N. Cleland, and J. M Martinis: *Nature* **461** 2009, 'Violation of Bell's Inequality in Josephson Phase Qubits,' p 504.

[4] A. D. Armour, M. P. Blencowe, and K. C. Schwab: *Physical Review Letters* **88** 2002, 'Entanglement and Decoherence of Micromechanical Resonator via Coupling to a Cooper-Pair Box,' 148301.

[5] A. Aspuru-Guzik, A. D. Dutoi, P. J. Love, M. Head-Gordon: *Science* **309** 2005, 'Simulated Quantum Computation of Molecular Energies,' p 1704.

[6] O. Astafiev, Y. A. Pashkin, Y. Nakamura, T. Yamamoto, and J. S. Tsai: *Physical Review Letters* **93** 2004, 'Quantum Noise in the Josephson Charge Qubit,' 267007.

[7] J. Bardeen, L. N. Cooper, and J. F. Schrieffer: *Physical Review* **108** 1957, 'Theory of Superconductivity,' p 1175.

[8] A. Barenco, C. Bennett, R. Cleve, D. P. DiVincenzo, N. Margolus, P. Shor, T. Sleator, J. A. Smolin, and H. Weinfurter: *Physical Review A* **52** 1995, 'Elementary Gates for Quantum Computation,' p 3457.

[9] A. J. Berkley, H. Xu, R. C. Ramos, M. A. Gubrud, F. W. Strauch, P. R. Johnson, J. R. Anderson, A. J. Dragt, C. J. Lobb, and F. C. Wellstood: *Science* **300** 2003, 'Entangled Macroscopic Quantum States in Two Superconducting Qubits,' p 1548.

[10] P. Bertet, I. Chiorescu, G. Burkard, K. Semba, C. J. P. M. Harmans, D. P DiVincenzo, and J. E. Mooij: *Physical Review Letters* **95** 2005, 'Dephasing of a Superconducting Qubit Induced by Photon Noise,' 257002.

[11] R. C. BIalczak, M. Ansmann, M. Hofheinz, E. Lucero, M. Neeley, A. D. O'Connell, D. Sank, H. Wang, J. Wenner, M. Steffen, A. N. Cleland, and J. M. Martinis: *Nature Physics* **6** 2010, 'Quantum Process Tomography of a Universal Entangling Gate Implemented with Josephson Phase Qubits,' p 409.

[12] A. Blais, R.-S. Huang, A. Wallraff, S. M. Girvin, and R. J. Schoelkopf: Phys. Rev. A **69** 2004, 'Cavity Quantum Electrodynamics for Superconducting Electrical Circuits: An Architecture for Quantum Computation,' 062320

[13] A. Blais, A. M. van den Brink, A. M. Zagoskin: *Physical Review Letters* **90** 2003: 'Tunable Coupling of Superconducting Qubits,' 127901.

[14] M. P. Blencowe: *Physics Reports* **395** 2004, 'Quantum Electromechanical Systems,' p 159.

[15] I. Buluta and F. Nori: *Science* **326** 2009, 'Quantum Simulators,' p 108.

[16] B. Boghosian and W. Taylor: arxiv:quant-ph 1997, 'Simulating Quantum Mechanics on a Quantum Computer,' quant-ph/9701019.

[17] Kenneth R. Brown, Robert J. Clark, and Isaac L. Chuang: *Physical Review Letters* **97** 2006, 'Limitations of Quantum Simulation Examined by Simulating a Pairing Hamiltonian Using Nuclear Magnetic Resonance,' 050504.

[18] O. Buisson and F. W. J. Hekking: Kluwer Academic Plenum Publishers 2001, 'Entangled States in a Josephson Charge Qubit Coupled to a Superconducting Resonator' in *Macroscopic Quantum Coherence and Computing*, edited by D. V. Averin, B. Ruggiero, and P. Silvestrini, p. 137.

[19] G. Burkard, D. Loss, and D. P. DiVincenzo: *Physical Review B* **59** 1999, 'Coupled Quantum Dots as Quantum Gates,' p 2070.

[20] J. M. Chow, J. M. Gambetta, L. Tornberg, J. Koch, L. S. Bishop, A. A. Houck, B. R. Johnson, L. Frunzio, S. M. Girvin, and R. J. Schoelkopf: *Physical Review Letters* **102** 2009, 'Randomized Benchmarking and Process Tomography for Gate Errors in a Solid-State Qubit,' 090502.

[21] J. I. Cirac and P. Zoller: *Physical Review Letters* **74** 1995, 'Quantum Computations with Cold Trapped Ions,' p. 4091.

[22] J. Clarke and F. K. Wilhelm: Nature 2008, 'Superconducting Quantum Bits,' p 1031.

[23] A. N. Cleland and M. R. Geller: *Physical Review Letters* **93** 2004, 'Superconducting Qubit Storage and Entanglement with Nanomechanical Resonators,' 070501.

[24] K. B. Cooper, M. Steffen, R. McDermott, R. W. Simmonds, S. Oh, D. A. Hite, D. P. Pappas, and J. M. Martinis: *Physical Review Letters* **93** 2004, 'Observation of Quantum Oscillations Between a Josephson Phase Qubit and a Microscopic Resonator Using Fast Readout,' 180401.

[25] M. H. Devoret and J. M. Martinis: *Quantum Information Processing* **3** 2004, 'Implementing Qubits with Superconducting Integrated Circuits,' No 1.

[26] M. H. Devoret, J. M. Martinis, and J. Clarke: *Physical Review Letters* **55** 1985, 'Measurements of Macroscopic Quantum Tunneling out of the Zero-Voltage State of a Current-Biased Josephson Junction,' p 1908.

[27] L. Dicarlo, J. M. Chow, J. M. Gambetta, L. S. Bishop, D. I. Schuster, J. Majer, A. Blais, L. Frunzio, S. M. Girvin, and R. J. Schoelkopf: *Nature* **460** 2009, 'Demonstration of Two-Qubit Algorithms with a Superconducting Quantum Processor,' p. 240.

[28] L. DiCarlo, M. D. Reed, L. Sun, B. R. Johnson, J. M. Chow, J. M. Gambetta, L. Frunzio, S. M. Girvin, M. H. Devoret, R. J. Schoelkopf, 'Preparation and Measurement of Three-Qubit Entanglement in a Superconducting Circuit,' arXiv: 1004.4324.

[29] J. Dodd, M. A. Nielsen, M. J. bremner, and R. T. Thew: *Physical Review A* **65** 2002, 'Universal Quantum Computation and Simulation Using any Entangling Hamiltonian and Local Unitaries,' 040301(R).

[30] J. Du, Nanyang Xu, X. Peng, P. Wang, S. Wu, D. Lu: *Phys. Rev. Lett.* **104** 2010, 'NMR Implementation of a Molecular Hydrogen Quantum Simulation with Adiabatic State Preparation,' 030502.

[31] T. Duty, D. Gunnarsson, K. Bladh, and P. Delsing: *Physical Review B* **69** 2004, 'Coherent Dynamics of Josephson Charge Qubit,' 140503.

[32] R. P. Feynman: *International Journal of Theoretical Physics* **21** 1982, 'Simulating Physics with Computers', p 467.

[33] A. Friedenauer, H. Schmitz, J. T. Glueckert, D. Porras, and T. Schaetz: *Nature Physics* **4** 2008, 'Simulating a Quantum Magnet with Trapped Ions,' p 757.

[34] J. Friedman, V. Patel, W. CHen, S. K. Topygo, and J. E. Lukens: *Nature* **406** 2000, 'Quantum Superposition of Distinct Macroscopic States,' p 43.

[35] A. Galiautdinov: *Physical Review A* **75** 2007, 'Generation of High-Fidelity Controlled-NOT Logic Gates by Coupled Superconducting Qubits,' 052303

[36] A. Galiautdinov: *Journal of Mathematical Physics* **48** 2007, 'Single-Step Controlled-NOT Logic from Any Exchange Interaction,' 112105.

[37] J. Gambetta, W. A. Braff, A. Wallraff, S. M. Girvin, and R. J. Schoelkopf: *Physical Review A* **76** 2007, 'Protocols for Optimal Readout of Qubits Using a Continuous Quantum Nondemolition Measurement,' 012325.

[38] M. R. Geller: World Scientific 2008, 'Quantum Computing with Electrical Circuits: Hamitonian Construction for Basic Qubit-Resonator Models' in *Condensed Matter Physics in the Prime of the 21st Century*, edited by Janusz Jedrezejewski, p 89.

[39] M. R. Geller: *Physical Review A* **71** 2005, 'Superconducting Qubits Coupled to Nano-electromechanical Resonators: An Architecture for Solid-State Quantum-Information Processing,' 032311.

[40] M. R. Geller, E. J. Pritchett, A. Galiautdinov, and J. M. Martinis: *Physical Review A* **81** 2010, 'Quantum Logic with Weakly Coupled Qubits,' 012320.

[41] M. R. Geller, E. J. Pritchett, A. T. Sornborger and F. K. Wilhelm: Springer 2006, 'Quantum Computing with Superconductors I: Architectures' in *Manipulating Quantum Coherence in Solid State Systems*, edited by M. E. Flatte and I. Tifrea, p 171.

[42] J. Ghosh and M. R. Geller: *Physical Review A* **81** 2010, 'CNOT Gate with Weakly Coupled Qubits: Dependence of Fidelity on Form of Interaction,' 052340.

[43] M. Grajcar, A. Izmalkov, E. Il'ichev, T. Wagner, N. Oukhanski, U. Hubner, T. May, I. Zhilyaev, H. E. Hoenig, Y. S. Greenberg, V. I. Snyrkov, D. Born, W. Krech, H.-G. Meyer, A. M. van den Brink: *Physical Review A* **69** 2004, 'Low Frequency Measurement of the Tunneling Amplitude in a Flux Qubit,' 060501(R).

[44] M. Greiner, O. Mandel, T. Esslinger, T. W. Hansch, and I. Bloch: *Nature* **415** 2002, 'Quantum Phase Transition from a Superfluid to a Mott Insulator in a Gas of Ultracold Atoms,' p 39.

[45] I. A. Grigorenko and D. V. Khveshchenko: *Physical Review Letters* **94** 2005, 'Robust Two-Qubit Quantum Registers,' 040506.

[46] I. A. Grigorenko and D. V. Khveshchenko: *Physical Review Letters* **95** 2005, 'Single-Step Implementation of Universal Quantum Gates,' 110501.

[47] L. K. Grover: *Physical Review Letters* **79** 1997, 'Quantum Mechanics Helps in Searching for a Needle in a Haystack,' p 325.

[48] S. Helgason: American Mathematical Society, Providence 1978, 'Differential Geometry, Lie Groups, and Symmetric Spaces.'

[49] M. Hofheinz, H. Wang, M. Ansmann, R. C. Bialczak, E. Lucero, M. Neeley, A. D. O'Connell, D. Sank, J. Wenner, J. M. Martinis, and A. N. Cleland: *Nature* **459** 2009, 'Synthesizing Arbitrary Quantum States in a Superconducting Resonator,' p 546.

[50] M. Hofheinz, E. M. Weig, M. Ansmann, R. C. Bialczak, E. Lucero, M. Neeley, A. D. O'Connell, H. Wang, J. M. Martinis, and A. N. Cleland: *Nature* **545** 2008, 'Generation of Fock States in a Superconducting Quantum Circuit,' p 310.

[51] A. A. Houck, J. Koch, M. H. Devoret, S. M. Girvin, R. J. Schoelkopf: cond-mat/0812.1865, 'Life After Charge Noise: Recent Results with Transmon Qubits.'

[52] A. A. Houck, J. A. Schreier, B. R. Johnson, J. M. Chow, J. Koch, J. M. Gambetta, D. I. Schuster, L. Frunzio, M. H. Devoret, S. M. Girvin, R. J. Schoelkopf: *Physical Review Letters* **101** 2008, 'Suppressing Charge Noise Decoherence in Superconducting Charge Qubits,' 080502.

[53] E. K. Irish and K. Schwab: *Physical Review B* **68** 2003, 'Quantum Measurement of a Coupled Nanomechanical Resonator–Cooper-Pair Box System,' 155311.

[54] J. Johansson, S. Saito, T. Meno, H. Nakano, M. Ueda, K. Semba, and H. Takayanagi: *Physical Review Letters* **96** 2006, 'Vacuum Rabi Oscillations in a Macroscopic Superconducting Qubit *LC* Oscillator System,' 127006.

[55] P. R. Johnson, F. W. Strauch, A. J. Dragt, R. C. Ramos, C. J. Lobb, J. R. Anderson, and F. C. Wellstood: *Physical Review B* **67** 2003, 'Spectroscopy of Capacitively Coupled Josephson-Junction Qubits,' 20509.

[56] I. Kassal, S. P. Jordan, P. J. Love, M. Mohseni, and A. Aspuru-Guzik: *Proceedings of the National Academy of Sciences of the United States of America* **105** 2008, 'Polynomial-Time Quantum Algorithm for the Simulation of Chemical Dynamics,' p 1868.

[57] N. Katz, M. Ansmann, R. C. Bialczak, E. Lucero, R. McDermott, M. Neeley, M. Steffen, E. M. Weig, A. N. Cleland, J. M. Martinis, and A. N. Korotkov: *Science* **312** 2006, 'Coherent State Evolution in a Superconducting Qubit from Partial-Collapse Measurement,' p 1498.

[58] N. Katz, M. Neeley, M. Ansmann, R. C. BIalczak, M. Hofheinz, E. Lucero, A. O'Connell, H. Wang, A. N. Cleland, J. M. Martinis, and A. N. Korotkov: *Physical Review Letters* **101** 2008, 'Reversal of the Weak Measurement of a Quantum State in a Superconducting Phase Qubit,' 200401.

[59] N. Khaneja, R. Brockett, and S. J. Glaser: *Physical Preview A* **63** 2001, 'Time Optimal Control in Spin Systems,' 032308.

[60] N. Khaneja, S. Glaser: *Chemical Physics* **267** 2001, 'Cartan Decomposition of $SU(2^n)$, Constructive Controllability of Spin Systems and Universal Quantum Computing,' p 11.

[61] J. S. Kline, H. Wang, S. oh, J. M. Martinis, and D. P. Pappas: *Superconductor Science and Technology* **22** 2009, 'Josephson Phase Qubit Circuit for the Evaluation of Advanced Tunnel Barrier Materials,' 015004.

[62] R. Knobel and A. N. Cleland: *Nature* **424** 2003, 'Nanometre-Scale Displacement Sensing Using a Single Electron Transistor,' p 291.

[63] J. Koch, T. M. Yu, J. M. Gambetta, A. A. Houck, D. I. Schuster, J. Majer, A. Blais, M. H. Devoret, S. M. Girvin, and R. J. SChoelkopf: *Physical Review A* **76** 2007, 'Charge Insensitive Qubit Design from Optimizing the Cooper-Pair Box,' 042319.

[64] M. D. LaHaye, O. Buu, B. Camarota, and K. C. Schwab: *Science* **304** 2004, 'Approaching the Quantum Limit of a Nanomechanical Resonator,' p 74.

[65] L. D. Landau and E. M. Lifshitz: Elsevier, Amsterdam, 1976. 'Mechanics.'

[66] B. P. Lanyon, T. J. Weinhold, N. K. Langford, M. Barbieri, D. F. V. James, A. Gilchrist, and A. G. White, *Physical Review Letters* **99** 2007, 'Experimental Demonstration of a Compiled Version of Shor's Algorithm with Quantm Entanglement,' 250505.

[67] B. P. Lanyon, J.D. Whitfield, G. G. Gillett, M. E. Goggin, M. P. Almeida, I. Kassal, J. D. Biamonte, M. Mohseni, B. J. Powell, M. Barbieri, A. Aspuru-Guzik, and A. G. White: *Nature Chemistry* **2** 2010, p 106.

[68] D. Leibfried, B. DeMarco, V. Meyer, M. Rowe, A. Ben-Kish, J. Britton, W. M. Itano, B. Jelenkovic, C. Langer, T. Rosenband, and D. J. Wineland: *Physical Review Letters* **89** 2002, 'Trapped Ion Quantum Simulator: Experimental Application to Nonlinear Interferometers,' 247901.

[69] C. Y. Lin, P. C. Stancil, H.-P. Liebermann, P. Funke, and R. J. Buenker: *Physical Review A* **78** 2008, 'Inelastic Processes in Collisions of Na($3s$,$3p$) with He at Thermal Energies,' 052706.

[70] S. Lloyd: *Science* **273** 1996, 'Universal Quantum Simuilators,' p 5273.

[71] D. Loss and D. P. DiVincenzo: *Physical Review A* **57** 1998, 'Quantum Computation with Quantum Dots,' p. 120.

[72] C.-Y. Lu, D. E. Browne, T. Yang, J.-W. Pan: *Physical Review Letters* **99** 2007, 'Demonstration of a Complied Version of Shor's Quantum Factoring Algorithm Using Photonic Qubits,' 250504.

[73] E. Lucero, M. Hofheinz, M. Ansmann, R. C. Bialczak, N. Katz, M. Neeley, A. D. O'Connell, H. Wang, A. N. Cleland, and J. M. Martinis: *Physical Review Letters* **100** 2008, 'High-fidelity Gates in a Josephson Qubit,' 247001.

[74] J. Majer, J. M. Chow, J. M. Gambetta, J. Koch, B. R. Johnson, J. A. Schreier, L. Frunzio, D. I. Schuster, A. A. Houck, A. Wallraff, A. Blais, M. H. Devoret, S. M. Girvin, and R. J. Schoelkopf: *Nature* **449** 2007, 'Coupling Superconducting Qubits via a Cavity Bus,' p 443.

[75] Y. Makhlin: *Quantum Information Processing* **1** 2003, 'Nonlocal Properties of Two-Qubit Gates and Mixed States, and the Optimization of Quantum Computation,' p 243.

[76] Y. Makhlin, G. Schon and A. Shnirman: *Nature* **398** 305, 'Josephson-junction qubits with Controlled Couplings,' p 305.

[77] Y. Makhlin, G. Schon and A. Shnirman: *Review of Modern Physics* **73** 2001, 'Quantum-state engineering with Josephson-junction devices,' p 357.

[78] F. Marquardt and C. Bruder: *Physical Review B* **63** 2001, 'Superposition of Two Mesoscopically Distinct Quantum States: Coupling a Cooper-Pair Box to a Large Superconducting Island,' 054514.

[79] J. M. Martinis (to be published)

[80] J. M. Martinis, M. H. Deveoret, and J. Clarke: *Physical Review Letters* **55** 1985, 'Energy-Level Quantization in the Zero-Voltage State of a Current-Biased Josephson Junction,' p 1543.

[81] J. M. Martinis, S. Nam, J. Aumentado, and C. Urbina: *Physical Review Letters* **89** 2002, 'Rabi Oscillations in a Large Josephson-Junction Qubit,' 117901.

[82] R. McDermott, R. W. Simmonds, M. Steffen, K. B. Cooper, K. Cicak, K. D. Osborn, D. P. Oh, S. Pappas, and J. M. Martinis: *Science* **307**, 'Simultaneous State Measurement of Coupled Josephson Phase Qubits,' p 1299.

[83] C. Monroe, D. M. Meekhof, B. E. King, W. M. Itano, and D. J. Wineland: *Physical Review Letters* **79** 1995, 'Demonstration of a Fundamental Quantum Logic Gate,' p 4714.

[84] J. E. Mooij, T. P. Orlando, L. S. Levitov, L. Tian, C. H. van der Wal, and S. Lloyd, *Science* **235** 1999, 'Josephson Persistent-Current Qubit,' 010301.

[85] F. Motzoi, J. M. Gambetta, P. Rebentrost, and F. K. Wilhelm: *Physical Review Letters* **103** 2009, 'Simple Pulses for Elimination of Leakage in Weakly Nonlinear Qubits,' 110501.

[86] Y. Nakamura, C. D. Chen, and J. S. Tsai: *Physical Review Letters* **79** 1997, 'Spectroscopy of Energy-Level Splitting Between Two Macroscopic Quantum States of Charge Coherently Superposed by Josephson Coupling,' p 2328.

[87] Y. Nakamura, Y. A. Pashkin, and J. S. Tsai: *Nature* **398** 1999, 'Coherent Control of Macroscopic Quantum States in a Single-Cooper-Pair Box,' p 786.

[88] Y. Nakamura, Y. A. Pashkin, T. Yamamoto, and J. S. Tsai: *Physical Review Letters* **88** 2002, 'Charge Echo in a Cooper-Pair Box,' 047901.

[89] M. Neeley, R. C. Bialczak, M. Lenander, E. Lucero, M. Mariantoni, A. D. O'Connell, D. Sank, H. Wang, M. Weides, J. Wenner, Y. Yin, T. Yamamoto, A. N. Cleland, John M. Martinis: 2010, 'Generation of Three-Qubit Entangled States using Superconducting Phase Qubits,' arxiv:1004.4246.

[90] M. A. Nielsen and I. L. Chuang, Cambridge University Press, Cambridge, *Quantum Computation and Quantum Information*, 2000.

[91] S. Oh, K. Cizak, R. McDermott, K. B. Cooper, K. D. Osborn, R. W. Simmonds, M. Steffen, J. M. Martinis, and D. P. Pappas: *Superconductor Science and Technology* **18** 2005, 'Low Leakage Superconducting Tunnel Junctions with a Single-Crystal Al)$_2$O$_3$ Barrier,' p 1396.

[92] Y. A. Pashkin, T. Yamamoto, O. Astafiev, Y. Nakamura, D. V. Averin, and J. S. Tsai: *Nature* **421** 2003, 'Quantum Oscillations in Two Coupled Charge Qubits,' p 823.

[93] G. Passante, O. Moussa, C. A. Ryan, and R. Laflamme: *Physical Review Letters* **103** 2009, 'Experimental Approximation of the Jones Polynomial with One Quantum Bit,' 250501.

[94] M. Paternostro, G. Falci, M. Kim, and G. M. Palma: *Physical Review B* **69** 2004, 'Entanglement Between Two Superconducting Qubits Via Interaction with Nonclassical Radiation,' 214502.

[95] M. Paternostro, W. Son, M. S. Kim, G. Falci, and G. M. Palma: *Physical Review A* **70** 2004, 'Dynamical Entanglement Transfer for Quantum-Information Networks,' 022320.

[96] F. Plastina and G. Falci: *Physical Review B* **67** 2003, 'Communicating Josephson Qubits,' 224514.

[97] E. J. Pritchett, C. Benjamin, A. Galiautdinov, M. R. Geller, A. T. Sornborger, P. C. Stancil, and J. M. Martinis: submitted to *Physical Review Letters* in 2010, 'Quantum Simulation of Molecular Collisions with Superconducting Qubits.'

[98] E.J. Pritchett and M. R. Geller: *Physical Review A* **72** 2005, 'Quantum Memory for Superconducting Qubits,' 010301(R).

[99] J. J. Sakuri: Addison-Wesley Publishing Company, Reading, 1994. 'Modern Quantum Mechanics.'

[100] J. A. Schreier, A. A. Houck, J. Koch, D. I. Schuster, B. R¿ Johnson, J. M. Chow, J. M. Gambetta, J. Majer, L. Frunzio, M. H. Devoret, S. M. Girvin, and R. J. Schoelkopf: *Physical Review B* **77** 2008, 'Suppressing Charge Noise Decoherence in Superconducting Charge Qubits,' 180502(R).

[101] J. R. Schrieffer: *Theory of Superconductivity*, Addison-Wesley Publishing Company, Inc., Redwood City, 1964.

[102] D. I. Schuster, A. A. Houck, J. A. Schreier, A. Wallraff, J. M. Gambetta, A. Blais, L. Frunzio, J. Majer, B. Johnson, M. H. Devoret, S. M. Girvin, and R. J. Schoelkopf, *Nature* **445** 2007, 'Resolving Photon Number States in a Superconducting Circuit,' p 515.

[103] R. W. Simmonds, K. M. Lang, D. A. Hite, S. Nam, D. P. Pappas, and J. M. Martinis: *Physical Review Letters* **93** 2004, 'Decoherence in Josephson Phase Qubits from Junction Resonators,' 077003.

[104] M. O. Scully and M. S. Zubairy: *Quantum Optics*, Cambridge University Press, Cambridge, 2007.

[105] A. Shnirman, G. Schon, and Z. Hermon: *Physical Review Letters* **79** 1997, 'Quantum Manipulations of Small Josephson Junctions,' 2371.

[106] P. W. Shor: *Proceedings, 35th Annual Symposium on Foundations of Computer Science* IEEE press, Los Alamitos, 'Algorithms for Quantum Computation: Discrete Logarithms and Factoring,' 1994.

[107] M. A. Sillanpaa, J. I. Park, and R. W. Simmonds: *Nature* **449** 2007, 'Coherent Quantum State Storage and Transfer Between Two Phase Qubits via a Resonant Cavity,' p 438.

[108] S. Somaroo, C. H. Tseng, T. F. Havel, R. Laflamme, and D. G. Cory: *Physical Review Letters* **82** 1999, 'Quantum Simulations on a Quantum Computer,' p 538.

[109] A.T. Sornborger and E.D. Stewart, *Physical Review A* **60** 1999, 'Higher Order Methods for Simulations on Quantum Computers,' p 1956.

[110] M. Steffen, M. Ansmann, R. McDermott, N. Katz, R. C. Bialczak, E. Lucero, M. Neeley, E. M. Weig, A. N. Cleland, and J. M. Martinis: *Physical Review Letters* **79** 2006, 'State Tomography of Capacitively Shunted Phase Qubits with High Fidelity,' 050502.

[111] M. Steffen, M. Ansmann, R. C. Bialczak, N. Katz, E. Lucero, R. McDermott, M. Neeley, E. M. Weig, A. N. Cleland, and J. M. Martinis: *Science* **313** 2006, 'Measurement of the Entanglement of Two Superconducting Qubits via State Tomography,' p 1423.

[112] M. Steffen, J. M. Martinis, and I. L. Chuang, *Physical Review B* **68** 2003, 'Accurate Control of Josephson Phase Qubits,' 224518.

[113] F. W. Strauch, P. R. Johnson, A. J. Dragt, C. J. Lobb, J. R. Anderson, and F. C. Wellstood: *Physical Review Letters* **91** 2003, 'Quantum Logic Gates for Coupled Superconducting Phase Qubits,' 167005.

[114] M. Tinkham: *Introduction to Superconductivity*, McGraw-Hill, New York, 1996.

[115] S. Trotzky, P. Cheinet, S. Folling, M. Feld, U. Schnorrberger, A. M. Rey, A. Polkovnikov, E. A. Demier, M. D. Lukin, I. Bloch: *Science* **319** 2008, p 295.

[116] C. H. van der Wal, A. C. J. ter Haar, F. K. Wilhelm, R. N. Schouten, C. J. P. M. Harmans, T. P. Orlando, S. Lloyd, and J. E. Mooij: *Science* **290** 2000, 'Quantum Superposition of Macroscopic Persisitent-Current States,' p 773.

[117] J. van Wezel, J. van den Brink, and J. Zaanen: *Physical Review Letter* **94** 2005, 'An Intrinsic Limit to Quantum Coherence due to Spontaneous Symmetry Breaking,' 230401.

[118] L. M. K. Vandersypen, M. Steffen, G. Breyta, C. S. Yannoni, M. H. Sherwood, and I. L. Chuang: *Nature* **414** 2001, 'Experimental Realization of Shor's Quantum Factoring Algorithm Using Nuclear Magnetic Resonance,' p 883.

[119] A. Wallraff, D. I. Schuster, A. Blais, L. Frunzio, R.-S. Huang, J. Majer, S. Kumar, S. M Girvin, and R. J. Schoelkopf: *Nature* **431** 2004, 'Strong Coupling of a Single Photon to a Superconducting Qubit Using Circuit Quantum Electrodynamics,' p 162.

[120] H. Wang, M. Hofheinz, M. Ansmann, R. C. Bialczak, E. Lucero, M. Neeley, A. D. O'Connell, D. Sank, M. Weides, J. Wenner, A. N. Cleland, and J. M. Martinis: *Physical Review Letters* **103** 2009, 'Decoherence Dynamics of Complex Photon States in a Superconducting Circuit,' 200404.

[121] S. Wiesner: arxiv:quant-ph 1996, 'Simulations of Many-Body Qantum Systems by a Quantum Computer,' quant-ph/9603028.

[122] F. K. Wilhelm, M. J. Storcz, U. Hartmann and M. R. Geller: Springer 2006, 'Superconducting Qubits II: Decoherence' in *Manipulating Quantum Coherence in Solid State Systems*, edited by M. E. Flatte and I. Tifrea, p 195.

[123] L.-A. Wu, M. S. Byrd, and D. A. Lidar: *Physical Review Letters* **89** 2002, 'Polynomial-Time Simulation of Pairing Models on a Quantum Computer,' 057904.

[124] T. Yamamoto, M. Neeley, E. Lucero, R. C. Bialczak, J. Kelly, M. Lenander, M. Mariantoni, A. D. O'Connell, D. Sank, H. Wang, M. Weides, J. Wenner, Y. Yin, A. N. Cleland, and J. M. Martinis: 'Quantum Process Tomography of Two-Qubit Controlled-Z and Controlled-Not Gates Using Superconducting Phase Qubits,' arXiv:1006.5084.

[125] T. Yamamoto, Y. A. Pashkin, O. Astafiev, Y. Nakamura, and J. S. Tsai, *Nature* **423** 2003, 'Demonstration of Conditional Gate Operation Using Superconducting Charge Qubits,' p 941.

[126] J. Q. You, J. S. Tsai, and F. Nori: *Physical Review Letters* **89** 2002, 'Scalable Quantum Computing with Josephson Charge Qubits,' 197902.

[127] S. P. Yukon: *Physica C* **368** 2002, 'A Multi Josephson Junction Qubit,' p 320.

[128] C. Zalka: *Proceedings: Mathematical, Physical and Engineering Sciences* **454** 1998, 'Simulating Quantum Systems on a Quantum Computer,' p 313.

[129] J. Zhang, J. Vala, S. Sastry, and K. B. Whaley: *Physical Review A* **67** 2003, 'Geometric Theory of Nonlocal Two-Qubit Operations,' 042313.

[130] J. Zhang and K. B. Whaley: *Physical Review A* **71** 2005, 'Generation of Quantum Logic Operations from Physical Hamiltonians,' 052317.

[131] X. Zhou, M. Wulf, Z. Zhou, G. Guo, and M. J. Feldman: *Physical Review A* **69** 2004, 'Dispersive Manipulation of Paired Superconducting Qubits,' 030301.

[132] S.-L. Zhu, Z. D. Wang, and K. Yang: *Physical Review A* **68** 2003, 'Quantum Information Processing Using Josephson Junction Coupled Through Cavities,' 034303.

[133] X. Zou and W. Mathis: *Physics Letters A* **324** 2004, 'Quantum Information Processing and Entanglement with Josephson Charge Qubits Coupled Through Nanomechanical Resonator,' p 484.